**N°d'ordre :

Université de Saida– Dr. Moulay Tahar
Faculté des sciences

Thèse

Présentée pour obtenir le diplôme de

DOCTORAT LMD (3ième Cycle)

Filière : Physique

Spécialité : Physique des matériaux

Par :
HAMLAT Mama

Thème :
Prédiction théorique des propriétés magnéto-électroniques de nouveaux composés pérovskite

Thèse soutenue le 23/06/2022 devant le jury composé de :

N°	Nom et prénom	Grade	Etablissement	Qualité
01	DJAAFRI Tayeb	MCA	Université de Saida – Dr. Moulay Tahar	Président
02	AMARA Kadda	prof	Université de Saida – Dr. Moulay Tahar	Rapporteur
03	KHELFAOUI Friha	MCA	Université de Saida – Dr. Moulay Tahar	Co-rapporteur
04	EL KEURTI Mohammed	prof	Université de Saida – Dr. Moulay Tahar	Examinateur
05	BELFEDAL Abdelkader	prof	Université de mascara	Examinateur
06	BERBER Mohamed	MCA	Centre universitaire Nour El-bachir El-bayadh	Examinateur

Order number:

UNIVERSITY OF SAIDA Dr. MOULAY TAHAR
Faculty of sciences

Dissertation

Presented to obtain the diploma of

DOCTORATE LMD diploma (3rd Cycle)

Specialty: physics

Option: materials physics

By:
HAMLAT Mama

Theme:

Theoretical prediction of the magneto-electronic properties of new perovskite compounds

Defended on 23/06/2022 in front of the jury composed of:

N°	Name	Grade	Affiliation	Quality
01	DJAAFRI Tayeb	MCA	University of Saida – Dr. Moulay Tahar	Chair man
02	AMARA Kadda	prof	University of Saida – Dr. Moulay Tahar	Thesis advisor
03	KHELFAOUI Friha	MCA	University of Saida – Dr. Moulay Tahar	Thesis Co-advisor
04	EL KEURTI Mohammed	prof	University of Saida – Dr. Moulay Tahar	Examiner
05	BELFEDAL Abdelkader	prof	University of mascara	Examiner
06	BERBER Mohamed	MCA	University center Nour El-bachir El-bayadh	Examiner

Dedication

I dedicate this modest work to my parents, for always loving
and supporting me.
To My dear brother Farid.
All the professors at the University of Saida.
My friends, colleagues and everyone who encouraged me.

HAMLAT Mama

Acknowledgments

Table of content

Nomenclature

List of most commonly used abbreviations:

- DM: Diamagnetic.
- PM: Paramagnetic Materials.
- FM: Ferromagnetic Materials.
- AFM: Antiferromagnetic Materials.
- FiM: Ferrimagnetic Materials.
- GMR: Giant Magneto Resistance.
- MRAM: Magnetic Random Access Memory.
- HMF: Half-Metal Ferromagnetic.
- HMFs: Half-Metallic Ferromagnetic materials.
- DFT: Density Functional Theory.
- KS: Kohn–Sham.
- HK: Hohenberg–Kohn.
- HF: Hartree-Fock.
- XC: Exchange-Correlation potentiel.
- LDA: Local Density Approximation.
- LSDA: Local Spin polarized Density Approximation.
- GGA: Generalized Gradient Approximation.
- TB-mBJ: Tran-Blaha modified beck Johnson (TB-mBJ) potentials.
- FP-LAPW: Full Potential Linearized Augmented Plane Waves.
- APW: Augmented Plane Waves.
- APW+ lo: Augmented Plane Waves + local orbitals.
- LAPW+ LO: Linearized Augmented Plane Waves + local orbitals.
- IBZ: Irreducible Brillouin Zone.
- SCF: Self-Consistent Field.
- MT: Muffin-Tin.
- E_f: Fermi Energy.
- DOS: Density of states.
- G: Shear modulus.
- E: Young Modulus.
- DMS: Dilute magnetic semiconductors.

List of figures

List of tables

General introduction

Introduction:

In the last few years, there has been a growing interest in the so called half-metallic ferromagnetic materials due to their outstanding physical, chemical, mechanical, optical, and magnetic properties [1], which are potentially promising in spintronic devices [2]. In a half metal, the electrons of one spin channel are metallic while those of the other are insulating, the spin polarization at Fermi level is complete (100%), and the magnetic moment is an integer. It is worth noting that the first prediction of a half metallic material was published in 1983 by De Groot et al in half-Heusler compound NiMnSb [3]. Later, numerous materials with different structures were also predicted with half-metallic ferromagnetism such as: the study of Japanese research groups on Co_2MnZ compounds, where Z match to Si and Ge [4], the quaternary Heusler CoFeCrAl by Iltaf Muhammad [5], The oxide compounds CrO_2 [6], TiO_2, and VO_2 [7] have been predicted as half-metallic ferromagnets, the double perovskites X_2FeMoO_6 (X = Ba, Ca, Sr) are reported to be HMs with 100% spin polarization [8] . Bouadjemi et al. [9] found that the cubic perovskite oxide $PrMnO_3$ presents a half-metallic behavior. The same character appears in Dilute magnetic semiconductors (DMSs), e.g. Cu-doped ZnO [10].

As above-mentioned, much effort has been spent to comprehend, forecast and grow new half metallic material. During the last decades, the HMF used in spintronics technology was based exclusively on transition metals. The latter have an electronic filling up to the d or f orbital [11]; and it is precisely these electrons which are at the origin of the magnetism and of the HMF in the materials based on these elements.

In contrast, recent research, theoretical and experimental, has revealed the existence of magnetism in materials involving light elements such as alkali and alkaline earth metals [12-14]. Used with carbon, nitrogen or oxygen, these materials have been predicted to be excellent HMF, the origin of which is no longer linked to d or f electrons as in transition metals, but to s and p electrons of these three elements. In this case the simple perovskite, not including transition elements are very promising candidates.

This is what motivated us to suggest a study of I^A-II^A-O_3 materials as $LiBeO_3$, $KBeO_3$ and $KMgO_3$ in the cubic phase, using ab-initio simulation studies [15], within the framework of the DFT according to the wien2k code [16] with a systematic study of the structural, elastic, magnetic, electronic and thermodynamic properties.

This thesis is organized as follows: In **chapter 1**, we try to provide a general overview on perovskite and ferromagnetic materials; also we consider the various possible applications. In **chapter 2**, we described the employed method.

Discussion of the results obtained in the present work will be presented in **chapter 3**. Finally, we will end this study with a general conclusion and our perspectives.

Bibliographical references:

[1] S. Wolf, D. Awschalom, R. Buhrman, J. Daughton, v.S. von Molnár, M. Roukes, A.Y. Chtchelkanova, D. Treger, Spintronics: a spin-based electronics vision for the future, science, 294 (2001) 1488-1495.

[2] J. Shah, P. Bhatt, K.D.D. Dayas, R. Kotnala, Significant role of antiferromagnetic $GdFeO_3$ on multiferroism of bilayer thin films, Materials Research Express, 5 (2018) 026416.

[3] R. De Groot, F. Mueller, P. Van Engen, K. Buschow, New class of materials: half-metallic ferromagnets, Physical Review Letters, 50 (1983) 2024.

[4] S. Ishida, S. Fujii, S. Kashiwagi, S. Asano, Search for half-metallic compounds in Co_2MnZ (Z= IIIb, IVb, Vb element), Journal of the Physical Society of Japan, 64 (1995) 2152-2157.

[5] I. Muhammad, J.-M. Zhang, A. Ali, S. Muhammad, Preserving the half-metallicity at the quaternary Heusler CoFeCrAl (001)-oriented thin films: A first-principles study, Materials Chemistry and Physics, 240 (2020) 122262.

[6] K. Schwarz, CrO_2 predicted as a half-metallic ferromagnet, Journal of Physics F: Metal Physics, 16 (1986) L211.

[7] V. Pardo, W.E. Pickett, Half-metallic semi-Dirac-point generated by quantum confinement in TiO 2/VO 2 nanostructures, Physical Review Letters, 102 (2009) 166803.

[8] Z. Szotek, W. Temmerman, A. Svane, L. Petit, G. Stocks, H. Winter, Half-metallic transition metal oxides, Journal of magnetism and magnetic materials, 272 (2004) 1816-1817.

[9] B. Bouadjemi, S. Bentata, A. Abbad, W. Benstaali, B. Bouhafs, Half-metallic ferromagnetism in $PrMnO_3$ perovskite from first principles calculations, Solid state communications, 168 (2013) 6-10.

[10] L.-H. Ye, A.J. Freeman, B. Delley, Half-metallic ferromagnetism in Cu-doped ZnO: density functional calculations, Physical Review B, 73 (2006) 033203.

[11] J.-H. Park, E. Vescovo, H.-J. Kim, C. Kwon, R. Ramesh, T. Venkatesan, Direct evidence for a half-metallic ferromagnet, Nature, 392 (1998) 794-796.

[12] O. Volnianska, P. Boguslawski, Magnetism of solids resulting from spin polarization of p orbitals, Journal of Physics: Condensed Matter, 22 (2010) 073202.

[13] C.M. Fang, G. De Wijs, R. De Groot, Spin-polarization in half-metals, Journal of Applied Physics, 91 (2002) 8340-8344.

[14] X. Wan, M. Kohno, X. Hu, Robust half-metallic character and large oxygen magnetism in a perovskite cuprate, Physical Review Letters, 95 (2005) 146602.

[15] D.J. Singh, L. Nordstrom, Planewaves, Pseudopotentials, and the LAPW method, Springer Science & Business Media, 2006.

[16] P. Blaha, K. Schwarz, G.K. Madsen, D. Kvasnicka, J. Luitz, wien2k, An augmented plane wave+ local orbitals program for calculating crystal properties, 60 (2001).

CHAPTER 1

I/- perovskite oxides and magnetic materials:

This first chapter constitutes a state of the art on Oxide perovskites where an overview on perovskite materials in view of their crystalline structures and practical properties is presented. In this chapter a short introduction on magnetism, its origin and some definitions of its different categories are also reported. Finally, some notions of ferromagnetic materials, spintronics, and half-metals are reminded.

I.1 Perovskites oxides generality:

I.1.1. Introduction:

Perovskite structural materials have been and still are the subject of various and varied studies. This interest stems from the fact that the perovskite solids have a relatively simple crystal structure with numerous electrical, magnetic, piezoelectric, optical, catalytic and magnetoresistance properties [1]. Depending on the crystal structure and the chemical composition of the perovskites Their properties change from one to another [2]. At low temperature, these materials can have an insulating behavior or semiconductor, and superconducting at relatively high temperatures [3]

The natural mineral, titanium oxide of calcium ($CaTiO_3$) is the first perovskite structure which was discovered in the mountains of the Urals of Russia in 1839 by German Gustave Rose [4].The name, perovskite, was subsequently given by Lev Aleksevich Von Perovski (1752-1856), a Russian mineralogist [5, 6], it can be schematically described as ABX_3, While most perovskites refer to oxides, some can be carbides, nitrides, halides and hydrides [7] ,cyanides, oxynitrides and sulfides.

.Perovskite exists in its natural state and is associated with several minerals such as: chlorite, talc, serpentine and melilite. It has a metallic appearance, with black, brown or brown-red color, but it can sometimes be slightly transparent.

There are several varieties of perovskites, we will cite among others:

- ✓ **Dysanalyte:** It is a niobiferous variety of perovskite (**Figure.I.1.a**) described initially from a sample from the quarry of Badloch, Mont-Orberg, Kaiserstuhl, BadenWürttemberg: one of the states making up Germany .
- ✓ **Knopite:** Variety of perovskite rich in cerium, of ideal formula (Ca, Ce, Na) (Ti, Fe) 3. It is described from samples from Långörsholmen, Alnön, Municipality of

Sundsvall, Medelpad, Sweden and dedicated to the German chemist Wilhelm Knop (1817-1891) (**Figure.I.1.b**).

✓ **Perovskite sodalite:** recognized in the form of clear crystals of very shiny sodalite and with large crystals, found in Udersdorf, Rhineland-Palatinate in Germany (**Figure.I.1.c**).

✓ **Clinochlore perovskite:** square in shape, it is an opaque perovskite on green clinochlore, very shiny and **with** large crystals, found in the Ilmen mountains, Chelyabinsk, Urals, Russia (**Figure. I.1.d**).

Figure. I.1: Perovskites in their natural state: (a) Dysanalyte ;(b) Knopite (c) sodalite and (d) clinochlore.

The next part is focused on the perovskite oxides family. The peculiarity of this family lies in the incredible variety of physicochemical properties sensitive to structural distortions, and to the chemical composition of crystals such as electrical transport, magnetism and elasticity.

I.1.2 Perovskites Materials:

I.1.2.1 ABX3 perovskite structure:

the general formula of perovskites is ABX_3 [9], A is an alkaline earth or a rare earth, B is a transition metal (A being the largest cation, B the smallest) and X is generally oxygen, fluorine or a halogen (chloride, bromide, iodide..). Anion X can also be found in the form of hydride H- or sulfide.[10, 11] see **figure. I. 2.**

The general formula of simple perovskites ABX₃
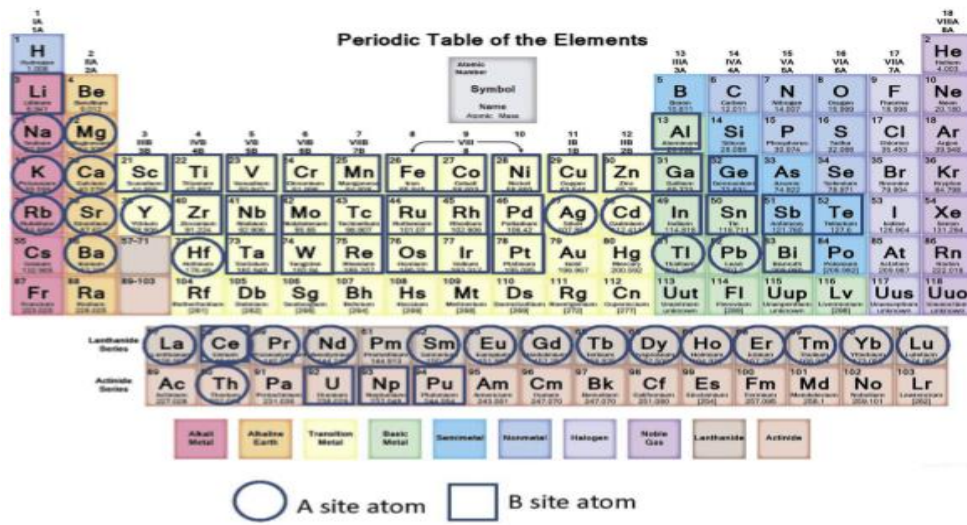
Figure I.2: general presentation of simple perovskites ABX$_3$.

The ideal perovskite is simple cubic and belongs to the space group Pm3m (N°
221) [12], where the atoms A occupy the corner of the cube, the atoms B in its center
and the atoms of oxygen O the faces of edges, where A is a monovalent, divalent, or
trivalent metal and B a pentavalent, tetravalent, or trivalent element, respectively
[13].

Perovskites are generally represented by a stack of BX$_6$ octahedral linked
together by their vertices. The cations B are in coordination 6 and the cations A
located in the cub octahedral cavity formed by 8 BX6 octahedral [14].

(a)   (b)   (c)

Atom	Site	positions
A	(2a)	(0, 0,0)
B	(2a)	(1/2,1/2, 1/2)
X	(6b)	(1/2,1/2, 0)
		(1/2,0, 1/2)
		(0,1/2, 1/2)
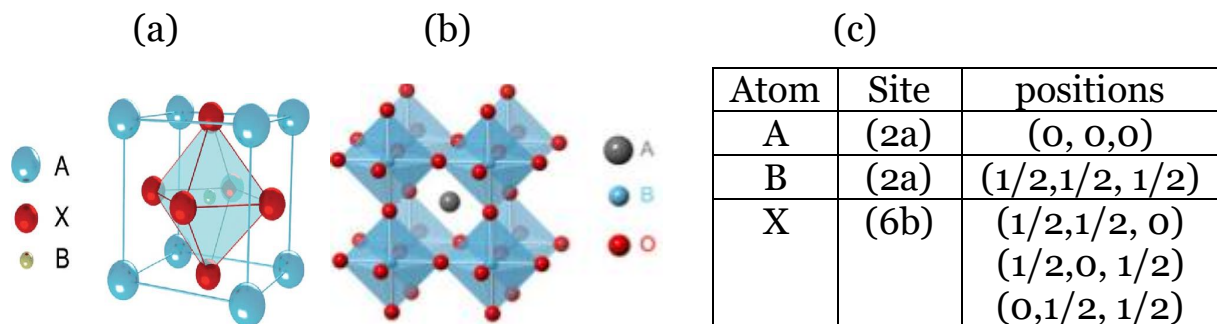
Figure I.3: (a-b) Two ways to represent the ideal perovskite structure, **(c)** atomic
positions [15].

There are generally two types of perovskites according to the occupation of sites A and B, **Figure I.4**:
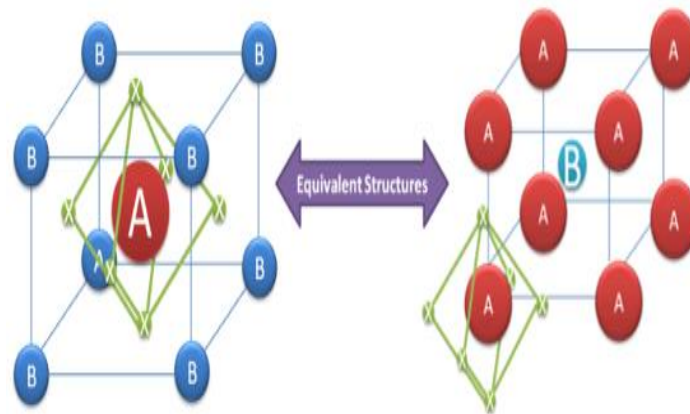
Figure I.4: A generic perovskite crystal structure of the form ABX_3.

Note that the two structures are equivalent – the left-hand structure is drawn so that atom B is at the <0, 0, 0> position while the right-hand structure is drawn so that atom (or molecule) A is at the <0,0,0> position. Also note that the lines are a guide to represent crystal orientation rather than bonding patterns.[16] Depending on the types of atoms occupying sites A and B, we distinguish:

- ✓ **Simple perovskite structures:** These are the ABO_3 structures whose sites A and B are occupied respectively by a single type of cation ($BaTiO_3$, $KNbO_3$, $NaTaO_3$, $CaTiO_3$, $PbTiO_3$, $BaMnO_3$, $KnbO_3$,).
- ✓ **Complex perovskite structures:** These are the structures of which one of the sites A or B is occupied by different types of cations ($PbMg_{1/3} Nb_{2/3} O_3$, $PbSc_{1/2} Ta_{1/2} O_3$, $Na_{1/2} Bi_{1/2} TiO_3$, $La_{0.8} Sr_{0.2}CoO_3$, $PbMg_{0.33} Nb_{0.67} O_3$, $PbCo_{0.25} Mn_{0.75} O_3$ ...).

I.1.2.2 Stability Criteria:

The stability of the perovskite structure depends essentially on two factors: the tolerance factor t and the iconicity of the anion-cation bond.

I.1.2.2.1Tolerance factor:

To describe the distortion of perovskite structures, the tolerance factor (Goldschmidt 1926) [17] is introduced and defined as an indicator of the stability and distortion of crystal structures (the size difference between A and B as follows) [18].

$$t = \frac{(r_A + r_o)}{(r_B + r_o)}$$

(I.3)

Where r_A, r_B and r_o are the ionic radii of A, B and O atoms, respectively.
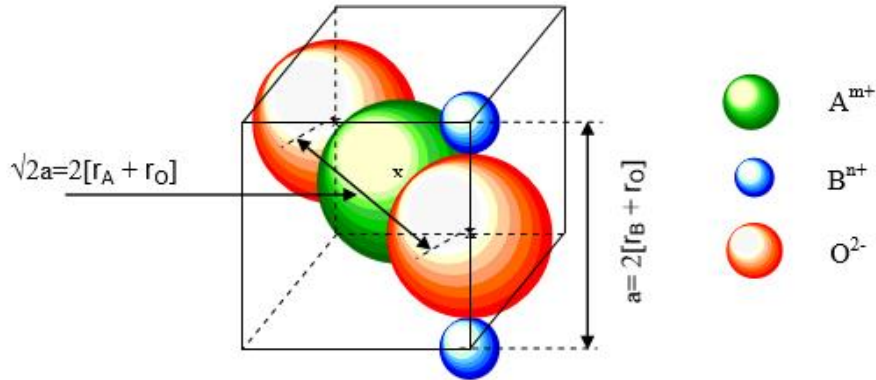
Figure I.5: In the cubic perovskite ABO_3, the axes of the mesh are described by the two expressions presented in the figure [19].

Note that From a theoretical point of view t must be equal to 1, but experimentally, we find that the perovskite compounds adopt the ideal cubic arrangement for 0.99 <t <1.06 [18, 20].

Several situations can therefore be distinguished depending on the value of the tolerance factor [21], as shown in **Table I.1**.

Table I.1: Evolution of crystal structures as a function of the value of the tolerance factor. [10]

at <0.75	0.75 <t<1.06			at>1.06
Ilmenite	perovskite			Hexagonal
	0.75<t<0.96	0.96<t<0.99	0.99<t<1.06	
	Orthorhombic distortion	rhombohedra distortion	cubic	

I.1.2.2.2 Ionicity of the anion-cation bonds:

The second parameter that defines a stability criterion is the ionicity of the anion connection. The ionic character of a perovskite structure of type ABX_3 is quantified

according to the Pauling scale [22] from the difference in electronegativity which is given by:

$$\bar{X} = \frac{X_{A-X} + X_{B-X}}{2}$$ (I.4)

Where X_{A-X} and X_{B-X} are respectively the differences in electronegativity between A, B and the associated oxygen or halogen.

The perovskite structure is more stable when the bonds involved have a strong ionic character. Thus lead-based perovskites of the covalent type are less stable than more ionic perovskites such as $BaTiO_3$ and $SrTiO_3$ [23].

I.1.3 Physicochemical properties of perovskites and their applications:

Perovskites are inorganic chameleons due to the diversity of physicochemical properties that they derive from them **(Table I.2),** either as reducers, catalysts, photocatalysts, conductors or semiconductors, ferroelectric, or piezoelectric, etc.

Table I.2: Materials with perovskite structure and their properties and application [24-26].

Materials	Properties	Applications
$BaTiO_3$	Dielectric	capacitor, sensor
(Ba,Sr)TiO$_3$	Pyroelectric	pyrodetector
$PbTiO_3$	pyroelectric piezoelectric	pyrodetector, acoustic transducer
Pb(Zr,Ti)O$_3$	dielectric pyroelectric piezoelectric electro-optic	nonvolatile memory, pyrodetector surface acoustic wave device, substrate waveguide device
(Pb,La)(Zr,Ti)O$_3$	pyroelectric electro-optic	pyrodetector waveguide device, optical memory display
$LiNbO_3$	Piezoelectric	pyrodetector, surface acoustic wave device
($LiNbO_3$/Ti)	electro-optic	waveguide device, second harmonic generation, optical modulator
K(Ta,Nb)O$_3$	pyroelectric electro-optic	pyrodetector waveguide device, frequency doubler
Pb(Mg$_{1/3}$Nb$_{2/3}$)O$_3$	Dielectric	memory, capacitor

I.2 Magnetism in perovskite materials
I.2.1 Introduction

Magnetism is a phenomenon by which materials assert an attractive or repulsive force or influence over other materials, has been known for thousands of years [27]. Magnetism has experienced considerable growth and technological importance; it occupies a remarkable place in the description of the fundamental properties of matter. Magnetic materials are present everywhere in electronics, electromechanics and electricity [28].

In addition, these materials have allowed science to open up to a new field called spintronics. It is a new technology where the two properties of the electron, namely its charge and its spin, are exploited.

I.2.2 Origin of Magnetism

The macroscopic magnetic properties of materials are a consequence of the magnetic moments associated with individual electrons. Each electron in an atom has magnetic moments which originate from two sources [29].
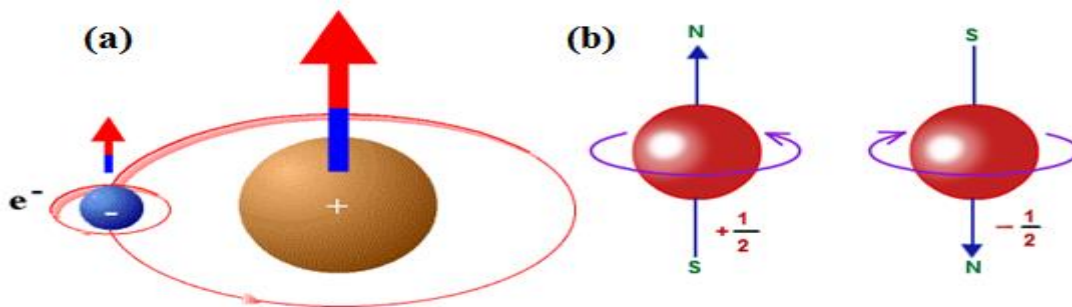
Figure I.6: magnetic moment (a): orbital magnetic moment, (b): magnetic moment of spin.

- ✓ The orbital magnetic moment: $\overrightarrow{\mu_l} = \frac{\mu_B}{\hbar}\vec{l}$ Where $\mu_B = 9.87.10^{-24}$A.m² is the magneto of Bohr and ℏ the reduced Planck constant.
- ✓ The magnetic moment of spin: $\overrightarrow{\mu_s} = -g\frac{\mu_B}{\hbar}\vec{S}$ where g is the Landé factor which is worth approximately 2 in the case of the electron.

When the sum of the magnetic moments is zero (all electrons are paired) the atom, or ion, is diamagnetic. Otherwise (unpaired electrons) the atom or ion is paramagnetic.

I.2.3 different forms of magnetism:[30]

The best way to introduce the different types of magnetism is to describe how materials respond to magnetic fields. This may be surprising to some, but all matter is magnetic. It's just that some materials are much more magnetic than others. The main distinction is that in some materials there is no collective interaction of atomic magnetic moments, whereas in other materials there is a very strong interaction between atomic moments.

In general, solid materials can be divided into two major classes from a magnetic point of view:

✓ **Unordered magnetic materials:** which correspond to ***non-cooperative magnetism***, a category in which we find diamagnetics and paramagnetics.
✓ **Ordered magnetic materials:** correspond to ***cooperative magnetism***, where ferromagnetics, antiferromagnetics and ferrimagnetics are found [30].

The magnetic behavior of materials can be classified into the following five major groups:

I.2.3.1 Diamagnetic Materials (DM):

Diamagnetism is weak magnetism, does not depend on temperature and is the fundamental property of all matter. Diamagnetism is mainly due to the non-cooperative behavior of orbital electrons under the application of the external magnetic field.

Diamagnetic substances are made up of atoms whose electronic configuration reveals only doublets or empty orbitals. So, no magnetic spin moment. However, when an external magnetic field is applied to these materials, they are magnetized opposite the direction of the field. So, they have negative magnetization. This means that for diamagnetic substances, the sensitivity is negative [31] (varies between 10^{-6} and 10^{-4} depending on the material) [32].Diamagnetism affects all materials but it is often masked by other manifestations of magnetism (paramagnetism or ferromagnetism). There are several typical diamagnetic materials. Example: silver and bismuth.
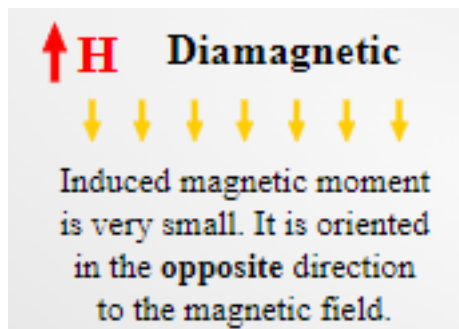
Figure I.7: magnetic moments of each atom are applied to the external magnetic field.

I.2.3.2 Paramagnetic Materials (PM):

Paramagnetism results from the presence of least one unpaired electron spin in a material's atoms or molecules. In other words, any material that possesses atoms with incompletely filled atomic orbitals is paramagnetic. The spin of the unpaired electrons gives them a magnetic dipole moment. Basically, each unpaired electron acts as a tiny magnet within the material. When an external magnetic field is applied, the spin of the electrons aligns with the field. Because all the unpaired electrons align the same way, the material is attracted to the field. When the external field is removed, the spins return to their randomized orientations. Examples of paramagnetic materials include magnesium, molybdenum, lithium, and tantalum. Example: manganese and tungsten.

The magnetization approximately follows curie's law, which states that the magnetic susceptibility χ is inversely proportional to temperature:

$$M = \chi_m = C_m/T \tag{I.5}$$

Where M is magnetization, χ_m is magnetic susceptibility, H is the auxiliary magnetic field, T is the absolute (Kelvin) temperature, and C is the material-specific Curie constant.
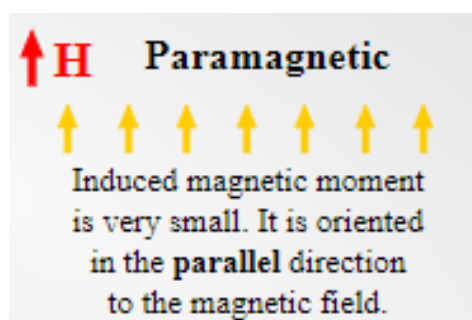
Figure I.8: magnetic moments of each atom align with the external magnetic field.

I.2.3.3 Ferromagnetic Materials (FM):

Ferromagnetic materials can form permanent magnets and are attracted to magnets. A ferromagnet has unpaired electrons, plus the magnetic moments of the electrons tend to remain aligned even when removed from a magnetic field. these materials also have a transition temperature, called Curie temperature θ_C [33] above which $(T > \theta_C)$ they become paramagnetic, their magnetic susceptibility χ_m positive and great. $(10^3 < \chi_m < 10^6)$ then following the law of Curie-Weiss [34].

$$\chi_m = \frac{C}{T - \theta_C} \tag{I.6}$$

where C is a constant sometimes called the Curie constant and Tc is the Curie temperature.

Examples of ferromagnetic materials include iron, cobalt, nickel, alloys of these metals, some rare earth alloys, and some manganese alloys.

As soon as the temperature drops again to become equal to θ_C $(T = \theta_C)$, the material reacquires ferromagnetic behavior. In other words, this phase transition is reversible.
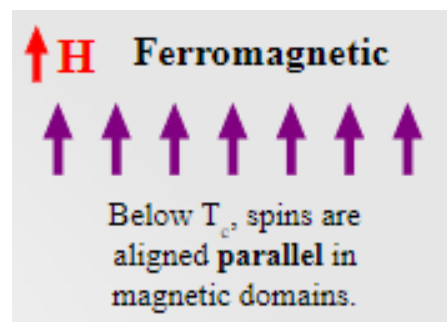
Figure I.9: magnetic moments of an atom are parallel with that of the neighboring atom.

I.2.3.4 Antiferromagnetic Materials (AFM):

In recent years, researchers have gone much further in the study of perovskites, discovering new explanations for behaviors previously unknown, everyone is now interested in antiferromagnetic behavior [35]. This new property is created in the case of a ferrimagnetic substance having two antiparallel sub-networks and whose sum of parallel and antiparallel moments is zero **Figure I.10**. These

materials never have a moment permanent magnetic. We note that Their susceptibility is low and increases with temperature up to a temperature at a critical temperature called the Néel temperature T_N . If T $> T_N$ the material becomes paramagnetic. Example: FeMn alloys and NiO oxide.
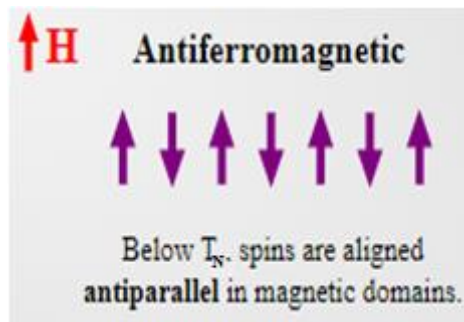
Figure I.10: magnetic moments of an atom are reversed with that of the neighboring atom.

I.2.3.5 Ferrimagnetic Materials (FiM):[36]

In a ferrimagnetic material, a particular case of the AFM materials, the directions of the magnetic moments are parallel and the directions of neighboring magnetic moments are opposite **Figure I.11** which should lead to a non-zero total magnetic moment because the different elementary magnetic moments do not have the same modulus. Enough to observe a spontaneous magnetization of the material, even in the absence of an external magnetic field applied. Magnetic susceptibility remains high up to Neel temperature T_N. If T $> T_N$ the material becomes paramagnetic.

However, the magnetization is generally weaker than in the case of a ferromagnetic material. Example of ferrimagnetic materials: Fe_3O_4, $BaFe_{12}O_{19}$.
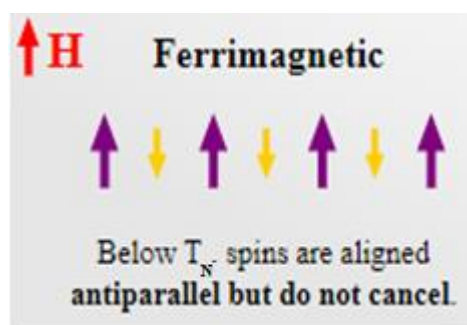
Figure I.11: Magnetic moments in one direction do not have the same intensity as those in the other direction.

I.3 Classification of ferromagnetic materials:

We separate the magnetic materials into two families which are distinguished by their curve B = (H):

I.3.1 Soft magnetic materials:

According to the criteria of the electrical engineer, a good soft metallic material, subjected to the action of relatively weak magnetic fields, should exhibit high magnetization, close to saturation magnetization. This ease of magnetization means very high magnetic permeability. The hysteresis cycle associated with this type of material is very narrow, therefore a very small coercive field **(Figure I.12.a)**.

These materials are generally widely used, in applications where it is necessary to guide the magnetic flux (transformers and motors). Quote:

- ✓ Electric steels.
- ✓ FeNi and FeCo alloys.
- ✓ Ferrites.
- ✓ Amorphous materials.

I.3.2 Hard magnetic materials

As opposed to soft magnetic materials which are easily magnetized and demagnetized, hard materials can only be demagnetized with difficulty, hence the interest in the realization of permanent magnets. These materials are characterized by wide hysteresis cycles and high coercive fields (**figure I.12.b)**. Hard materials are permanent magnets [37].

Among the hard magnetic materials we have:

- ✓ Ceramic materials: hard ferrites.
- ✓ Alloys based on rare earth elements.
- ✓ Alloys based on Iron- Nickel- Aluminum (Alnico).
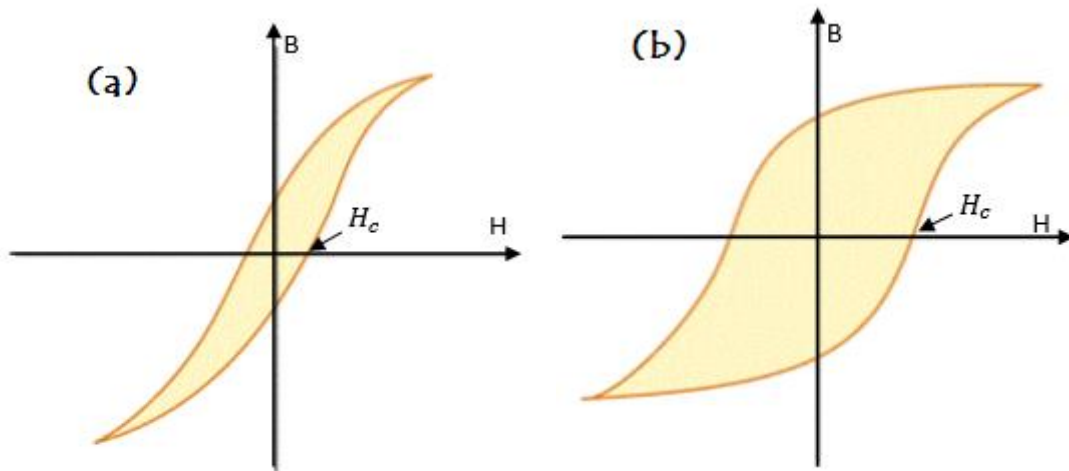
Figure I.12: Hysteresis cycle **(a):** soft material, **(b):** hard material. The point H_c indicates the coercive field.

I.4 Spintronic:

"Spintronic is a new area of research at the interface between magnetism and electronics, electronics that harness a quantum characteristic of the electron, its spin" underlines (says) Albert Fert , scientific director at the CNRS / Thalès joint physics unit and professor emeritus at the University of Orsay [38].

Spintronics can be described as electronics that exploit not only the charge, but also the spin of electrons. Its development followed the discovery of giant magnetoresistance (GMR) in 1988 [39, 40] by the teams of Albert Fert in France and Peter Grünberg in Germany, and for which the Nobel Prize for Physics 2007 was co-awarded to them. The general concept of spintronics is to place ferromagnetic materials in the path of electrons and to use the influence of spin on the mobility of electrons in these materials. This influence, first suggested by Mott [41] in 1936, was then demonstrated experimentally and theoretically described in the late 1960s [42, 43]. The discovery of GMR led to the first practical uses of this influence. Many other phenomena also exploiting the spin of electrons were then revealed and, today, spintronics is developing in many directions: tunnel magnetoresistance, spin transfer phenomena, spintronics with semiconductors, molecular spintronics, spintronics with multiferroics, etc [38].

It can be applied to the writing of magnetic memories (MRAM for our computers) and to the generation of microwave waves (application in telecommunications) [8].

I.5 Half metals:

Since the spintronic discovery in the early 1980s [44], half metallic ferromagnet (HMF) materials have been the subject of intense theoretical and experimental investigations in materials science. The idea of HM ferromagnetism was introduced by de Groot et al (1983) in NiMnSb and PtMnSb half-Heusler alloys [44]. In idealized HM ferromagnet, the spin-polarized system exhibits metallic nature in one spin channel ("up" or "down") and semiconducting / insulating in the other spin channel that reveals the100% spin polarization at Fermi level [44, 45] **(Figure I.13).** Half-metallic ferromagnetic materials (HFMs) have attained significant interest from both the academic as well as industrial point of view.[46], due to their promising potential applications in spintronic devices [47], magnetic tunnel junctions, magnetic disk drives, spin injection devices and nonvolatile magnetic random access memories. [48]
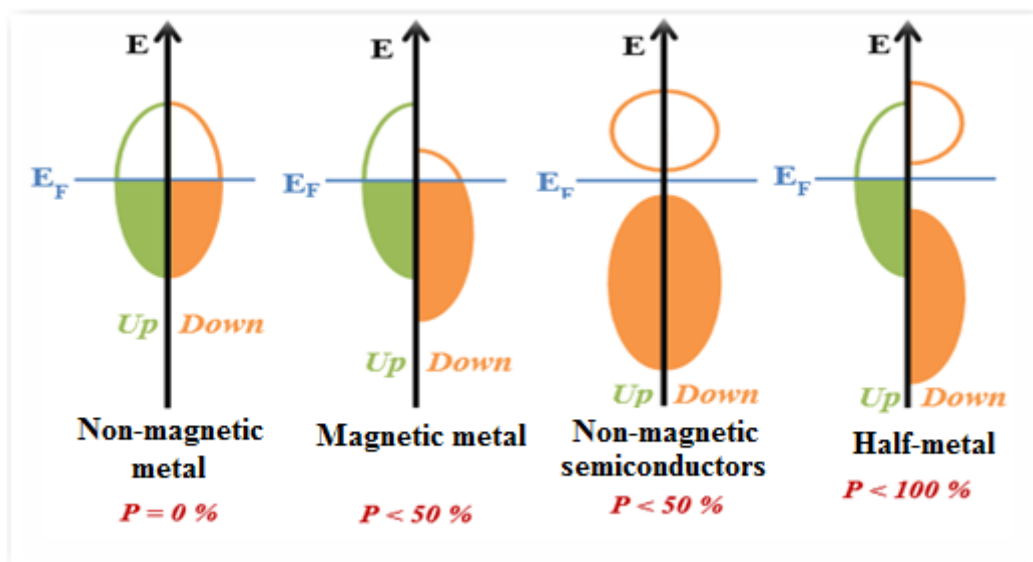
Figure I.13: Schematic illustration of the density of states of a: non-magnetic metal, magnetic metal, non-magnetic semiconductor and half-metal.[49]

Half-metallic character has been reported theoretically and experimentally in many other compounds such as:

✓ Heusler alloys (e.g., half Heusler CoCrZ (Z=S, and Se)[50], full Heusler Zr_2PdZ (Z= Al, Ga, and In) [51], and quaternary Heusler CoFeCrZ (Z= Al, Si, Ga, Ge, P, As and Sb) [52, 53]).

- ✓ The oxide compounds, such as CrO_2 [54-56], TiO2, and VO_2 [57], within their rutile structure, have been predicted as half-metallic ferromagnets.

- ✓ Ali [58], Park [59] have also found that some ternary compounds, specifically spinels (minerals with the general formula AB_2O_4), such as Fe_3O_4, $LiMn_2O_4$ [60] are half-metals.

- ✓ Dilute magnetic semiconductors (DMSs), e.g. Cu-doped ZnO [61], Cr-doped CdZ (Z= S, Se, and Te) [62], and Mn-doped GaN [63] behave like half metallic systems.

- ✓ Perovskites (e.g., $BaCrO_3$, $BaCr_{0.5}Ti_{0.5}O_3$ [64]) are found to be half-metallic ferromagnets with an integral magnet moments per unit.

Bibliographical references:

[1] T. Wolfram, S. Ellialtioglu, Electronic and optical properties of d-band perovskites, Cambridge University Press, 2006.

[2] A. Maameri, La Structure électronique des pérovskites défectives en atome d'oxygène de type MNbO3-x (M= Ba, Sr): Calcul de premiers-principes, in, Université d'Oran1-Ahmed Ben Bella, 2011.

[3] M.B. Bouabdellah, DIPLOME DE DOCTORAT EN SCIENCE Spécialité ELECTRONIQUE, in, Université de Mostaganem, 2013.

[4] B.C. Youcef, Structures Magnétiques des Pérovskites de type ABC3 Etude du premier principe, in, Université de Mostaganem, 2018.

[5] N.-G. Park, Perovskite solar cells: an emerging photovoltaic technology, Materials today, 18 (2015) 65-72.

[6] F. Hawthorne, R. Ferguson, The crystal structure of roselite, The Canadian Mineralogist, 15 (1977) 36-42.

[7] M. Pena, J. Fierro, Chemical structures and performance of perovskite oxides, Chemical reviews, 101 (2001) 1981-2018.

[8] F. Albert, [Vidéo]. Canal-U. SPINTRONIQUE : ORIGINES, DÉVELOPPEMENTS RÉCENTS ET PERSPECTIVES., https://www.canal-u.tv/chaines/iap/spintronique-origines-developpements-recents-et-perspectives, (2009).

[9] C. Li, K.C.K. Soh, P. Wu, Formability of ABO3 perovskites, Journal of Alloys and Compounds, 372 (2004) 40-48.

[10] C. Nassima, Etude ab-intio des différentes propriétés structurales, électroniques, optiques et thermiques des composés ternaires (CaLiF3 et SrLiF3) par la méthode FP-LAPW, in, Université Badji Mokhtar, 2015.

[11] O.B. Mya, Synthèse et Caractérisation de la pérovskite La1-xSrxFe0. 7Ni0. 3O3, in, 2015.

[12] A. Rabie, Etude des propriétés structurales, électroniques et mécaniques des composés fluoro-pérovskites à base de sodium NaXF3 (X= Mg, Zn) par la méthode FP-LAPW, in, 2018.

[13] F. Jona, G. Shirane, Chap. IV, in, Dover New York, 1993, pp. 108.

[14] R.H. Mitchell, Perovskites: modern and ancient, Almaz Press Thunder Bay, 2002.

[15] F. Marlec, Nouveaux matériaux perovskites ferroélectriques: céramiques et couches minces issues de la solution solide (Sr2Ta2O7) 100- x (La2Ti2O7) x, in, Université Rennes 1, 2018.

[16] D.J. Mullassery, PEROVSKITE SOLAR CELLS.

[17] V.M. Goldschmidt, Geochemische verteilungsgesetze der elemente, In Kommission bei J. Dybwad, 1927.

[18] R.J. Tilley, Perovskites: structure-property relationships, John Wiley & Sons, 2016.

[19] M.S. Mahboub, Synthèse, caractérisation par diffraction X et spectroscopie Raman des composés Ca1-xSrxFeO2. 5-δ (δ= 0, 0.5), (2012).

[20] J. Philipp, P. Majewski, L. Alff, A. Erb, R. Gross, T. Graf, M. Brandt, J. Simon, T. Walther, W. Mader, Structural and doping effects in the half-metallic double perovskite A 2 CrWO 6 (A= Sr, Ba, and Ca), Physical Review B, 68 (2003) 144431.

[21] M. Marezio, J. Remeika, P. Dernier, The crystal chemistry of the rare earth orthoferrites, Acta Crystallographica Section B: Structural Crystallography and Crystal Chemistry, 26 (1970) 2008-2022.

[22] L. Pauling, The Nature of the Chemical Bond, Cornell university press Ithaca, NY, 1960.

[23] T.R. Shrout, A. Halliyal, Preparation of lead-based ferroelectric relaxors for capacitors, (1987).

[24] S. Pradhan, G. Roy, Study the crystal structure and phase transition of $BaTiO_3$– A pervoskite, Researcher, 5 (2013) 63-67.

[25] K. Hooshyari, M. Javanbakht, A. Shabanikia, M. Enhessari, Fabrication $BaZrO_3$/PBI-based nanocomposite as a new proton conducting membrane for high temperature proton exchange membrane fuel cells, Journal of Power Sources, 276 (2015) 62-72.

[26] Y. Mao, H. Zhou, S.S. Wong, Synthesis, properties, and applications of perovskite-phase metal oxide nanostructures, Material Matters, 5 (2010) 50.

[27] Y. GUERMIT, Magnetic properties of Heusler alloys Ni2XY (X= Mn, Co. Y= Al, Ga, Sn), in, 2018.

[28] M.A. CHOUIAH, Etude Ab-initio des Propriétés structurales, optoélectroniques, thermodynamiques et magnétiques des pérovskites, in, Université de Mostaganem, 2019.

[29] J. Degauque, Magnétisme et matériaux magnétiques: introduction, Le Journal de Physique IV, 2 (1992) C3-1-C3-13.

[30] A. SOUIDI, Etude des propriétés spintroniques du double Perovskite type ABCO6, in, Université de Mostaganem-Abdelhamid Ibn Badis.

[31] L.C. Pauling, The theoretical prediction of the physical properties of many electron atoms and ions. Mole refraction, diamagnetic susceptibility, and extension in space, Proceedings of the Royal Society of London. Series A, Containing Papers of a Mathematical and Physical Character, 114 (1927) 181-211.

[32] C. Pigot, La lévitation diamagnétique à l'échelle micrométrique: applications et possibilités, in, Institut National Polytechnique de Grenoble-INPG, 2008.

[33] A. LABDELLI, Etude ab-initio des propriétés optoélectroniques et magnétiques de l'alliage pérovskite GdxBa1-xRuO3, in, Université de Mostaganem-Abdelhamid Ibn Badis.

[34] C. Kittel, P. McEuen, Introduction to solid state physics, Wiley New York, 1996.

[35] D. Bloch, R. Georges, I. Jacobs, Étude de la susceptibilité magnétique de l'oxyde de manganèse et du sulfure de manganèse en poudre dans l'état ordonné, Journal de Physique, 31 (1970) 589-595.

[36] J.-P. Pérez, R. Carles, R. Fleckinger, Electromagnétisme: fondements et applications avec 300 exercices et problèmes résolus, Dunod, 2002.

[37] D. Jiles, Introduction to magnetism and magnetic materials, CRC press, 2015.

[38] A. Fert, Les débuts de la spintronique-Travaux précurseurs et magnétorésistance géante, Reflets de la Physique, (2009) 5-10.

[39] M.N. Baibich, J.M. Broto, A. Fert, F.N. Van Dau, F. Petroff, P. Etienne, G. Creuzet, A. Friederich, J. Chazelas, Giant magnetoresistance of (001) Fe/(001) Cr magnetic superlattices, Physical Review Letters, 61 (1988) 2472.

[40] G. Binash, P. grunberg, F. Saurenbach and W. Zinn, Phys. Rev. B, 39 (1989) 4828.

[41] N.F. Mott, The electrical conductivity of transition metals, Proceedings of the Royal Society of London. Series A-Mathematical and Physical Sciences, 153 (1936) 699-717.

[42] B. Loegel, F. Gautier, Origine de la resistivite dans le cobalt et ses alliages dilues, Journal of Physics and Chemistry of Solids, 32 (1971) 2723-2735.

[43] J. Wajnflasz, R. Pick, Transitions «Low spin»-«High spin» dans les complexes de Fe2+, Journal de Physique Colloques, 32 (1971) C1-91-C91-92.

[44] R. De Groot, F. Mueller, PG v. Engen, and KHJ Buschow, Phys. Rev. Lett, 50 (1983) 2024-2027.

[45] C. Vargas-Hernández, R.B. Cruz, Half-metallic ferromagnetism of ZnxMn1− xO compounds: a first-principles study, Computational Condensed Matter, 4 (2015) 1-5.

[46] M.R. ur rehman Hashmi, M. Zafar, M. Shakil, A. Sattar, S. Ahmed, S. Ahmad, First-principles calculation of the structural, electronic, and magnetic properties of cubic perovskite RbXF3 (X= Mn, V, Co, Fe), Chinese Physics B, 25 (2016) 117401.

[47] S. Wolf, D. Awschalom, R. Buhrman, J. Daughton, v.S. von Molnár, M. Roukes, A.Y. Chtchelkanova, D. Treger, Spintronics: a spin-based electronics vision for the future, science, 294 (2001) 1488-1495.

[48] S. Terkhi, R. Bentata, F. Bendahma, T. Lantri, S. Bentata, Z. Aziz, B. Abbar, Half-metallic ferromagnetic behavior of cubic lanthanide based on perovskite-type oxide NdCrO 3: first-principles calculations, Indian Journal of Physics, 95 (2021) 833-839.

[49] M.H. GOUS, Calcul des propriétés structurales, élastiques, électroniques et magnétiques des semi-conducteurs magnétiques dilués à base de MgS et des alliages demi-heusler demi-métalliques CoVTe et RuVTe, in, GUELMA, 2018.

[50] H.-M. Huang, C.-K. Zhang, Z.-D. He, J. Zhang, J.-T. Yang, S.-J. Luo, Electronic and mechanical properties of half-metallic half-Heusler compounds CoCrZ (Z= S, Se, and Te), Chinese Physics B, 27 (2018) 017103.

[51] F. Khelfaoui, A. Boudali, A. Bentayeb, L. El Hachemi Omari, Y. Si Abderrahmane, Investigations of Structural, Elastic, Electronic, Magnetic and Transport Properties of the Heusler Compounds Zr2PdZ (Z= Al, Ga, and In): FP-LAPW Method, Acta Physica Polonica, A., 133 (2018).

[52] A. Bahnes, A. Boukortt, H. Abbassa, D. Aimouch, R. Hayn, A. Zaoui, Half-metallic ferromagnets behavior of a new quaternary Heusler alloys CoFeCrZ (Z= P, As and Sb): Ab-initio study, Journal of Alloys and Compounds, 731 (2018) 1208-1213.

[53] G. Gao, L. Hu, K. Yao, B. Luo, N. Liu, Large half-metallic gaps in the quaternary Heusler alloys CoFeCrZ (Z= Al, Si, Ga, Ge): A first-principles study, Journal of Alloys and Compounds, 551 (2013) 539-543.

[54] K. Schwarz, CrO2 predicted as a half-metallic ferromagnet, Journal of Physics F: Metal Physics, 16 (1986) L211.

[55] H. Hwang, S.-W. Cheong, Enhanced intergrain tunneling magnetoresistance in half-metallic CrO2 films, science, 278 (1997) 1607-1609.

[56] I. Mazin, D. Singh, C. Ambrosch-Draxl, Transport, optical, and electronic properties of the half-metal CrO 2, Physical Review B, 59 (1999) 411.

[57] V. Pardo, W.E. Pickett, Half-metallic semi-Dirac-point generated by quantum confinement in TiO 2/VO 2 nanostructures, Physical Review Letters, 102 (2009) 166803.

[58] S. Ali, M. Rashid, M. Hassan, N. Noor, Q. Mahmood, A. Laref, B.U. Haq, Ab-initio study of electronic, magnetic and thermoelectric behaviors of LiV2O4 and LiCr2O4 using modified Becke-Johson (mBJ) potential, Physica B: Condensed Matter, 537 (2018) 329-335.

[59] M.S. Park, S. Kwon, S. Youn, B. Min, Half-metallic electronic structures of giant magnetoresistive spinels: Fe 1− x Cu x Cr 2 S 4 (x= 0.0, 0.5, 1.0), Physical Review B, 59 (1999) 10018.

[60] D. Santos-Carballal, P.E. Ngoepe, N.H. De Leeuw, Ab initio investigation of the thermodynamics of cation distribution and of the electronic and magnetic structures in the LiMn 2 O 4 spinel, Physical Review B, 97 (2018) 085126.

[61] L.-H. Ye, A.J. Freeman, B. Delley, Half-metallic ferromagnetism in Cu-doped ZnO: density functional calculations, Physical Review B, 73 (2006) 033203.

[62] H.S. Saini, M. Singh, A.H. Reshak, M.K. Kashyap, Variation of half metallicity and magnetism of Cd1− xCrxZ (Z= S, Se and Te) DMS compounds on reducing dilute limit, Journal of magnetism and magnetic materials, 331 (2013) 1-6.

[63] T. Sasaki, S. Sonoda, Y. Yamamoto, K.-i. Suga, S. Shimizu, K. Kindo, H. Hori, Magnetic and transport characteristics on high Curie temperature ferromagnet of Mn-doped GaN, Journal of Applied Physics, 91 (2002) 7911-7913.

[64] Z. Zhu, X. Yan, Half-metallic properties of perovskite BaCrO 3 and BaCr 0.5 Ti 0.5 O 3 superlattice: LSDA+ U calculations, Journal of Applied Physics, 106 (2009) 023713.

CHAPTER II

In this chapter, we give an overview about the theoretical foundations on which the density functional theory is based, by discussing the different approximations generally adopted in solving the Schrödinger equation and by describing the different possible implementations.

II.1 Introduction:

There are many fields within the physical sciences and engineering where the key to scientific and technological progress is understanding and controlling the properties of matter at the level of individual atoms and molecules [1].The so-called Density functional theory (DFT) has proved to be highly successful approach in describing structure and   electronic structure properties (principally the ground state) in a vast class of materials, ranging from atoms and molecules to simple crystals to complex extended systems (including glasses and liquids). Furthermore DFT is computationally simple. For these reasons DFT has become a common tool in first-principles calculations aimed at describing – or even predicting – properties of molecular and condensed matter systems.

II.2 what is Density Functional Theory?

Density functional theory is a useful and interesting topic. But what is it exactly? We begin with the observation that one of the most profound scientific advances of the twentieth century was the development of quantum mechanics and the repeated experimental observations that confirmed that this theory of matter describes, with astonishing accuracy, the universe in which we live. In this section, we begin a review of some key ideas from quantum mechanics that underlie DFT (and other forms of computational chemistry).

To get a first idea of what density-functional theory is about, it is useful to take a step back and recall some elementary quantum mechanics. In quantum mechanics we learn that all information we can possibly have about a given system is contained in the system's wave function, Ψ.

Our goal here is not to present a complete derivation of the techniques used in DFT. Instead, our goal is to give a clear, brief, introductory presentation of the most basic equations important for DFT.

Here we will exclusively be concerned with the electronic structure of atoms, molecules and solids. The nuclear degrees of freedom (e.g., the crystal lattice in a solid) appear only in the form of potential v (r) acting on the electrons, so that the wave function depends only on the electronic coordinates. Nonrelativistically, this wave function is calculated from Schrodinger's equation.

II.3 Schrödinger Equation:

Schrödinger equation; the fundamental equation of the science of submicroscopic phenomena known as quantum mechanics. The equation, developed (1926) by the Austrian physicist Erwin Schrödinger, has the same central importance to quantum mechanics as Newton's laws of motion have for the large-scale phenomena of classical mechanics, it predicts the future behavior of a dynamic system. It is a wave equation in terms of the wave function which predicts analytically and precisely the probability of events or outcome. Schrödinger's equation can be separated into two equations, one for time $\hat{H}\,\Psi\big(\vec{r},\vec{R},t\big) = i\frac{\partial\,\Psi(\vec{r},\vec{R},t)}{\partial t}$ and another for space $\hat{H}\,\Psi\,(\vec{r},\vec{R}) = E\Psi\,(\vec{r},\vec{R})$.

Let's assume a system made up of N atomic nuclei (of mass M_I and atomic number Z_I) in mutual interaction, and of Ne electrons (of spin σ_i, mass m_e and electric charge e) positioned at $\vec{R} = (\vec{R_I}; I = 1, \ldots \ldots, N)$ and at $\vec{r} = \{(\vec{r_i}, \sigma_i); i = 1, \ldots, Ne)\}$, respectively, gravitating around these, uses the Schrödinger equation [2].

$$\hat{H}\,\Psi{=}\hat{E}\,\Psi \tag{II.1}$$

The total Hamiltonian corresponding to such a system is expressed in the following exact form:

$$\hat{H} = \hat{V}_{NN} + \hat{T}_N + \hat{V}_{eN} + \hat{V}_{ee} + \hat{T}_e \tag{II.2}$$

In which the terms correspond respectively

$\hat{T}_N = \Sigma_I\,\hat{T}_I = \Sigma_I\left(-\frac{\hbar^2}{2M_I}\Delta_I\right)$: The kinetic energy of the nuclei.

$\hat{T}_e = \Sigma_i\,\hat{T}_i = \Sigma_i\left(-\frac{\hbar^2}{2m_e}\Delta_i\right)$: The kinetic energy of the electrons.

$\hat{V}_{eN} = -\frac{1}{2}\,\Sigma_{i,I}\frac{Z_Ie^2}{4\pi\,\varepsilon_0\,\|\vec{r_i}-\vec{R_I}\|}$: The potential energy of attraction nuclei-electrons.

$\widehat{V}_e = \frac{1}{2} \sum_{i,i \neq j} \frac{e^2}{4\pi \, \varepsilon_0 \, \|\vec{r_i} - \vec{r_j}\|}$: The potential energy of repulsion between the electrons.

$\widehat{V}_{NN} = \frac{1}{2} \sum_{I \neq J} \frac{Z_i Z_j e^2}{4\pi \, \varepsilon_0 \, |\vec{R_I} - \vec{R_J}|}$: The potential energy of interaction between the nuclei.

So, Schrodinger's equation is written:

$$\left(\sum_I \left(-\frac{\hbar^2}{2M_I} \Delta_I \right) + \sum_i \left(-\frac{\hbar^2}{2m} \Delta_i \right) + \widehat{V}_{eN} + \widehat{V}_{ee} + \widehat{V}_{NN} \right) \Psi\left(\vec{r}, \vec{R} \right) = E\Psi\left(\vec{r}, \vec{R} \right) \qquad (II.3)$$

The search for solutions to this macroscopic system (energy and wave functions) is called a multi-body (or N-body) problem.

The Schrödinger equation can be solved with accuracy for simple single electron systems such as hydrogen. In last form, the Schrödinger equation (II.3) is too complex to be solved analytically because the complexity of the solution increases with the increasing number of particles in the system, so, the challenge is to introduce judicious approximations in order to achieve satisfactory and realistic results.

The rest of this paragraph will therefore aim to present the reasonable approximations allowing the resolution of this problem.

II.3.1 Born-Oppenheimer Approximation (adiabatic):

It is based on the principle of separation of nuclear and electronic movements in a molecule. Max Born (1882-1970) and Robert Oppenheimer (1904-1967) proposed an approximation to simplify the resolution of Schrödinger's equation [3].

The Born-Oppenheimer approximation plays a vital role in electronic structure calculations. It consists in decoupling the movement of a proton compared to that of the electrons, which is justified by the fact that the mass of a proton is approximately 1836 times larger than the mass of an electron. It is the minimum mass ratio of electron to nucleus (hydrogen atom) and becomes even higher for heavier atoms, another simplification can be introduced. The so called Born-Oppenheimer approximation states that due to the mass difference the nucleus can be, in comparison to the electrons, considered nonmoving, i.e. spatially fixed ($\widehat{V}_{NN} = cst$). It can be said that the motion of the nucleus can be neglected on the time scale of

electronic transitions, which means that the motion of the nucleus has no influence on them [4].

It can be simplified, since the kinetic energy of the nuclei becomes zero ($\hat{T}_N = 0$), the interaction energy of the nuclei becomes constant ($\hat{V}_{NN} = $ cst), but we can take it as the origin of the energies ($\hat{V}_{NN} = 0$).As a consequence, the general Hamiltonian is replaced by the so-called electronic Hamiltonian:

$$\widehat{H_e} = \sum_i \left(-\frac{\hbar^2}{2m} \nabla^2_i \right) - \frac{1}{2} \sum_{i,I} \frac{Z_I e^2}{4\pi\,\varepsilon_0\,\|\vec{r_i}-\vec{R_I}\|} + \frac{1}{2} \sum_{i,i\neq j} \frac{e^2}{4\pi\,\varepsilon_0\|\vec{r_i}-\vec{r_j}\|} \tag{II.4}$$

Schrödinger's equation is therefore rewritten as follows:

$$\widehat{H_e}\,\Psi_e = E_e\,\Psi_e \tag{II.5}$$

With Ψ_e and E_e: the eigenstate and the eigenenergy of the N_e electrons system. The total energy of the system is then given by: $\boldsymbol{E_{TOTALE} = E_e + E_n}$.

So the total wave function $\Psi\,(\vec{r},\vec{R})$ of the system can be described as the product of 2 wave functions because we have 2 independent systems.

$$\Psi\,(\vec{r},\vec{R}) = \Psi_n(\vec{R})\,\Psi_e(\vec{r}) \tag{II.6}$$

$\Psi_e(\vec{r})$: Wave function describing the electrons.

$\Psi_n(\vec{R})$: Wave function describing the nuclei.

The electronic wave function describes the movement of electrons in the field of nuclei.

Although the problem is greatly simplified, the exact resolution of (II.4) is still impossible. However, it is possible to access the fundamental state of the system, the associated energy responding to a variational principle. Indeed the fundamental state of the N_e electrons system is by definition the state which minimizes the energy E_e. It is in the search for minimum energy that the ab-initio techniques will intervene.

The difficulties in solving $\widehat{H_e}\,\Psi_e = E_e\,\Psi_e$ lies in the electron-electron interaction, $V(\vec{r_{i,j}})$, which includes all the quantum effects of the electrons. Despite the intractable nature of these interactions, many approximate methods have been developed to solve Schrodinger-like equations.

II.3.2 Hartree approximation (free electrons):

One of the first and most simple approximations aimed to solve the problem posed in the previous section is due to Douglas Hartree in 1927. In this approximation, Hartree [5, 6] Consists that the electrons move independently of each other, their movement is correlated. Thus, if we consider two electrons 1 and 2, the probability of the presence of the electron of coordinate's $\vec{r_1}$ in the orbital 1 is independent of that of the electron of coordinate's $\vec{r_2}$. Thus, the Hamiltonian can be put in the following form:

$$H_e = \sum H_i \tag{II.7}$$

$$H_i = -\frac{\hbar^2}{2m}\Delta_i + V_{ext}(\vec{r}) + V_i(\vec{r_i}) \tag{II.8}$$

Where:

$V_{ext}(\vec{r}) = -\sum_I \frac{Z_I e^2}{4\pi\,\varepsilon_0\,\|\overrightarrow{r_i}-\overrightarrow{R_I}\|}$: is the potential energy of the electron in the field of all the nuclei (I).

R_I: The fixed position of nuclei (I).

$V_i(r_i) = \frac{1}{2}\sum_j \frac{e^2}{4\pi\,\varepsilon_0\,\|\overrightarrow{r_i}-\overrightarrow{r_j}\|}$: is the effective field of Hartree.

The total wave function is constrained to be a product (typically referred to as Hartree product [7]) of N one-electron orbitals (monoelectronic functions [5].)

$$\Psi_e(\boldsymbol{r_1}, \dots .\boldsymbol{r_N}) = \prod_{i=1}^{N}\varphi_i(\boldsymbol{r_i}) \tag{II.9}$$

Hartree's field reduces the multiple equations to a single electron equation system:

$$\left[-\frac{\hbar^2}{2m}\Delta_i + V_{ext}(\vec{r}) + V_i(\vec{r_i})\right]\varphi_i(\vec{r}) = \varepsilon_i\varphi_i(\vec{r}) \tag{II.10}$$

This approximation is based on the free electron hypothesis which does not take into account the interactions between electrons and spin states up or down. To remedy this problem, other approximations have been made.

II.3.3 Hartree - Fock approximation

Unfortunately, the Hartree product does not satisfy all the important criteria for wave functions. Because the Hartree theory lacks an ingredient that turns out to be essential to correctly describe the behavior of molecular species: the indisernability of the electrons .as long as the electrons are fermions, the wave function must change sign if two electrons change places with each other, which is known as the Pauli Exclusion Principle. One of its usual formulations, equivalent to the one proposed originally by Wolfgang Pauli in 1925 [8], is the following:

$$\Psi(\vec{r_1};\vec{r_2}) = -\Psi(\vec{r_2};\vec{r_1}) \qquad (II.11)$$

Pauli's Exclusion Principle—No two electrons can share the same quantum [9]numbers (antisymmetric).

This is a property that is certainly not met by the Hartree product, which is a serious drawback. This was noticed independently by Fock [10] and Slater [11] in 1930, and it was corrected by proposing a variational principle for the total wave function that takes the form of a so-called Slater determinant.

Slater Determinants:

$$\Psi^S (\vec{r_1};\vec{r_2} \ \dots\dots \ ;\vec{r_N}) = \frac{1}{\sqrt{N!}} \begin{pmatrix} \varphi_1(\vec{r_1}) & \varphi_2(\vec{r_1}) & \dots\dots\dots\dots & \varphi_N(\vec{r_1}) \\ \varphi_1(\vec{r_2}) & \varphi_2(\vec{r_2}) & \dots\dots\dots\dots & \varphi_N(\vec{r_2}) \\ \vdots & \vdots & & \ddots \\ . & . & & . \\ \varphi_i(\vec{r_N}) & \varphi_j(\vec{r_N}) & \dots\dots\dots\dots & \varphi_N(\vec{r_N}) \end{pmatrix} \qquad (II.12)$$

The Hartree and Hartree-Fock approximation are the most used in quantum chemistry for the study of atoms and molecules, and they can give very good results, compared to those of the experiment; but for solids, they are less accurate [12]. However there is a modern and certainly more powerful method which is the Density Functional Theory.

In the next section, we will show the main foundations of this theory, the approximations related to it and its implementation in a numerical code.

II.4 Density Functional Theory (DFT):

Density functional theory was established in 1964 by Hohenberg-Kohn [13] and Kohn-Sham [14]. It is a reformulation of Schrödinger's equation for the problem of N interacting electrons, to give in principle an exact ground state solution of this equation.

The main idea of DFT is to describe a system of interacting electrons at through its density and not through the wave function of each electron.

In the DFT, the states of the N electrons of the system are determined by applying the variational principle to a functional, i.e. a function of another function, the first being the total energy and the second the electron density $\rho(\vec{r})$. The total energy must be a unique functional of the density, and this energy is minimal for the density of the ground state, the latter remaining unknown, one must resort to various approximations.

Nowadays, the DFT remains the most used method in the calculations of the electronic structure; it owes its success to the approach proposed by Kohn and Sham (KS).

II.4.1 Theorems of Hohenberg and Kohn:

The objective of DFT is to determine, using only knowledge of the electron density, the properties of the ground state of a system composed of a fixed number of electrons in Coulomb interaction with point nuclei. It is based on two theorems attributed to Hohenberg and Kohn [13]:

➢ <u>First theorem:</u> *For an interacting electron system, the external potential $V_{ext}\,(\vec{r})$ is determined uniquely, by the ground state electron density $\rho(\vec{r})$ and all properties of the system are determined as a function of $\rho(\vec{r})$. Therefore, the total energy of the ground-state system is also a unique functional of the electron density, that is:* $E = E\,[\rho]$
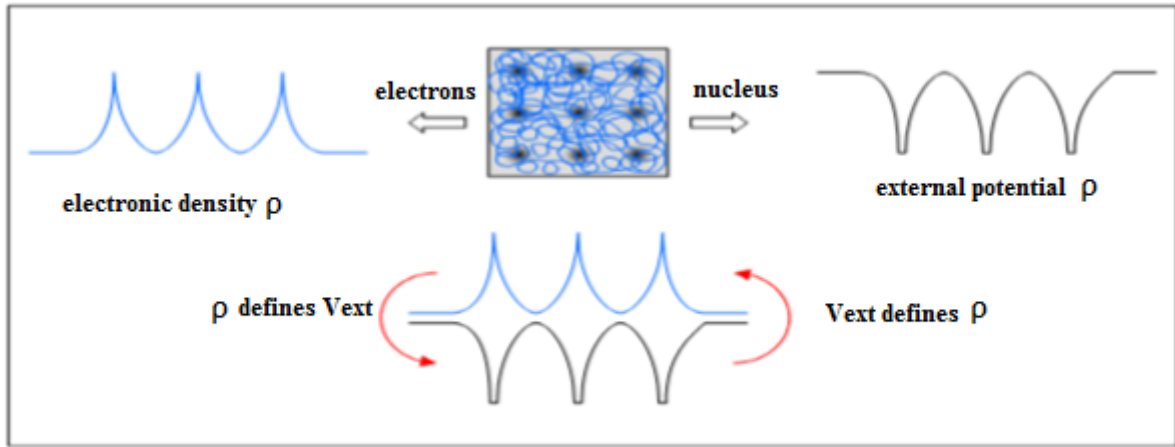
Figure II.1: First kohn and Hohenberg theorem.

➢ Second theorem: *The total ground state energy is minimal for a ground state density with respect to all densities leading to the correct number of electrons.*

$$E[\rho_0] = min\ [E(\rho)] \tag{II.13}$$

The functional of the total energy of the ground state is written as follows:

$$E[\rho(\vec{r})] = \langle\Psi|\hat{T} + \hat{V}_{ee}|\Psi\rangle + \langle\Psi|\hat{V}_{ext}|\Psi\rangle \tag{II.14}$$

$$E[\rho(\vec{r})] = F_{HK}[\rho] + \int \rho(\vec{r})\,V_{ext}(\vec{r})\,d\vec{r} \tag{II.15}$$

Where:

$$F_{HK}[\rho] = T[\rho] + V_{ee}[\rho] \tag{II.16}$$

$F_{HK}[\rho]$: The Hohenberg and Kohn functional.

$T[\rho]$: The kinetic energy.

$V_{ee}[\rho]$: The interaction between the electrons.

Where the Hohenberg-Kohn density functional $F_{HK}[\rho]$ is universal for any many-electron system. $E[\rho(\vec{r})]$ reaches its minimal value (equal to the ground state total energy) for the ground state density corresponding to V_{ext}.

Note: The theorems of Hohenberg and Kohn were stated for non-polarized systems in spin, but their extension to systems polarized in spin is immediate: E and the properties of the ground state become functional of the two densities of spin down and spin up :

$$E = E\left[\rho_\uparrow, \rho_\downarrow\right] \tag{II.17}$$

The work of Hohenberg and Kohn made it possible to reformulate the problem concerning the resolution of the Schrödinger equation; however $F_{HK}[\rho]$ remains impossible to calculate because of the complexity of the N-electron system. This difficulty was overcome by Kohn and Sham.

II.4.2 Kohn-Sham equations:

The last problem left by the Hohenberg-Kohn theorems was solved a year after the publication of their work by Lu Jeu Sham and Walter Kohn in 1964 [14]. The resolution of F_{HK} [ρ] was accomplished by replacing the problem of N interacting electrons with each other subjected to the real potential, into a problem with N independent fictive particles having the same electronic density ρ (r) and bathing in an effective potential VS.

The energy functional can be expressed by the following expression:

$$E\left[\rho(\vec{r})\right] = T_0[\rho(\vec{r})] + E_H[\rho(\vec{r})] + E_{xc}[\rho(\vec{r})] + \int V_{ext}\,(\vec{r})\rho(\vec{r})\,\mathrm{d}^3\vec{r} \tag{II.18}$$

Where:

$T_0[\rho(\vec{r})]$: The kinetic energy of the electron gas without interaction.

$E_H[\rho(\vec{r})]$: The Coulomb energy of electron-electron interaction (also appearing in classical mechanics and described by the Hartree energy).

$E_{xc}[\rho(\vec{r})]$: The energy of exchange-correlation which is an additional functional describing the inter-electronic interaction.

$V_{ext}\,(\vec{r})\rho(\vec{r})$: includes the Coulomb interaction of electrons with nuclei.

So the equation of Schrödinger's transforms into Mono-electronic equations of Schrödinger commonly called Kohn-Sham equations:

$$\left(-\frac{\hbar^2}{2m}\nabla^2 + V_{eff}\,(\vec{r})\right)\varphi_i(\vec{r}) = \varepsilon_i\,\varphi_i(\vec{r}) \tag{II.19}$$

Where the effective potential is defined by:

$$V_{eff} = V_{ext} + V_H + V_{xc} \qquad (II.20)$$

With:

$$V_H = e^2 \int \frac{\rho(\vec{r'})}{|\vec{r}-\vec{r'}|} \, \overrightarrow{dr'} \quad : \text{Hartree potential.}$$

$$V_{xc}(\vec{r}) = \frac{\delta E_{xc}\,[\rho(\vec{r})]}{\delta\rho(\vec{r})} \quad : \text{Exchange–correlation potential.}$$

The exact ground state density $\rho(\vec{r})$ of an N-electron system is:

$$\rho(\vec{r}) = \sum_{i=1}^{N}|\varphi_i(\vec{r})|^2 \qquad (II.21)$$

For the spin-dependent system, the total density is just divided into the sum of both density spins:

$$\rho(r) = \rho(r,\uparrow) + \rho(r,\downarrow) \qquad (II.22)$$

With each spin-density state being the sum of the particles wave-functions with the spin established by the density spin state:

$$\rho(r,\uparrow) = \sum_i^N|\Psi_i(r,\uparrow)|^2 \qquad\qquad \rho(r,\uparrow) = \sum_i^N|\Psi_i(r,\downarrow)|^2 \qquad (II.23)$$

With the Kohn-Sham equations well defined and giving an exact solution, we still have a problem: the exact form of the exchange-correlation energy is not known, which remains a real challenge today, and the only solution is to find an approximation that gives an accurate result.
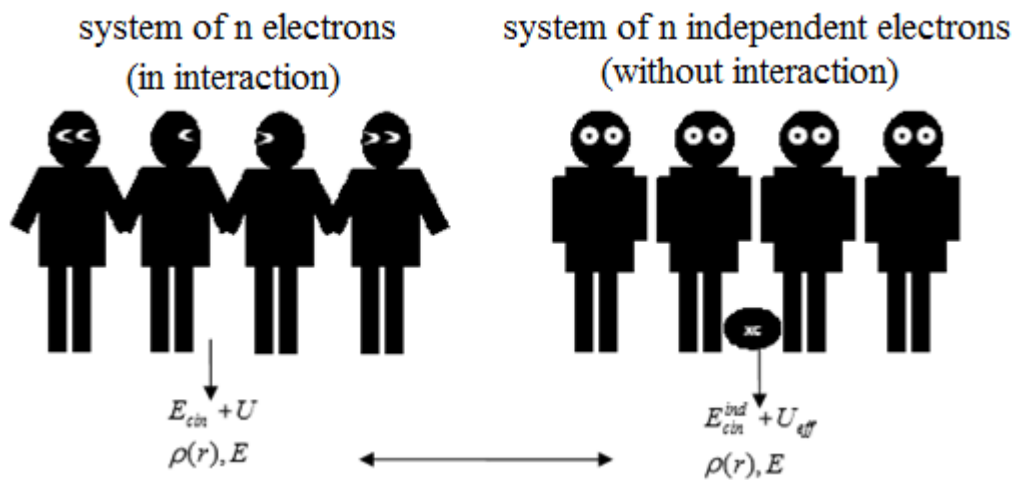
Figure II.2: comparison diagram between a real system and the kohn -sham approach [15].

II.5 Exchange-correlation functionals (XC):

The Kohn-Sham equation can be solved if the exchange-correlation functional is known. Given the fact that an exact expression is not available, the introduction of an approximation is needed. Two such often used approximations are LDA (Local Density Approximation "LSDA/LDA/LDS") and GGA (Generalized Gradient Approximation).

To find an expression for the E_{XC} term, various correlation exchange functionals have been developed by researchers: Local Density Approximation (LDA), Generalized Gradient Approximation (GGA) and (Meta-GGA) functionals such as the so-called Tran-Blaha modified Becke-Johnson potential (TB − mBJ) and the more expensive calculation cost hybrid functionals.

II.5.1 Local density approximation (LDA):

In order to obtain an approximation of the exchange-correlation functional $E_{xc}[\rho(\vec{r})]$, Kohn and Sham proposed as early as 1965 the local density approximation (LDA) (The oldest and simplest approximation for the exchange-correlation).

The underlying idea is very simple. At each point in space the exchange-correlation energy is approximated locally by the exchange-correlation energy of a homogeneous electron gas with the same electron density as present at that point. In other words, it is based on the assumption that the terms of exchange-correlation depend only on the local value of $\rho(\vec{r})$, that is to say that it treats a non homogeneous system as being locally homogeneous. The exchange-correlation energy is then expressed as follows [16]:

$$E_{xc}^{LDA} = \int \boldsymbol{\rho}(\vec{r}) \varepsilon_{xc}^{LDA}[\boldsymbol{\rho}(r)] \, \boldsymbol{d^3\vec{r}} \tag{II.24}$$

Here, the term ε_{xc}^{LDA} is the electron exchange and correlation energy in an electron gas whose distribution is assumed to be uniform. Explicitly, the quantity ε_{xc} can be separated in two terms, exchange energy ε_x and correlation energy ε_c.

$$\varepsilon_{xc}(\boldsymbol{\rho}(\vec{r})) = \varepsilon_x(\boldsymbol{\rho}(\vec{r})) + \varepsilon_c(\boldsymbol{\rho}(\vec{r})) \tag{II.25}$$

The exchange part, E_x^{LDA} , was originally derived by Bloch and Dirac [17] in the late 1920's $\varepsilon_x = -\frac{3}{4}(\frac{3\rho(\vec{r})}{\pi})^{\frac{1}{3}}$ [18].

Ceperley and Alder [19] calculated numerically the correlation energy ε_c using the quantum Monte-Carlo method(QMC), then Perdew and Zunger [20] fitted the numerical data to analytical expressions.

There are thus many parameterizations for correlation energy such as, for example, that of Hedin Lundqvist [21], that of Wigner [22], or that of Vosko-Wilkes-Nusair [23].

In spite of its simplicity, LDA performs quite well even for more realistic systems.

II.5.2 Local Spin Density Approximation (LSDA):

The local density approximation has been generalized by Kohn and Sham when the spin polarization is considered as for magnetic systems (those with incomplete shells d, f).The new one is called the local spin-density approximation (LSDA) [24], where the energy of exchange and correlation becomes a functional of the two densities of (spin-up) and (spin-down):

$$E_x^{LDA}[\rho^{\uparrow},\rho^{\downarrow}] = \int d^3\vec{r}\,\boldsymbol{\rho}(\vec{r})\left[\varepsilon_x^{hom}(\rho^{\uparrow}(\vec{r}),\rho^{\downarrow}(\vec{r}) + \varepsilon_c^{hom}(\rho^{\uparrow}(\vec{r}),\rho^{\downarrow}(\vec{r}))\right] \qquad (II.26)$$

The LSDA is an ab-initio approximation. By construction, it is exact for systems with homogeneous electronic distribution and a good approximation for those where the variation in electronic density is sufficiently slow (itinerant electronic systems).

However, it has been shown on several application examples since its implementation in different calculation methods, that the *LSDA* gives sufficiently reliable results for systems where the electron density does not vary very slowly, hence its enormous success [25].

I.5.3 Generalized Gradient Approximation (GGA):

These are the second generation functionals (sitting on the second rung of Jacob's ladder) [26].

the local density approximation (LDA) used in the DFT calculations is increasingly replaced by the methods known as GGA ("Generalized Gradient Approximation"), sometimes also called non-local methods. This approximation was

developed in order to improve the quality of the LDA results [17, 27] and to remedy certain anomalies obtained by the LDA in certain cases, where there was a contradiction with the experimental results. Most of the corrections that have been made to the LDA are based on the idea of accounting for variations in density by expressing the exchange and correlation energies as a function of the density but also of its gradient ($\vec{\nabla}\rho$) and thus correcting the defects of the LDA. The expression exchange-correlation is written in its general form:

$$E_{xc}^{GGA}[\rho;\vec{\nabla}\rho] = \int \varepsilon_{xc}^{GGA}(\rho(r),\vec{\nabla}\rho(r))\mathrm{d}^3\mathrm{r} \qquad (\text{II.27})$$

Where: $\varepsilon_{xc}^{GGA}(\rho(r),\vec{\nabla}\rho(r))$ represents the exchange-correlation energy per electron in a simultaneously interacting electron system of inhomogeneous density.

The GGA is given by different parameterizations, we can quote among others that of Perdew and Wang (1992) [28], and Perdew et al (1996) [27].

Series of tests on different systems have shown promising results.

In particular, there are several versions of GGA: WC (Wu-Cohen) [29] and EV (Engel Vosko) [30], Different approximations have been derived from equation (17) give rise to the GGAs functionals family. Among them, we cite Perdew, Burke and Ernzerhof (PBE) [27]; Becke (B88) [31]; Perdew (PW86) [32]; Handy and Cohen (OPTX) [33] and the functional of Yang Parr (BLYP) [34]. The most currently used in solid state physics is the PBE functional from Perdew, Burke and Ernzerhof [27]. These non-empirical methods are simple and precise. Indeed, compared to the LDA, the GGA increases the precision and improves the cell parameters of the crystals and the cohesion energies. On the other hand, the improvement is not always systematic. The GGA fails to deal well with systems characterized by Vander Walls interactions, involving long-term correlations.

Note:

It should be noted that the GGA approximation does not necessarily lead to more reliable results than the LDA, depending on the properties that are calculated and the system that is treated.

II.5.4 Meta-GGAs:

GGA methods allow an improvement of results compared to a local approach. However, the GGA approach is not always sufficient for a correct description of various chemical properties of the compounds. This is why, from the mid-1990s, new functionals were proposed to improve the results provided by the GGA methods. At This next level the density functionals so-called meta-GGAs [35-37](or m-GGA) include not only the gradient of the density, but also the second derivatives of the density. These functionals allow an improvement in the determination of the molecular properties but present some numerical stability problems. As an example of the m-GGA functional, we can cite the correlation functional B95 developed by Becke [38].

II.5.5 Modified Becke and Johnson potential TB-mBJ:

Among the meta-GGA functionals the modified Becke and Johnson potential TB-mBJ developed by Tran and Blaha [39], is a new version of the Becke and Johnson potential BJ [40] which can be further improve the BJ potential for the description of band gaps.

Tran and Blaha tested the potential of exchange proposed by Becke and Johnson (BJ) [39] designed for reproducing the shape of the exact exchange potential, i.e. the optimized effective potential (PEO) [41].They observed that the BJ potential combined with the correlation potential of the LDA always gives underestimated gap energies.

In order to improve these results, Tran and Blaha introduced a simple modification of the original BJ potential and obtained a good agreement with other more expensive approaches (because of their high self-consistency) such as the hybrid functional [42, 43] and the GW method [44-46].

The modified Becke-Johnson potential (TB-mBJ) proposed by Tran and Blaha takes the following form:

$$V_{x,\sigma}^{TB-mBJ}(r) = cV_{x,\sigma}^{BR}(r) + \frac{(3c-2)1}{\pi}\sqrt{\frac{5}{6}}\sqrt{\frac{t_\sigma(r)}{\rho_\sigma(r)}} \qquad \text{(II.28)}$$

With:

$\rho_\sigma(r) = \sum_{i=1}^{n_\sigma} \left| \psi_{i,\sigma}(r) \right|^2$: is the electron density.

$t_\sigma(r) = \frac{1}{2} \sum_{i=1}^{n_\sigma} \nabla \Psi_{i,\sigma}^*(r) \nabla \Psi_{i,\sigma}(r)$: is the kinetic energy density.

$V_{x,\sigma}^{BR}(r)$: is the potential of Becke-Roussel.

The Becke-Roussel potential [47] proposed here is roughly equivalent to the Slater potential used by Becke and Johnson for the case of atoms that they are almost identical.

II.6 Solving Kohn-Sham equations: (Self-consistency of charge density).

To solve the Kohn-Sham equation, the equations (II.18) must be solved in a self-coherent way, i.e. by starting from a certain initial density, a potential is obtained for which the equation (II.19) is solved and a new electronic density is then determined. From this new density, a new effective potential can be calculated. This process is repeated in a self-consistent manner until convergence is reached, i.e. until the new electronic density is equal to or very close to the previous one (corresponding to the fixed convergence criterion).
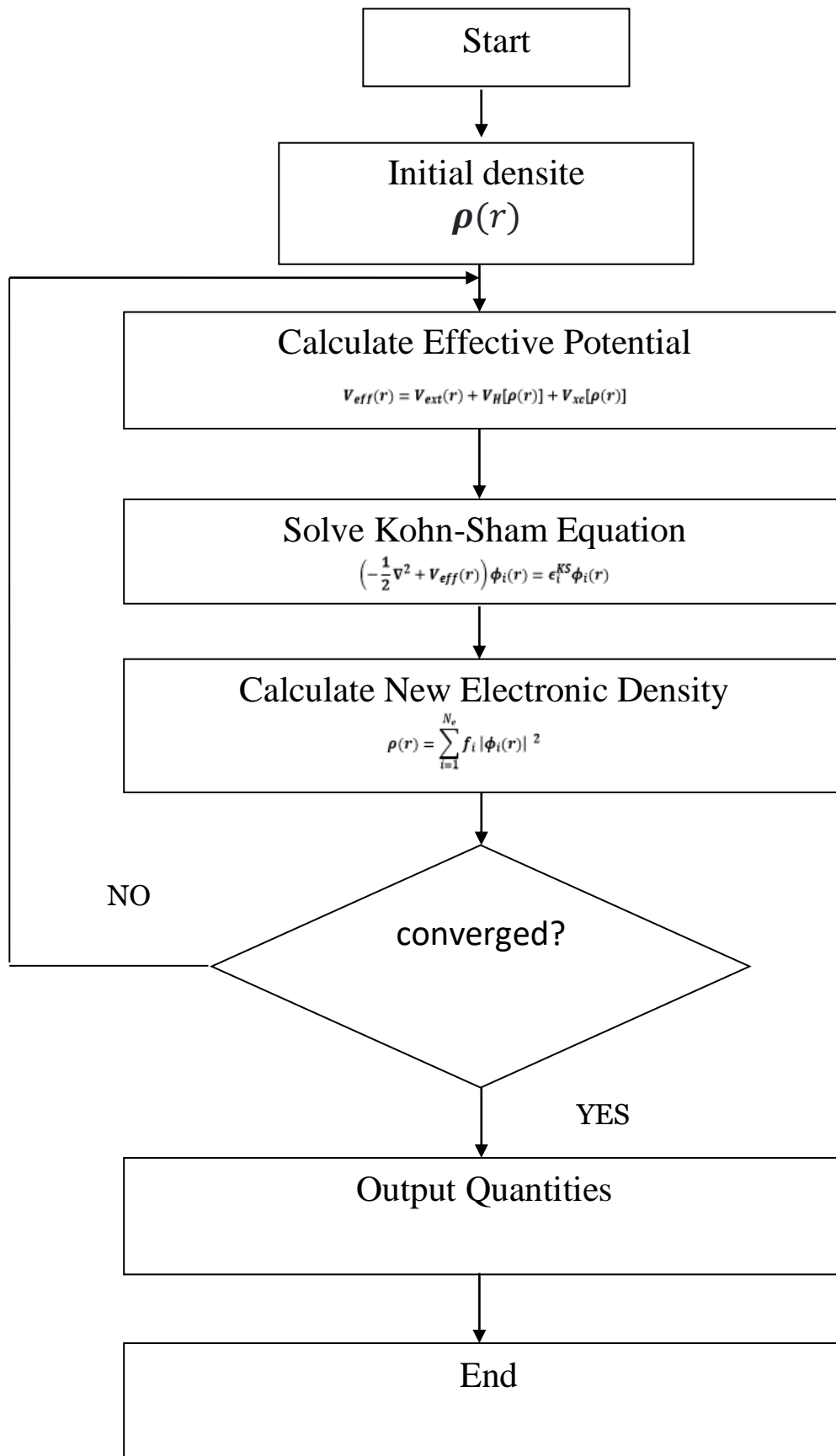
Figure II.3: Flowchart of the self-coherent cycle of the Functional Density Theory.

II.7. Full-potential linearized augmented plane wave

In order to predict the electronic properties of materials, various methods have been used, ranging from classical methods to approaches to quantum mechanics. Thus several calculation methods have emerged, these methods are classified into three categories according to the data used (experimental results or fundamental data), namely:

- Empirical methods for which calculations require experimental results.

-Semi-empirical methods for which calculations require both experimental results and fundamental data.

-The ab-initio methods for which the calculations require only the fundamental data.

There are several methods of calculating the properties of solids, and their common point is to solve the Kohn and Sham equations in a self-consistent manner. The latter is the origin of several numerical methods used in the first principles calculation. Among them, the Full Potential Linearized Augmented Plane Wave method (FP-LAPW) saves several orders of magnitude over the calculation time.

II.7.1 Augmented plane wave method (APW):

In 1937, Slater [48, 49]introduced augmented plane waves (APW) as basic functions for solving the Schrödinger equation with a single electron, the latter corresponds to the equation of Kohn and Sham based on the DFT (this method is detailed even more in Loucks' book [50]). In the APW scheme the unit cell is divided into two regions: (i) Muffin-tin regions (MT): spheres centered on each constituent atomic site r_α with a radius R_α, and (ii) the remaining interstitial region, abbreviated as I presented in **Figure II.4**. In this case the wave functions are expanded into PWs each of which is augmented by atomic solutions in the form of partial waves, i.e. a radial function time's spherical harmonics. In particular, radial solutions of Schrödinger's equation are employed inside non overlapping atom centered spheres and plane waves in the remaining interstitial zone.
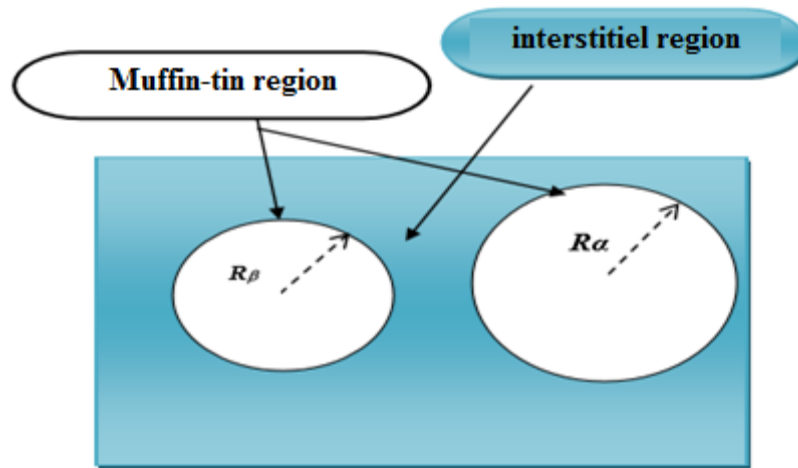
Figure II.4: Adaptation of the basis set by dividing the unit cell into atomic spheres and interstitial regions.

The introduction of such a basis set is due to the fact that close to the nuclei the potential and wave functions are very similar to those in an atom, while between the atoms then are smoother. The APWs consist of:

$$\phi(\vec{r}) = \begin{cases} \varphi_i(\vec{r}) = \frac{1}{\Omega^{\frac{1}{2}}}\sum_G C_G\, e^{i(\vec{k}+\vec{G})\vec{r}} & r > r_0 \ (I) \\ \varphi_s(\vec{r}) = \sum_{lm} A_{lm} U_l^\alpha(r, E_l) Y_{lm}(\hat{\vec{r}}) & r < r_0 \ (MT) \end{cases} \qquad (II.29)$$

r_0 : Represents the radius of the muffin-tin sphere.

r: The length of $\vec{r}$.

$\hat{\vec{r}}$: The angles θ and ϕ specifying the direction of $\vec{r}$ in spherical coordinates.

Ω: The volume of the elementary cell.

G: is the vector of the reciprocal space.

C_G, A_{lm} : The coefficients of development in spherical harmonics $Y_{lm}(\hat{\vec{r}})$

$\vec{k}$: is the wave vector in the irreducible Brillouin zone (IBZ).

Note that the origin of the spherical coordinates is taken from the centers of the atomic spheres.

The function $(U_l^\alpha(r))$ is a regular solution of Schrödinger's equation for the radial part which is written in the form:

$$\left\{-\frac{d^2}{dr^2} + \frac{l(l+1)}{r^2} + V(r) - E_{nl}\right\} r\, U_l^\alpha(r) = 0 \qquad (II.30)$$

E_{nl}: is the linearization energy and V (r) is the spherical component of the potential in the sphere.

The radial functions defined by equation (II.30) are orthogonal to any core eigenstate. This orthogonality disappears at the boundary of the sphere [50] as shown by the following Schrödinger equation:

$$(E_2 - E_1)r U_1 U_2 = U_2 \frac{d^2 r U_1}{dr^2} - U_1 \frac{d^2 r U_2}{dr^2} \qquad (II.31)$$

Where U_1 and U_2 are the radial solutions for the energies E_1 and E_2. The overlap is constructed using equation (II.31) and integrated by parts.

Slater justifies the particular choice of these functions by noting that:

✓ The plane waves are solutions of the Schrödinger equation when the potential is constant.

✓ The radial functions are solutions in the case of a spherical potential, when E is an eigenvalue.

This approximation is very good for the materials with cfc structure, and less satisfactory with the decrease of the symmetry.

To ensure continuity of the function φ (r) on the surface of the muffin-tin sphere, the A_{lm} coefficients must be developed according to the C_G coefficients of plane waves existing in the interstitial regions. These coefficients are given by the following relation:

$$A_{lm} = \frac{4\pi i^l}{\Omega^{\frac{1}{2}} U_l(R_\alpha)} \Sigma_G\, C_G\, j_l\,(|K + g|R_\alpha) Y_{ml}^*(\overrightarrow{K + G}) \qquad (II.32)$$

j$_l$ is the Bessel function given by: $j_l = \sqrt{\frac{\pi}{2x}}\, J_{j+\frac{1}{2}}(x)$

The APW method thus constructed represents some calculation difficulties, including those related to the function $U_l^{\alpha}(r)$ which appears in the denominator of the equation (II.32). It is therefore possible to find values of the energy for which the value $U_l^{\alpha}(r)$ vanishes at the limit of the sphere. This is called the asymptote problem. The calculations become more complicated when the bands appear near the asymptote. Therefore, in order to overcome this problem, several modifications to the APW method have been made, notably those proposed by Koelling [51]and by Andersen [52].

II.7.2 Linearized augmented plane wave method (LAPW) (Andersen-1975):

The linearized augmented plane wave (LAPW) method is developed by Andersen [52]; basically, it is an improvement of the (APW) method.

In the Linearized augmented plane wave (LAPW) method, the basic functions inside the "Muffin-tin" sphere are a linear combination of the radial functions $U_l(r)y_{lm}(\hat{\vec{r}})$ and their derivatives $\dot{U}_l(r)y_{lm}(\hat{\vec{r}})$ with respect to energy. The basic functions are given by:

$$\phi(\vec{r}) = \begin{cases} \varphi_i(\vec{r}) = \frac{1}{\Omega^{\frac{1}{2}}}\sum_G C_G \, e^{i(\vec{k}+\vec{G})\vec{r}} & r > R \\ \varphi_s(\vec{r}) = \sum_{lm}[A_{lm}U_l(r,E_0) + B_{lm}\dot{U}_l(r,E_0)]Y_{lm}(\hat{\vec{r}}) & r < R \end{cases} \quad \text{(II.33)}$$

The functions U_l are defined as in the method (APW) and the function $U_l(\vec{r})y_{lm}(\hat{\vec{r}})$ must satisfy the following condition:

$$\left\{-\frac{d^2}{dr^2} + \frac{l(l+1)}{r^2} + V(r) - E_l\right\}r\dot{U}_l(r) = rU_l(r) \quad \text{(II.34)}$$

$$\dot{U}_l(r,E_0) = \frac{\partial U_l(r)}{\partial E} \quad \text{(II.35)}$$

- In the interstitial zone, the basic functions are plane waves as in the APW method, while in the MT spheres, the basic functions depend not only on U_l but also on $\dot{U}_l$ It is very clear that the LAPW method is therefore more flexible than the APW method. In the MT spheres, the coefficients B_{lm} are of the same nature as A_{lm}.

- When E_l differs slightly from the band energy E, a linear combination is used to better represent the radial function $U_l(r)$:

$$U_l(r, E) = U_l(r, E_l) + (E - E_l)\dot{U}_l(r, E_l) + O((E - E_l)^2) \qquad \text{(II.36)}$$

- Note that, compared to the APW method, the errors on the wave functions and on the band energy are respectively of the order of $(E - E_l)^2$ and $(E - E_l)^4$.

- The asymptote problem is definitively eliminated since, even if U_l is equal to zero on the surface of the sphere, $\dot{U}_l$ will be different from zero.

II.7.3 Advantages of the LAPW method compared to the APW method:

If we want to make a comparison between the two methods APW and LAPW we can mention the following points:

- In the LAPW method, the energies of the bands, at the given K-point, are obtained precisely with a single diagonalization. Whereas in the APW, it is necessary to calculate the energy for each band.

- In the APW method, the asymptote problem is solved by adding the derivative of the radial function which ensures that the plane waves are not decoupled from the radial functions.

- The basic functions of the LAPW method have a great flexibility inside the spheres, which presents a consequence of the variational freedom, on the other hand in the APW method, the energy parameter must be fixed instead of being variational.

- In the LAPW method, the computation time is considerably reduced so convergence is quickly reached.

Note:

Recall that, the core electrons, entirely localized in the MT sphere, are called core states. The other type of electrons, are the valence electrons and found outside the MT sphere which can be bound to other atoms.

However, for many elements, electrons cannot be clearly distinguished like that. Some states are not contained in the core states, nor are they in the valence states and are, therefore called semi-core states, they have the same angular quantum number l as the valence states but their principal quantum number n is less. It is therefore difficult to use an energy E_l to determine the states having the same value of l. This dilemma is resolved by introducing local orbitals (LO).

II.7.4 Development in local orbitals (LO):

In this technique, all energy states are treated with a single energy window. Takeda [53], Smrčka [54], Petrů [55], Shaughnessy [56] and Singh [57] propose a linear combination of two radial functions. The derivatives of these functions with respect to energy are equal, but the corresponding linearization energies are different.

I.7.4.1 APW+ lo Method:

The problem with the APW method was the energy dependence of the set of basic functions. This dependency could be eliminated in the LAPW + LO method, at the cost of a larger set of basic functions.

Recently, an alternative approach is proposed by Sjösted et al [58] called the APW + lo method. In this method, the set of basic functions will be energy independent and always the same size as that of the APW method. In this sense, APW + lo combines the advantages of the APW method and those of the LAPW + LO method.

The basic set of functions of APW + lo contains both types of wave functions. The first are augmented plane waves APW, with a set of fixed energies E_l:

$$\phi(\vec{r}) = \begin{cases} \frac{1}{\Omega^{\frac{1}{2}}} \sum_G C_G \, e^{i(\vec{k}+\vec{G})\vec{r}} & r > R_\alpha \\ \sum_{lm} A_{lm} U_l^\alpha(r, E_l) Y_{lm}(\hat{\vec{r}}) & r < R_\alpha \end{cases} \qquad (\text{II}.37)$$

The second type of functions is local orbitals (lo) different from that of the LAPW + LO method, defined by:

$$\phi(\vec{r}) = \begin{cases} 0 & r > R_\alpha \\ \left[A_{lm} U_l(r, E_l) + B_{lm} \dot{U}_l(r, E_l) \right] Y_{lm}(\hat{\vec{r}}) & r < R_\alpha \end{cases} \qquad (\text{II}.38)$$

II.7.4.2 LAPW + LO method:

The development of the (LAPW) method in local orbitals consists in modifying the orbitals of its base to avoid the use of several windows. The principle is to process all the bands from a single energy window. Singh [57] gave these orbitals, denoted

"LO" as a linear combination of two radial functions corresponding to two different energies and the derivative with respect to the energy of one of these functions [7]:

$$\phi(\vec{r}) =$$
$$\begin{cases} 0 & r > R_\alpha \\ [A_{lm}U_l(r, E_{1.l}) + B_{lm}U_l(r, E_{1.l}) + C_{lm}U_l(r, E_{2.l})]Y_{lm}(\hat{\vec{r}}) & r < R_\alpha \end{cases} \qquad (II.39)$$

Where the coefficients C_{lm} are of the same nature as the coefficients A_{lm} and B_{lm} defined above. In addition, this modification reduces the error made in the calculation of the conduction and valence bands.

II.8 Concept of the linearized augmented plane waves with full potential (FP-LAPW) method:

A new technique to solve the Poisson equation [59] has been added to the LAPW method in order to be able to treat molecular absorption on surfaces. In the LAPW method, which ensures the continuity of the potential on the surface of the muffin-tin sphere MT, the potential is developed in the following form:

$$V(r) = \begin{cases} \sum_{lm} V_{lm}(r)Y_{lm}(\hat{\vec{r}}) & r < R_\alpha \\ \sum_K V_k(r)\, e^{i\vec{K}\vec{r}} & r > R_\alpha \end{cases} \qquad (II.40)$$

No shape approximations are made. It is expanded in Fourier series in the interstitial regions and has an angular dependence inside each atomic sphere, a procedure frequently called a " full-potential" method.

II.9 WIEN2K code:

The WIEN2k code is an implementation of the FP-LAPW method. This code is produced by a team from the University of Vien in Austria led by professors, P.Blaha, K.Schwarz, and P.Sorantin [60], it has successfully treated high temperature superconducting systems [61], minerals [62], surfaces of transition metals [63], non-ferromagnetic oxides [64], molecules and the gradient of the electric field [65].Versions of the original WIEN code have been developed under UNIX, which have been called WIEN93, WIEN95 and WIEN97[66] .Now a new version, WIEN2k, is available, which is based on a basic alternative set. This allows a significant improvement, particularly in terms of speed, universality, ease of use and new devices. WIEN2k is written in Fortran 90 and requires the UNIX operating system;

since the programs are linked together through C-shell scripts. In the WIEN2k code The calculation procedure goes through three stages:

1) Initialization: it consists in building the spatial configuration (geometry), the symmetry operations, the starting densities, the number of special points necessary for integration in the irreducible Brillouin zone … etc. All these operations are carried out thanks to a series of auxiliary programs which generate:

- **structgen:** generated the input file, which defines the structure and constitutes the main input file used in all programs.
- **nn:** calculates the distances between the nearest neighbors
- **sgroup:** determines the space group, as well as the point group.
- **symmetry:** generates the symmetry operations of the spatial group, the point group of different atomic sites, LM expansion for spherical harmonics and the local rotation matrices.
- **lstart:** produces the electronic densities of free atoms.
- **kgen:** generates a k–points mesh in the irreducible Brillouin zone.
- **dstart:** produces an initial density for the self-consistent cycle by a superposition of atomic densities generated by lstart.

2) SCF calculation:

In this step, the energies and the electronic density of the ground state are calculated according to a convergence criterion (energy, charge density, force). The sub-programs used are:

- **lapw0:** (POTENTIAL) generates the potential from density.
- **lapw1:** (BANDS) calculates the valence bands.
- **lapw2:** (RHO) computes valence densities from eigenvectors and Fermi energy.
- **lcore:** computes core states and densities.
- **mixer:** mixes input and output densities.

3) calculating properties:

After the successful completion of SCF, different properties of selected problems are caculated and analyzed as:

- **Optimize:** determines the total energy according to the volume, used in the calculation of cell parameters, using the equation of state.

- **Spaghetti:** calculates the band structure using the eigenvalues generated by LAPW1.

- **Tetra:** calculates the DOS (density of states) and LDOS (local density of states).
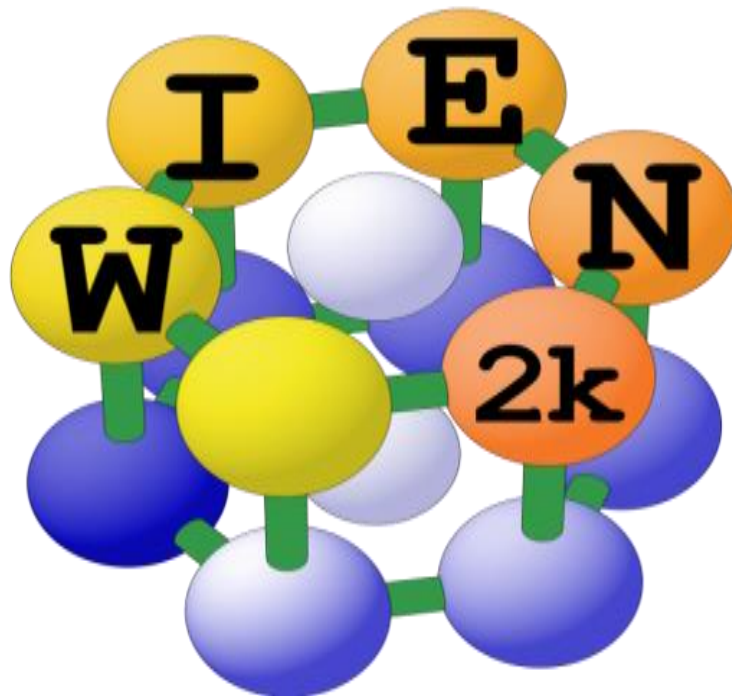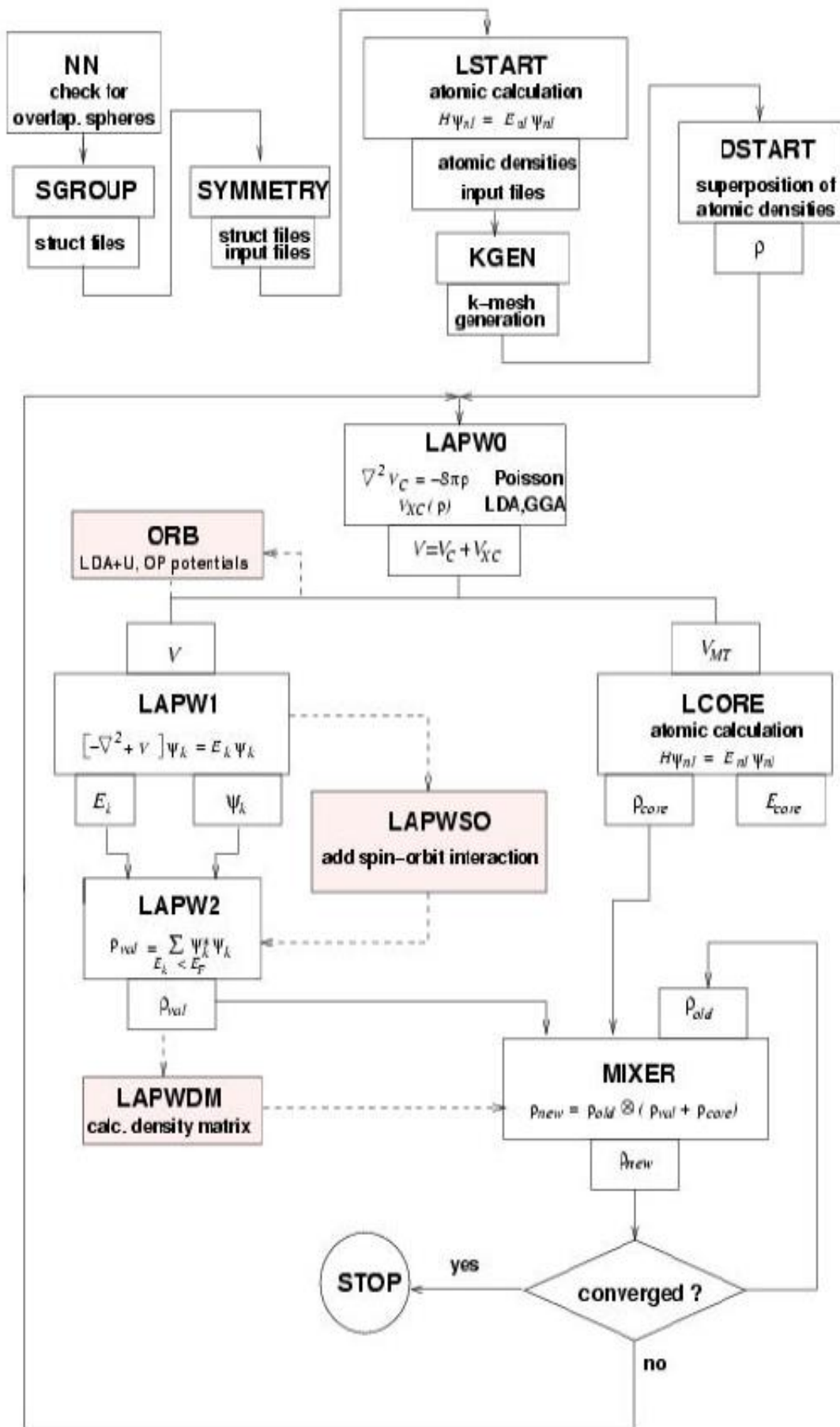
FigureII.5:   The   wien2K   code   program   flowchart   [60].

Bibliographical references:

[1] D. Sholl, J.A. Steckel, Density functional theory: a practical introduction, John Wiley & Sons, 2011.

[2] E. Schrödinger, SCHRÖDINGER 1926C, Annalen der Physik, 79 (1926) 734.

[3] M. Born, R. Oppenheimer, Zur quantentheorie der molekeln, Annalen der Physik, 389 (1927) 457-484.

[4] D.J. Griffiths, Introduction to quantum mechanics, Pearson International Edition (Pearson Prentice Hall, Upper Saddle River, 2005), 1960.

[5] D.R. Hartree, The wave mechanics of an atom with a non-Coulomb central field. Part I. Theory and methods, in: Mathematical Proceedings of the Cambridge Philosophical Society, Cambridge university press, 1928, pp. 89-110.

[6] D.R. Hartree, H.C.W.P.P. Fund, The calculation of atomic structures, J. Wiley, 1957.

[7] J.-L. Rivail, Éléments de chimie quantique à l'usage des chimistes (2e édition), EDP Sciences, 2012.

[8] W. Pauli, On the connexion between the completion of electron groups in an atom with the complex structure of spectra, Zeitschrift für Physik, 31 (1925) 765.

[9] Y. Omar, Indistinguishable particles in quantum mechanics: An introduction, Contemporary Physics, 46 (2005) 437-448.

[10] V. Fock, Näherungsmethode zur Lösung des quantenmechanischen Mehrkörperproblems, Zeitschrift für Physik, 61 (1930) 126-148.

[11] J.C. Slater, Note on Hartree's method, Physical Review, 35 (1930) 210.

[12] S. Cottenier, Density Functional Theory and the family of (L) APW-methods: a step-by-step introduction, Instituut voor Kern-en Stralingsfysica, KU Leuven, Belgium, 4 (2002) 41.

[13] P. Hohenberg, W. Kohn, Density functional theory (DFT), Phys. Rev, 136 (1964) B864.

[14] W. Kohn, L.J. Sham, Self-consistent equations including exchange and correlation effects, Physical Review, 140 (1965) A1133.

[15] J.G. Lee, Computational materials science: an introduction, CRC press, 2016.

[16] V. Sahni, Physical interpretation of electron correlation in the local-density approximation, in: Density Functional Theory, Springer, 1995, pp. 217-233.

[17] P.A. Dirac, Note on exchange phenomena in the Thomas atom, in: Mathematical proceedings of the Cambridge philosophical society, Cambridge University Press, 1930, pp. 376-385.

[18] R.M. Martin, Electronic structure: basic theory and practical methods, Cambridge university press, 2020.

[19] D.M. Ceperley, B.J. Alder, Ground state of the electron gas by a stochastic method, Physical Review Letters, 45 (1980) 566.

[20] J.P. Perdew, A. Zunger, Self-interaction correction to density-functional approximations for many-electron systems, Physical Review B, 23 (1981) 5048.

[21] L. Hedin, B.I. Lundqvist, Explicit local exchange-correlation potentials, Journal of Physics C: Solid state physics, 4 (1971) 2064.

[22] E. Wigner, Low-density correlation for an electron gas, Phys. Rev, 46 (1934) 1002.

[23] S.H. Vosko, L. Wilk, M. Nusair, Accurate spin-dependent electron liquid correlation energies for local spin density calculations: a critical analysis, Canadian Journal of physics, 58 (1980) 1200-1211.

[24] H.R. Eisenberg, R. Baer, A new generalized Kohn–Sham method for fundamental band-gaps in solids, Physical Chemistry Chemical Physics, 11 (2009) 4674-4680.

[25] A.F. LAMRANI, Modélisation et Simulation par la DFT des Propriétés Magnétiques et Structures Electroniques des Oxydes Magnétiques Dilués., in, Faculté des Sciences,Rabat-Maroc.

[26] J.P. Perdew, K. Schmidt, Jacob's ladder of density functional approximations for the exchange-correlation energy, in: AIP Conference Proceedings, American Institute of Physics, 2001, pp. 1-20.

[27] J.P. Perdew, K. Burke, M. Ernzerhof, Generalized gradient approximation made simple, Physical Review Letters, 77 (1996) 3865.

[28] J. Perdew, J. Chevary, S. Vosko, K. Jackson A., Pederson MR, Singh DJ, et Fioljais. C.,"Atoms, molecules, solids ans surfaces: Applications of generalized gradient approximation for exchange and correlation, Phys. Rev. B, 46 (1992) 6671.

[29] Z. Wu, R.E. Cohen, More accurate generalized gradient approximation for solids, Physical Review B, 73 (2006) 235116.

[30] J.P. Perdew, Y. Wang, Accurate and simple analytic representation of the electron-gas correlation energy, Physical Review B, 45 (1992) 13244.

[31] A.D. Becke, Density-functional exchange-energy approximation with correct asymptotic behavior, Physical review A, 38 (1988) 3098.

[32] J.P. Perdew, W. Yue, Accurate and simple density functional for the electronic exchange energy: Generalized gradient approximation, Physical Review B, 33 (1986) 8800.

[33] N.C. Handy, A.J. Cohen, Left-right correlation energy, Molecular Physics, 99 (2001) 403-412.

[34] C. Lee, W. Yang, R.G. Parr, Development of the Colle-Salvetti correlation-energy formula into a functional of the electron density, Physical Review B, 37 (1988) 785.

[35] E. Proynov, E. Ruiz, A. Vela, D. Salahub, Determining and extending the domain of exchange and correlation functionals, International Journal of Quantum Chemistry, 56 (1995) 61-78.

[36] T. Van Voorhis, G.E. Scuseria, A novel form for the exchange-correlation energy functional, The Journal of chemical physics, 109 (1998) 400-410.

[37] A.D. Becke, A new inhomogeneity parameter in density-functional theory, The Journal of chemical physics, 109 (1998) 2092-2098.

[38] A.D. Becke, Density-functional thermochemistry. IV. A new dynamical correlation functional and implications for exact-exchange mixing, The Journal of chemical physics, 104 (1996) 1040-1046.

[39] F. Tran, P. Blaha, Accurate band gaps of semiconductors and insulators with a semilocal exchange-correlation potential, Physical Review Letters, 102 (2009) 226401.

[40] A.D. Becke, E.R. Johnson, A simple effective potential for exchange, The Journal of chemical physics, 124 (2006) 221101.

[41] H. Zaari, Etude ab initio des propriétés optiques des matériaux: cas du ZnTe, CdFe2O4, MgB2, (2015).

[42] J. Heyd, J.E. Peralta, G.E. Scuseria, R.L. Martin, Energy band gaps and lattice parameters evaluated with the Heyd-Scuseria-Ernzerhof screened hybrid functional, The Journal of chemical physics, 123 (2005) 174101.

[43] J. Paier, M. Marsman, K. Hummer, G. Kresse, I.C. Gerber, J.G. Ángyán, Screened hybrid density functionals applied to solids, The Journal of chemical physics, 124 (2006) 154709.

[44] M. Shishkin, M. Marsman, G. Kresse, Accurate quasiparticle spectra from self-consistent GW calculations with vertex corrections, Physical Review Letters, 99 (2007) 246403.

[45] W.G. Aulbur, M. Städele, A. Görling, Exact-exchange-based quasiparticle calculations, Physical Review B, 62 (2000) 7121.

[46] S.V. Faleev, M. Van Schilfgaarde, T. Kotani, All-Electron Self-Consistent G W Approximation: Application to Si, MnO, and NiO, Physical Review Letters, 93 (2004) 126406.

[47] A.D. Becke, M.R. Roussel, Exchange holes in inhomogeneous systems: A coordinate-space model, Physical review A, 39 (1989) 3761.

[48] J.C. Slater, Wave functions in a periodic potential, Physical Review, 51 (1937) 846.

[49] J. Slater, Energy band calculations by the augmented plane wave method, in: Advances in quantum chemistry, Elsevier, 1964, pp. 35-58.

[50] T.L. Loucks, Augmented plane wave method: a guide to performing electronic structure calculations, WA Benjamin, 1967.

[51] D. Koelling, G. Arbman, Use of energy derivative of the radial solution in an augmented plane wave method: application to copper, Journal of Physics F: Metal Physics, 5 (1975) 2041.

[52] O.K. Andersen, Linear methods in band theory, Physical Review B, 12 (1975) 3060.

[53] T. Takeda, J. Kubler, Linear augmented plane wave method for self-consistent calculations, Journal of Physics F: Metal Physics, 9 (1979) 661.

[54] L. Smrčka, Linearized augmented plane wave method utilizing the quadratic energy expansion of radial wave functions, Czechoslovak Journal of Physics B, 34 (1984) 694-704.

[55] J. Petrů, L. Smrčka, Quadratic augmented plane wave method for self-consistent band structure calculations, Czechoslovak Journal of Physics B, 35 (1985) 62-71.

[56] D. Shaughnessy, G. Evans, M. Darby, An improved LAPW method for the calculation of self-consistent electronic band structures, Journal of Physics F: Metal Physics, 17 (1987) 1671.

[57] D. Singh, Planes Waves, Pseudopotentials and the LAPW, in, Method, Kluwer Academic, 1994.

[58] E. Sjöstedt, L. Nordström, D. Singh, An alternative way of linearizing the augmented plane-wave method, Solid state communications, 114 (2000) 15-20.

[59] E. Wimmer, H. Krakauer, M. Weinert, A. Freeman, Full-potential self-consistent linearized-augmented-plane-wave method for calculating the electronic structure of molecules and surfaces: O 2 molecule, Physical Review B, 24 (1981) 864.

[60] P. Blaha, K. Schwarz, G.K. Madsen, D. Kvasnicka, J. Luitz, wien2k, An augmented plane wave+ local orbitals program for calculating crystal properties, 60 (2001).

[61] K. Schwarz, C. Ambrosch-Draxl, P. Blaha, Charge distribution and electric-field gradients in YBa 2 Cu 3 O 7− x, Physical Review B, 42 (1990) 2051.

[62] B. Winkler, P. Blaha, K. Schwarz, Ab initio calculation of electric-field-gradient tensors of forsterite, American Mineralogist, 81 (1996) 545-549.

[63] B. Kohler, P. Ruggerone, S. Wilke, M. Scheffler, Frustrated H-induced instability of Mo (110), Physical Review Letters, 74 (1995) 1387.

[64] X.-G. Wang, W. Weiss, S.K. Shaikhutdinov, M. Ritter, M. Petersen, F. Wagner, R. Schlögl, M. Scheffler, The hematite (α-Fe 2 O 3)(0001) surface: evidence for domains of distinct chemistry, Physical Review Letters, 81 (1998) 1038.

[65] P. Dufek, P. Blaha, K. Schwarz, Determination of the nuclear quadrupole moment of 57 Fe, Physical Review Letters, 75 (1995) 3545.

[66] P. Blaha, K. Schwarz, J. Luitz, WIEN97: full potential linearized augmented plane wave package for calculating crystal properties; release 97.8 (April 1999), University of Technology, Inst. of Physical and Theoretical Chemistry, 1999.

CHAPTER III

In this section, we present a comparative study in cubic phases of three important perovskites: $LiBeO_3$, $KBeO_3$ and $KMgO_3$, describing their structure, elastic, magnetic, electronic and thermodynamic properties. Useful findings and conclusive discussion of these materials along with the possible applications has been mentioned in this part.

III.1 Computational methodology:

The present section shows the computational procedure employed for the investigation of different properties of $LiBeO_3$, $KBeO_3$ and $KMgO_3$. First-principle calculations, based on the formalism of the density functional theory (DFT)[1, 2] and the method of Full potential augmented and linearized plane waves (FP-LAPW) [3] implemented in the Wien2k code [4], were used to calculate their structural, electronic, magnetic, elastic and thermodynamic properties. The exchange and correlation effects were treated by the following two approximations: generalized gradient approximation (GGA) [5] and Tran-Blaha modified beck Johnson (TB-mBJ) potentials [6],[7], which was introduced to compute the band structure (improve the calculation of the energy gap). In all the studied configurations: non-magnetic (NM), anti-ferromagnetic (AFM) and ferromagnetic (FM). The plane wave cut-off value $R_{mt}K_{max} = 8$ is used (R_{mt} is the smallest radius of the MT sphere and K_{max} is the maximum of the K wave vector), The wave functions inside MTS are expanded in terms of the multiplication of spherical harmonics and the radial eigenfunctions up to lmax =10, While the charge density was Fourier expended up to $G_{max}= 14$ $Ry^{1/2}$. In the iteration process of self-coherence calculations, the convergence of energy has been taken up to 10^{-4} Ry whereas the charge convergence of $10^{-5}e$ is applied as a convergence criterion for all calculations performed. The integration of the Brillouin zone is carried out with 3000 k-points. Obviously, these parameters are determined by convergence tests process.

First of all, we started by determining the optimum sphere radii Rmt for each atom. The Muffin-Tin Sphere radius values (MTS) have been chosen such that there will be no overlap of the Muffin-Tin spheres. The values chosen in our calculations are grouped together in **table III.1**.

Table III.1: The R_{mt} Values used in our calculations.

Compound	LiBeO$_3$			KBeO$_3$			KMgO$_3$		
GGA	**Li**	**Be**	**O**	**K**	**Be**	**O**	**K**	**Mg**	**O**
R_{mt}	1.96	1.43	1.33	2	1.42	1.33	1.94	1.74	1.33

III.2 Results and discussion:

III.2.1 Structural properties:

Due to the current growing research about half-metals for applications in spintronics by an ab- initio study based on DFT, we have focused our interest on perovskite oxides of formula I^A-II^A-O3 (I^A is an alkali metal and II^A is an alkaline earth metals) because of their interesting properties. Therefore, in this work, we studied the cubic perovskites oxide: LiBeO$_3$, KBeO$_3$ and KMgO$_3$. These compounds crystallize in the space group Pm-3m (221) described by a = b = c and α = β = γ = 90 °.The Wyckoff positions of the atoms I^A (Li, K), II^A (Be, Mg) and O are (0, 0, 0), (1/2,1/2,1/2) and (1/2,1/2,0), respectively. The cubic structure I^A-II^A-O3 is illustrated in **Figure III.1**.
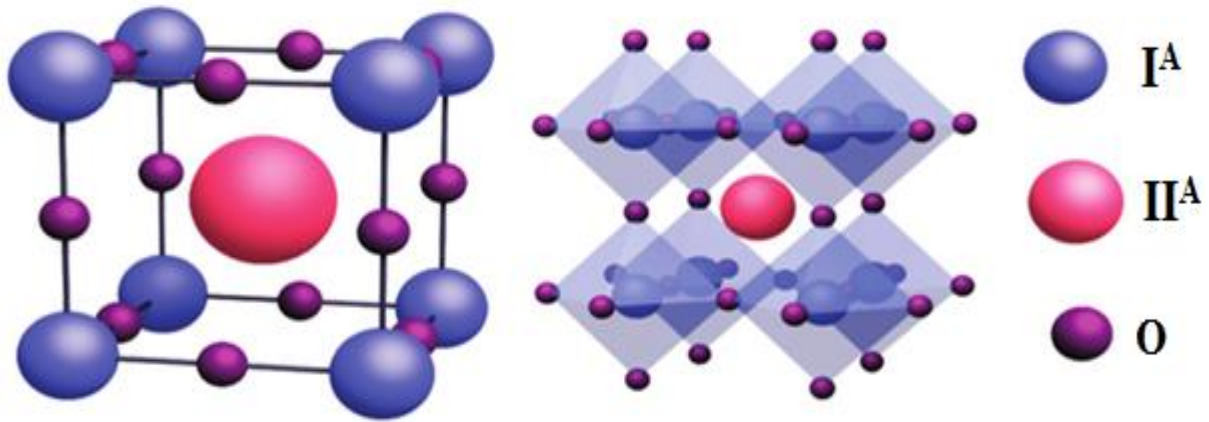
Figure III.1: Representation of the structure of I^A-II^A-O$_3$ used.

We remind the electronic configurations of our elements:

Li: 1s^2 2s^1 Be: 1s^2 2s^2 O: 1s^2 2s^2 2p^4
K: [Ar] 4s^1 Mg: [Ne] 3s^2

These different configurations will allow us to explain certain physical phenomena that we will observe later.

The magnetic structure of the AFM phase is obtained by constructing a supercell of 1×1×2 which contains two cubic cells where in the magnetic sub-lattice (O atoms), the AFM order is along z-axis, as schematically represented in **Figure III.2.**
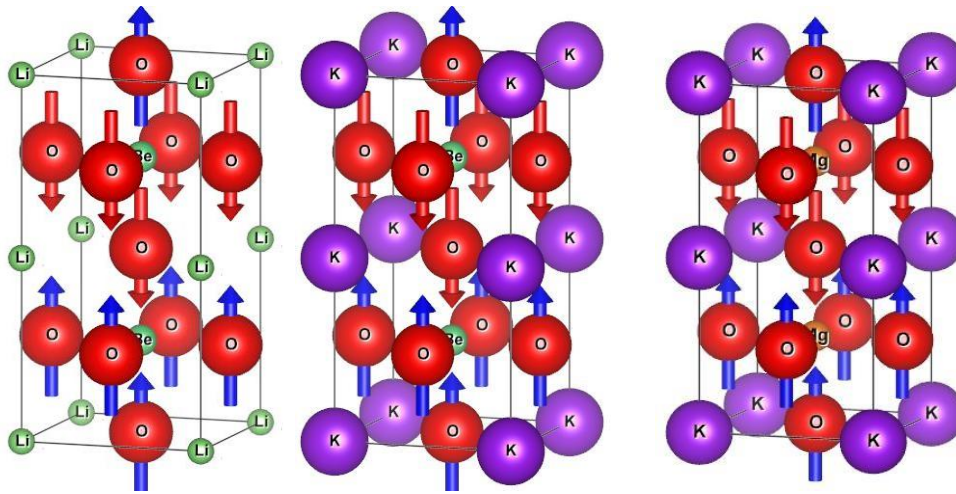
Figure III.2 Magnetic structure of the AFM configuration of $LiBeO_3$, $KBeO_3$ and $KMgO_3$ respectively.

Determining structural properties namely the lattice parameters (a), the compressibility modulus (B) and its derivative (B ') is the first important step in any calculation (an ab-initio calculation), as they gives us more information on the microscopic scale of the material to be studied and will therefore have a relatively large impact on the prediction of other properties (elastic, electronic and magnetic..).

The stability of the materials is the key parameter of their selection for device applications. For that, the relative stability of $LiBeO_3$, $KBeO_3$ and $KMgO_3$ compound has been investigated by calculating the total energy as function of the volume of the unit cell in (NM), (FM) and (AFM) states within GGA−PBE method, the total energy-volume curves are depicted in **Figure III. 3**.
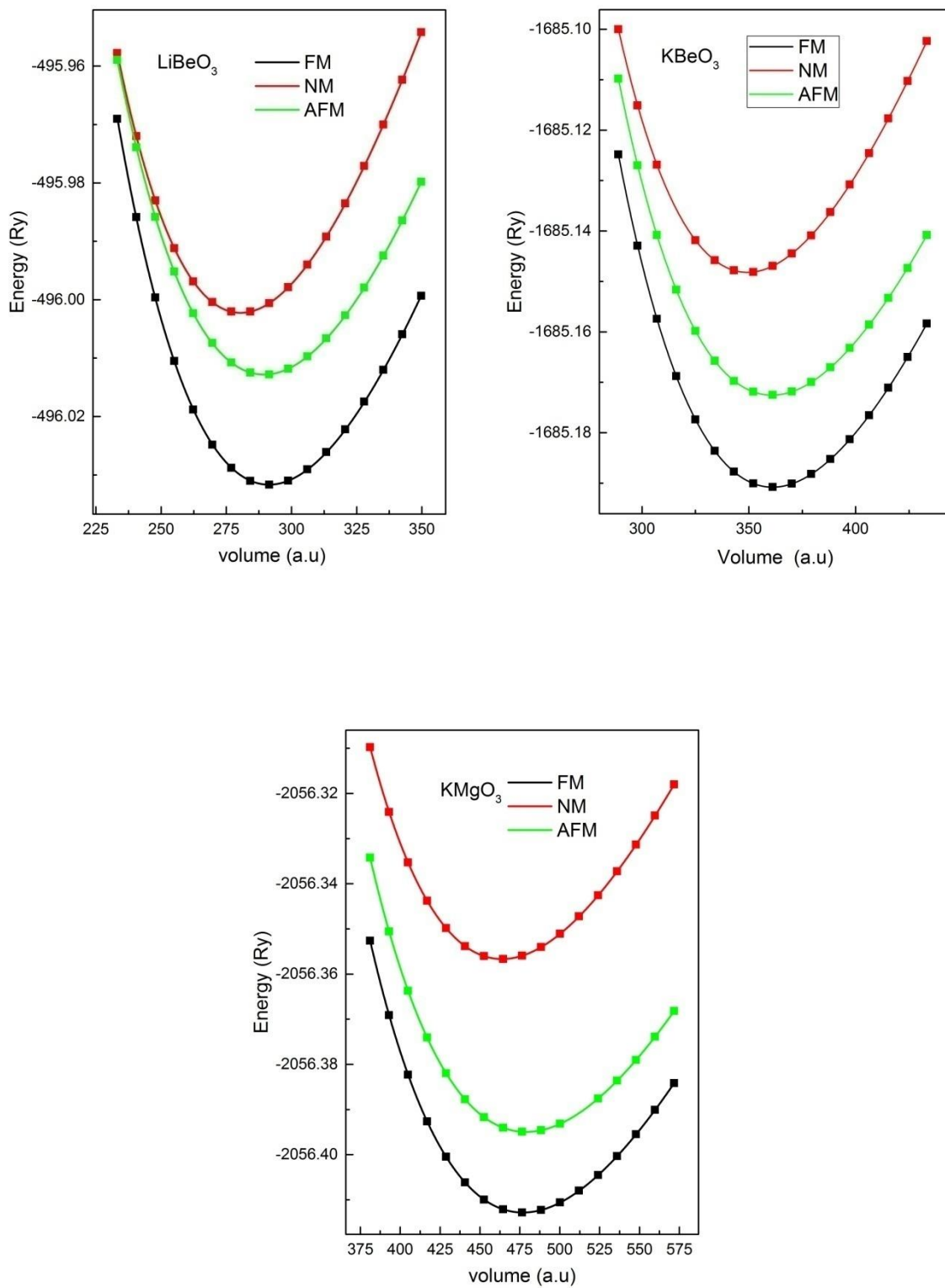
Figure III.3: Calculated total energy of $LiBeO_3$, $KBeO_3$ and $KMgO_3$ compounds as a function of the volume for FM, NM, and AFM phases.

As can be seen from these figures, the ferromagnetic phase (FM) has the lowest total energy for the three compounds, which suggests that it is energetically more stable with regard to the other (NM) and (AFM) phases.

The curves of total energy as functions of different volumes are fitted by using Birch Murnaghan equation of state [8], defined by the equation (III.1) ,in order to obtain the ground state properties of the studied compounds such as the equilibrium lattice constant, the bulk modulus, its pressure derivative , and the total energy of the compounds.

$$E(V) = E_0 + \frac{9V_0 B_0}{16}\left\{\left[\left(\frac{V_0}{V}\right)^{2/3} - 1\right]^3 \grave{B_0} + \left[\left(\frac{V_0}{V}\right)^{2/3} - 1\right]^2 \left[6 - 4\left(\frac{V_0}{V}\right)^{2/3}\right]\right\} \quad \text{(III.1)}$$

And the compressibility modulus B is determined by:

$$B = V\frac{\partial^2 E}{\partial V^2} \quad \text{(III.2)}$$

Where E (V) represents the energy of the ground state with cell volume V, and V_0 the unit cell volume at zero pressure, corresponding to the equilibrium lattice parameter a_0, B_0 and $\grave{B_0}$ are the compressibility modulus and its derivative, respectively. These parameters are computed for each state and their values are reported in **Table III.2**.

Table III.2: Calculated lattice parameter (Å), bulk modulus (GPa), its derivative pressure, and ground state energy (Ry) for $LiBeO_3$, $KBeO_3$ and $KMgO_3$ in their FM, NM, and AFM phases. The values in parentheses are from [9-11].

Compound	Phase	a_0	B	B'	E_{min}
LiBeO3	FM	3.51	110.20	3.9666	-496.0316
		(3.47 [9])	(122.54 [9])		
	NM	3.4639	120.111	4.089	-496.0022
	AFM	3.50	103.930	3.647	-496.0128
KBeO3	FM	3.77	90.90	4.2754	-1685.1907
		(3.70 [9])	(103.75 [9])		
		(3.77 [10])	(95.18 [10])	(2.89 [10])	(-1685.1878 [10])
	NM	3.7269	97.3655	4.2529	-1685.1482
	AFM	3.7678	87.8309	4.172	-1685.1725
KMgO3	FM	4.134	61.8	4.35	-2056.4128
		(4.126 [11])	(63.9 [11])	(4.42 [11])	
	NM	4.0964	65.8905	4.3618	-2056.3567
	AFM	4.9287	59.8364	4.2946	-2056.3950

To further confirm the stability of our studied compounds, we calculated the formation energy, in order to check the chemical stability related to their synthesizability. The formation energy can be computed by the following relation:

$$E_{Formation}^{I^A-II^A-O_3} = (E_{Total}^{I^A-II^A-O_3} - (E_{bulk}^{I^A} + E_{bulk}^{II^A} + 3/2\,E_{gaz}^{O_2})) \qquad (III.3)$$

Where $E_{Total}^{I^A-II^A-O_3}$ and $E_{gaz}^{O_2}$ are the total energy of I^A-II^A-O_3 and O_2 molecule, respectively. $E_{bulk}^{I^A}$ and $E_{bulk}^{II^A}$ are the bulk energies of I^A and II^A elements, respectively.

The obtained negative formation energy of -4.49, −3.81 and -5.10 eV for $LiBeO_3$, $KBeO_3$ and $KMgO_3$ respectively, as showed in **table III.3** indicates that these materials are chemically stable. Therefore, they can be synthesized in the normal conditions.

Table III.3: Bulk energies of Li, Be, K, Mg elements (in Ry), total energy of O_2 molecule (in Ry), total energy (in Ry /unit cell) and formation energies (in eV) of $LiBeO_3$, $KBeO_3$ and $KMgO_3$. The Results in parentheses are from [9-11].

Li	Be	O_2	$LiBeO_3$	$E_{Formation}$
-15.0441	-29.5410	-300.7426	-496.0317	-4.49 (-1.34 eV [9])
K	Be	O_2	$KBeO_3$	$E_{Formation}$
-1204.2548 (-1204.1913 [10])	-29.5410 (-29.2657[10])	-300.7426 (-300.2338[10])	-1685.1908 (-1685.1878[10])	-3.81 (-1.22 eV [9]) (-1.38 [10])
K	Mg	O_2	$KMgO_3$	$E_{Formation}$
-1204.2548	-400.6689	-300.7426	-2056.4128	-5.10 (-0.46[11])

III.2.2 Elastic properties:

To investigate the mechanical stability of our compounds, the calculation of the elastic constants using IRelast package, integrated in the WIEN2k code is performed. The elastic properties give various kinds of important information, on the

behavior of this compound with regard to the ductility, brittleness and application of the external forces.

For compounds that have a cubic structure only three elastic constants C_{11}, C_{12} and C_{44} are sufficient. We have calculated these constants for the cubic oxide perovskites $LiBeO_3$, $KBeO_3$ and $KMgO_3$ compounds in their energetically favorable phases.

The first equation involves the elastic modulus ($C_{11} - C_{12}$) which is related to the bulk modulus B by the following:

$$B = \frac{C_{11} + 2C_{12}}{3} \tag{III.4}$$

The second one by applying volume-conserving orthorhombic strain tensor:

$$\bar{\varepsilon} = \begin{bmatrix} \delta & 0 & 0 \\ 0 & -\delta & 0 \\ 0 & 0 & \frac{1}{1-\delta^2} \end{bmatrix} \tag{III.5.a}$$

Where the expression of total energy has the following form:

$$E(\delta) = E(-\delta) = E(0) + 3(C_{11} - C_{12})V_0\delta^2 + O(\delta^3) \tag{III.5.b}$$

To determine C_{44}, we used a volume-conserving monoclinic strain tensor:

$$\bar{\varepsilon} = \begin{bmatrix} \frac{\delta}{2} & 0 & 0 \\ 0 & -\frac{\delta}{2} & 0 \\ 0 & 0 & \frac{\delta^2}{4-\delta^2} \end{bmatrix} \tag{III.6.a}$$

The total energy of the system has become:

$$E(\delta) = E(0) + \frac{1}{6}(C_{11} + 2C_{12} + 4C_{44})V_0\delta^2 + O(\delta^3) \tag{III.6.b}$$

The mechanical stability of a cubic system requires that the criteria for Born stability are satisfied [12].

$$C_{44} > 0 \tag{III.7.a}$$

$$C_{11} - C_{12} > 0 \tag{III.7.b}$$

$$C_{11} + 2C_{12} > 0 \quad and \quad C_{12} < B < C_{11} \tag{III.7.c}$$

The obtained elastic constants satisfied all the Born's stability criteria; so, we confirm that the cubic oxide perovskites $LiBeO_3$, $KBeO_3$ and $KMgO_3$ compounds are mechanically stable. The computed C_{ij} constants are given in **Table III.4**.

Table III.4: Elastic constants C_{11}, C_{12}, C_{44} for $LiBeO_3$, $KBeO_3$ and $KMgO_3$ respectively. The values in parentheses are from [9-11].

Compound	C_{11}	C_{12}	C_{44}
LiBeO3	174.40 (219.88 [9])	87.03 (52.59 [9])	34.53 (39.94 [9])
KBeO3	124.08 (140.43 [9])	83.73 (78.33 [9])	45.77 (24.30 [9])
KMgO3	121.54 (123.48 [11])	32.57 (28.36 [11])	9.04 (15.96 [11])

Using the C_{ij} the shear modulus G, bulk modulus B and Young's modulus E are calculated in the Voigt −Reuss −Hill (VRH) averaging scheme [13]. The Voigt and Reuss bounds on the bulk and shear modulus for a cubic system can be given as follows:

$$B_V = B_R = \frac{(C_{11}+2C_{12})}{3} \tag{III.8}$$

$$G_V = \frac{(C_{11}-C_{12}-3C_{44})}{5} \tag{III.9}$$

$$G_R = \frac{5C_{44}(C_{11}-C_{12})}{4C_{44}+3(C_{11}-C_{12})} \tag{III.10}$$

The bulk and shear modulus can be determined as follows:

$$B = \frac{1}{2}(B_R + B_V) \tag{III.11}$$

$$G = \frac{1}{2}(G_R + G_V) \tag{III.12}$$

Other polycrystalline elastic moduli can be estimated using the following equations (III .13), (III .14), (III .15), such as Young's modulus (*E)*, Poisson's ratio (*v),* Zener anisotropy parameter *A*.

$$E = \frac{9BG}{3B+G} \tag{III.13}$$

$$v = \frac{3B-E}{6B} \tag{III.14}$$

$$A = \frac{2C_{44}}{C_{11}-C_{12}} \qquad \text{(III.15)}$$

Also, shear moduli of a crystal can be calculated from:

$$G = \frac{C_{11}-C_{12}+3C_{44}}{5} \qquad \text{(III.16)}$$

For $LiBeO_3$, $KBeO_3$ and $KMgO_3$ these quantities are also reported in **Table III.5** and **Table III.6**.

Table III.5: Calculated results for bulk, shear and Young modulus (in GPa) of $LiBeO_3$, $KBeO_3$ and $KMgO_3$ compound by Voigt, Reuss, and Hill approaches.

Compound	B			G			E		
	B_V	B_R	B_H	G_V	G_R	G_H	E_V	E_R	E_H
LiBeO3	116.15	116.15	116.15	38.19	37.69	37.94	103.26	102.04	102.65
KBeO3	97.18	97.18	97.18	35.53	30.37	32.95	95.02	82.50	88.81
KMgO3	62.23	62.23	62.23	23.21	13.26	18.23	61.93	37.15	49.84

Table III. 6: calculated results for B/G, and Poisson's ratios (v) and Zener anisotropy parameter A of $LiBeO_3$, $KBeO_3$ and $KMgO_3$ compound. The values in parentheses are from [9, 11].

Compound	A	B/G	v
LiBeO3	0.79	3.04 (2.02 [9])	0.35 (0.29 [9])
KBeO3	2.27	2.73 (3.69 [9])	0.337 0.375 [9])
KMgO3	0.20 (0.34[11])	2.68 (2.39 [11])	0.37 (0.31 [11])

It is known that bulk modulus is a measure of resistance to volume change by applied pressure (The material hardness). From **Table III.5 data**, we observe that the bulk modulus values resulting through the elastic constants for the three compounds agree with that obtained from the total energy optimization.

The same values of B_V, B_R and B_H indicate that the Bulk modulus is isotropic. This result is confirmed from the spherical shape by the 3D visualization of bulk modulus, as shown in **Figure III. 3**, using the directional variation of bulk modulus in the spherical coordinates, for a cubic structure[14, 15]:

$$\frac{1}{B} = 3(S_{11} + 2S_{12}) \qquad\qquad (III.17)$$

Where S_{ij} are the elastic compliance constants (The compliance matrix S_{ij} is the inverse of the matrix C_{ij}).

The observed spherical shapes of Bulk modulus surface for the three compounds suggest that these perovskites have a stronger capability to resist deformation.
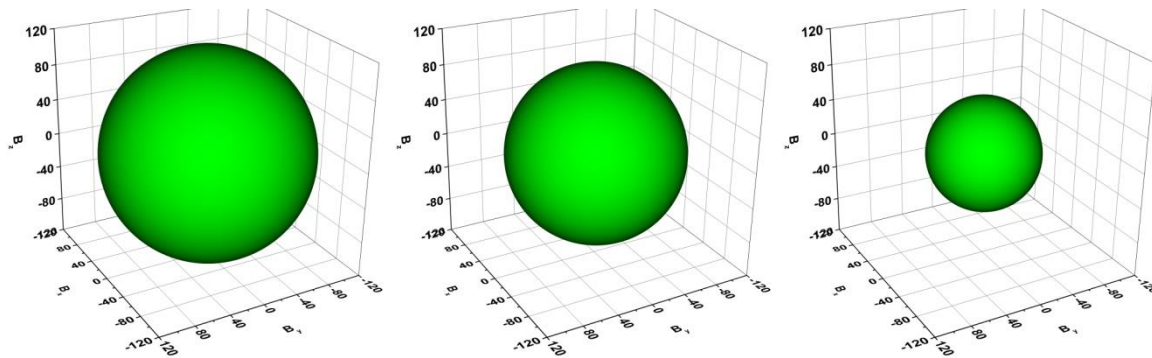

Figure III.4: 3D-visualized directional dependence of Bulk modulus B for LiBeO$_3$, KBeO$_3$ and KMgO$_3$, respectively.

From the point of view of the brittleness and ductility of a material, it is necessary to present two factors: the index B / G and the Cauchy pressure C$_p$. First, we started with the interpretation of the B / G ratio where the critical value which separates the ductile and brittle behavior is equal to 1.75 (brittle <1.75 <ductile) [16], according to our case B/G ratios are greater than 1.75 for all compounds which classified them as ductile materials.

Another parameter of ductility which is called the Cauchy pressure Cp= (C$_{12}$ - C$_{44}$) [17, 18]: if this pressure is positive (negative), the material is ductile (brittle). The positive value of the Cauchy's pressure for the three compounds LiBeO$_3$, KBeO$_3$ and KMgO$_3$ is 52.49, 37.96 and 23.54, respectively, further confirms the ductility of these materials, and it decreases from LiBeO$_3$ to KMgO$_3$.

 Generally, Poisson's ratio (ν) can give information   on the nature of the bonding force in a compound. Indeed, as reported, if ν is between the lowest (0.25) and upper (0.5) limits [19], the crystal can be considered as ionic and its corresponding interatomic forces are central. In the other hand, if this value is typically between 0.1 and 0.25, the material is covalent with non-central interatomic

forces [20] . In our case from **Table III.6**, the Poisson's ratios are higher than 0.25. Thus, all three compounds have an ionic-bonding character and interatomic central forces.

The Zener anisotropy factor A, given by equation (III.15), is another important physical quantity which tells about the structural stability and it is highly correlated with the possibility of inducing micro-cracks in the materials [21]. For an entirely isotropic system, A is unity and the deviation from unity measures the degree of elastic anisotropy. From **Table III.6**, one can be noticed that all of our compounds present a significant degree of anisotropy.

In addition to Zener anisotropy parameter A, the anisotropic elastic properties have been visualized in 3D map. The directional dependence of young's (E) and shear (G) modulus of cubic system are given in the following equations[14, 15]:

$$\frac{1}{E} = S_{11} - 2(S_{11} - S_{12} - \frac{S_{44}}{2})(\sin^4 \theta \cos^2 \varphi \sin^2 \varphi + \cos^2 \theta \sin^2 \theta) \qquad \text{(III.18)}$$
$$\frac{1}{G} = S_{44} + 4(S_{11} - S_{12} - \frac{S_{44}}{2})(\sin^4 \theta \cos^2 \varphi \sin^2 \varphi + \cos^2 \theta \sin^2 \theta) \qquad \text{(III.19)}$$

In **Figures III.5.**, our studied compounds exhibit the distinctive 3D figures of Young's and shear modulus with various deviations from a sphere which confirm their anisotropy. Among the three compounds, the A of LiBeO$_3$ is the closest to 1 and consequently it exhibits a small relative deviation. With regard to KBeO$_3$, we note that A>1 with a large deformation from the sphere shape along the <111> directions for young's modulus and along <001> directions for shear modulus. The situation becomes the opposite in the case of KMgO$_3$ since A<1.
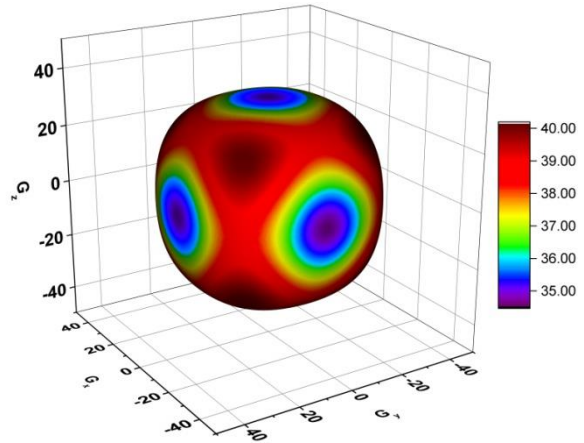
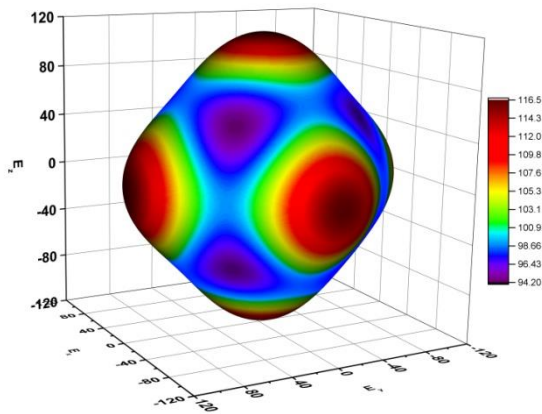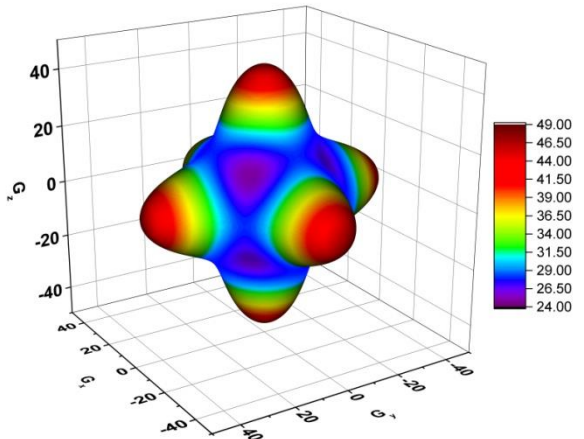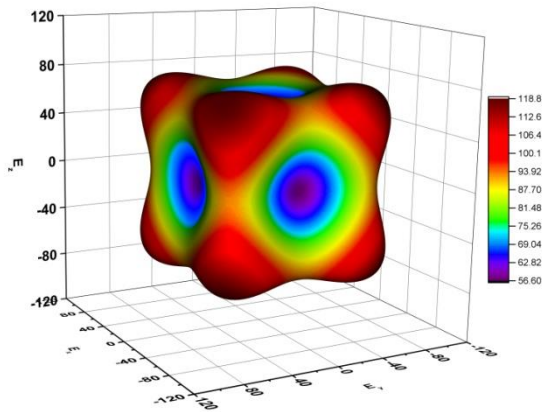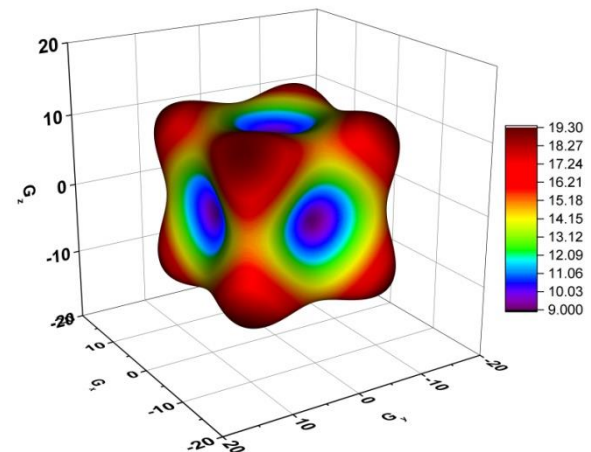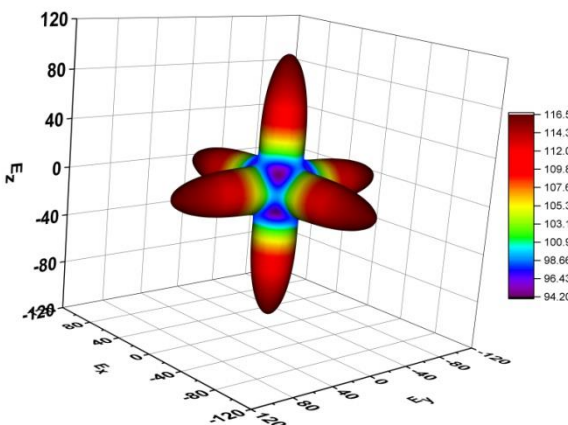**Young's modulus**   **shear modulus**

1/- LiBeO$_3$:

2/- KBeO$_3$:

3/- KMgO$_3$:

Figure III.5: 3D-Visualized directional dependence of Young's modulus E and shear modulus G (in GPa) of LiBeO$_3$, KBeO$_3$ and KMgO$_3$.

Debye temperature:

Debye temperature θ_D is an important fundamental parameter related to several physical properties such as specific heat and melting temperature and zero point vibration energy.

We estimated the Debye temperature using the average wave velocity v_m, by the following equation:

$$\theta_D = \frac{\hbar}{k_B}\left[\frac{3n}{4\pi}\left(\frac{N_A \rho}{M}\right)\right]^{\frac{1}{3}} v_m \tag{III.20}$$

where $\hbar$ is the Planck constant, k_B the Boltzmann constant, N_A the Avogadro number, n the number of atoms per formula unit, M the molecular mass per formula unit, the density $\rho = (M / V)$, the average wave velocity is given by the equation:

$$v_m = \left[\frac{1}{3}\left(\frac{2}{v_t^3} + \frac{1}{v_l^3}\right)\right]^{\frac{1}{3}} \tag{III.21}$$

Where v_l and v_t, is the longitudinal and transverse velocity respectively, and are given by the following expressions:

$$v_l = \sqrt{\frac{3B+4G}{3\rho}} \qquad and \qquad v_t = v\sqrt{\frac{G}{\rho}} \tag{III.22}$$

The results of our calculations are shown in **Table III.7**.

Table III.7: Average wave velocity, longitudinal and transverse speed of sound propagation (v_m, v_l and v_t respectively in m /s, and Debye temperature θ_D in K, the melting temperature T_m in K).

compound	v_m	v_l	v_t	θ_D	T_m
LiBeO3	2755.28	7272.92	2421.86	399.84	1492 ± 300
KBeO3	3735.79	6878.45	3323.76	504.71	1286 ± 300
KMgO3	2974.44	5750.05	2639.65	366.26	1271 ± 300

It is noteworthy to estimate an important parameter so-called the Goldschmidt's tolerance factor which gives the structural preference for the perovskites and has been calculated from the relation:

$$\tau = \frac{(r_A + r_o)}{\sqrt{2}(r_B + r_o)} \qquad\qquad (\text{III.23})$$

Where r_A, r_B and r_o are the ionic radii of A, B and O atoms, respectively.

The following tables show the ionic radius of the constituent elements [22] and the values of tolerance factor for the three compounds, respectively:

Table III.8.a: Ionic radii of the constituent elements [22].

Element	Li	K	Be	Mg	O
Ionic radius (A°)	0.92	1.64	0.45	0.72	1.35

Table III.8.b: Tolerance factor of $LiBeO_3$, $KBeO_3$ and $KMgO_3$.

Compound	$LiBeO_3$	$KBeO_3$	$KMgO_3$
Tolerance factor	0.89	1.17	1.02

It come out from the values found for the tolerance factor t, that the cubic structure is the preferred one for only the $KMgO_3$ since its t value is between 0.99 *et* 1.06 [23]. Although this fact, in the cubic structure both $LiBeO_3$ and $KBeO_3$ are metastable and probably synthesizable.

III.2.3 Electronic properties:

Firstly, the following electronic properties are inspected at equilibrium lattice constants using GGA method. Furthermore, it is extended to TB-mBJ potential in order to more precisely describe the electron profile and results are discussed.

III.2.3.1 Band structures:

For the resulting plot, see **Figures III.6, III.7 and III.8**, We notice that the curves of the three compounds have almost the same shape and show a gap separating the valance and the conduction bands in majority spin directions (spin-up); whereas, the minority spin states (spin –dn) are strongly metallic with bands crossing Fermi level.

From GGA method, there are indirect gaps R-Γ, it is observed from **Table III.9,** that $KBeO_3$ have a band gap of 8.61eV greater than that of $LiBeO_3$ and $KMgO_3$. The half-metallic gap resulting from $KMgO_3$ is slightly larger as compared to the

other compounds. These electronic results confirm their half-metallic nature with full spin polarization (P = 100%).

With using TB-mBJ potential, the band gap and half-metallic gap in spin-up state of our three compounds are increased. This method opens a band gap and keeps VBM at R-point and CBM at Γ-point. As we can see from **Table III.9**, The LiBeO3 exhibits the highest band gap of 11.81eV, while its half-metallic gap value is 2.85 eV which is the lowest one. KMgO3 shows the highest half metallic gap value of 3.33 eV. Thus, the half metallic character is maintained as we can also see from TB- mBJ band structure.
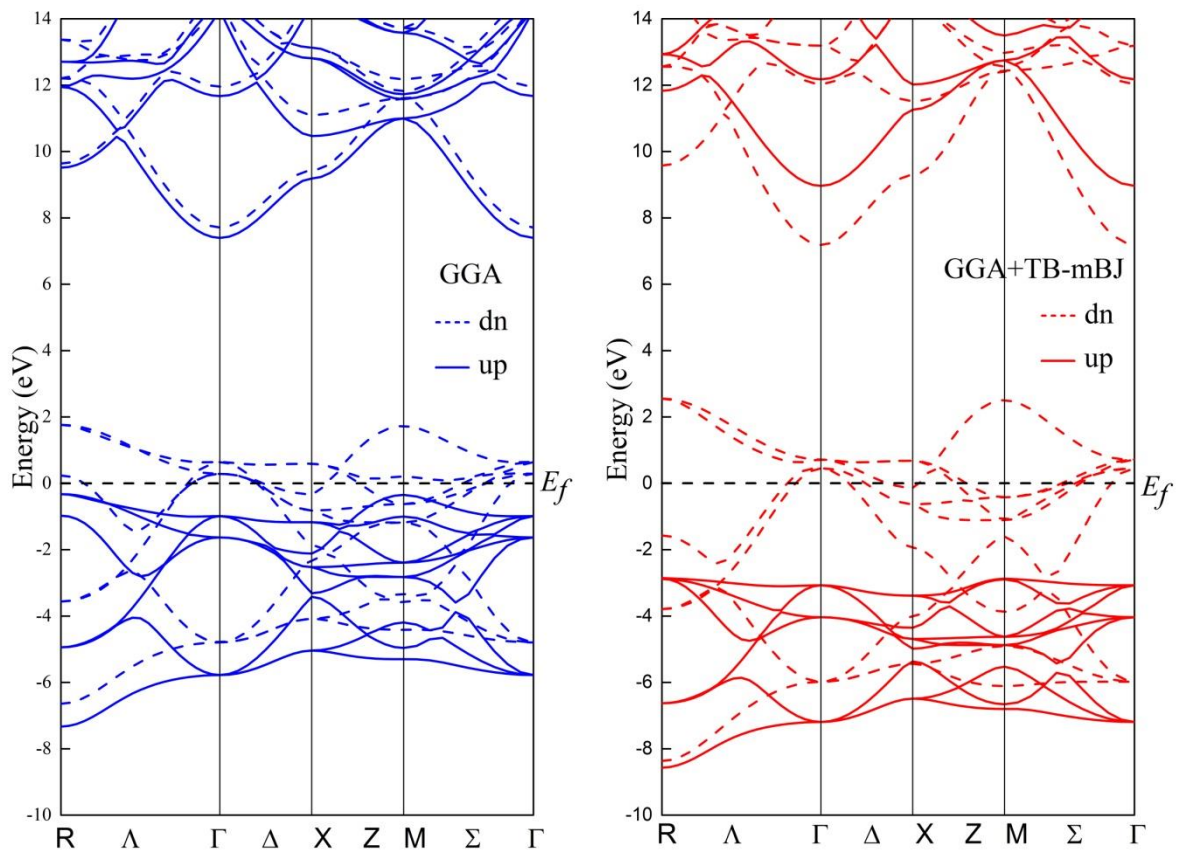

Figure III.6: spin resolved band structure of LiBeO$_3$ by GGA (left panel) and GGA+TB-mBJ (right panel) approximations. (Dash line for spin down and solid line for spin up).

Figure III.7: spin resolved band structure of $KBeO_3$ by GGA (left panel) and GGA+TB-mBJ (right panel) approximations. (Dash line for spin down and solid line for spin up).
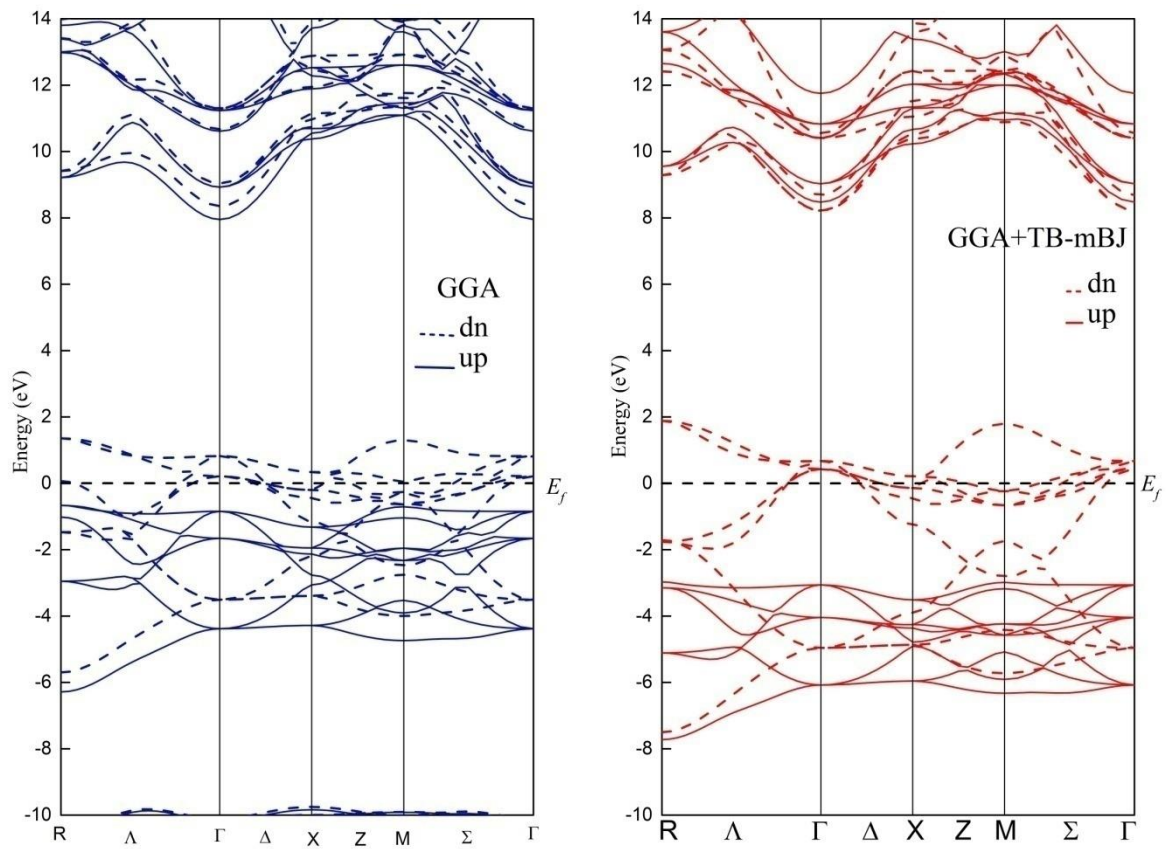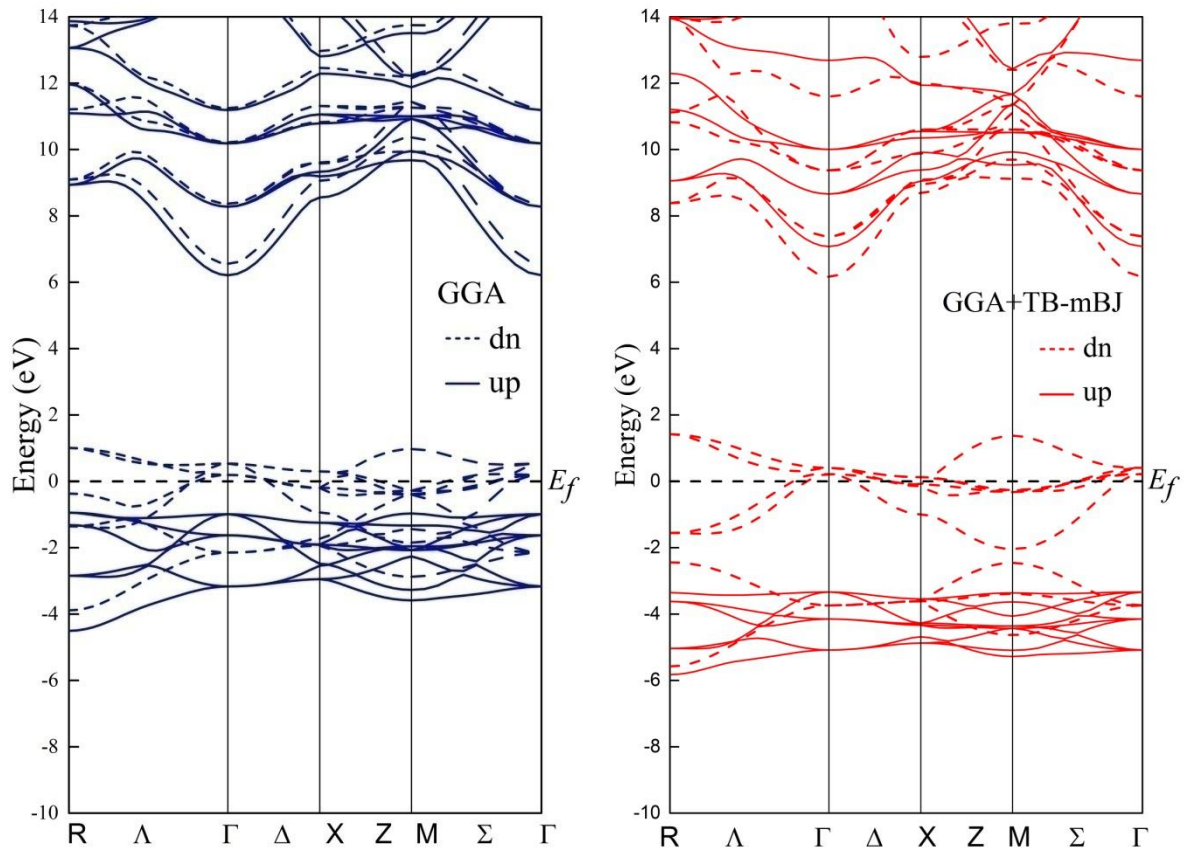
Figure III.8: spin resolved band structure of $KMgO_3$ by GGA (left panel) and GGA+TB-mBJ (right panel) approximations. (Dash line for spin down and solid line for spin up).

Table III.9: Obtained band gap, half-metallic gap (HM gap) in eV, of $LiBeO_3$, $KBeO_3$ and $KMgO_3$. The values in parentheses are from [9-11].

Compound	method	Band gap	HM gap
$LiBeO_3$	GGA	7.73	0.34(1.75 [9])
	TB-mBJ	11.81	2.85
$KBeO_3$	GGA	8.61 (10.4 [10])	0.67 (0.63 [10]) (1.43 [9])
	TB-mBJ	11.44(11.44 [10])	2.97 (3.02 [10])
$KMgO_3$	GGA	7.15 (6.44 [11])	0.99 (0.81 [11])
	TB-mBJ	10.41	3.33

III.2.3.2 Densities of electronic states:

Total and partial spin-resolved density of states (DOS) of the three perovskites oxides are calculated and depicted in **Figures III.9, III.10 and III.11**. The Fermi energy (E_f) is taken at 0.0 eV. Partial DOS of valence orbitals of each atom expose their individual contribution and explain the existence of ferromagnetism.

From the TDOSs, the results confirm the half-metallic nature of LiBeO$_3$, KBeO$_3$ and KMgO$_3$ compounds that is demonstrated already by the band structure inspections.

For each compound and from partial DOS, It is clear that exchange spin -splitting in both approaches (GGA and TB-mBJ) is fundamentally originated from p states of oxygen (O) atom. There are no contributions from valence orbitals of Li, Be and Mg. But, p states of K have a little contribution to the spin-down channel states around (E$_f$) level, in both spin channels.

As we have seen from the band structures by employing TB-mBJ method, the perovskite oxides LiBeO$_3$, KBeO$_3$ and KMgO$_3$ keep their half metallicity with a wider band gap at the spin-up channel compared to GGA method. So, and from PDOSs, the observed half-metallic character is chiefly originated by robust spin polarization of O-p orbital, which is due to that the Hund energy of O is nearby to that of transition metals [24].
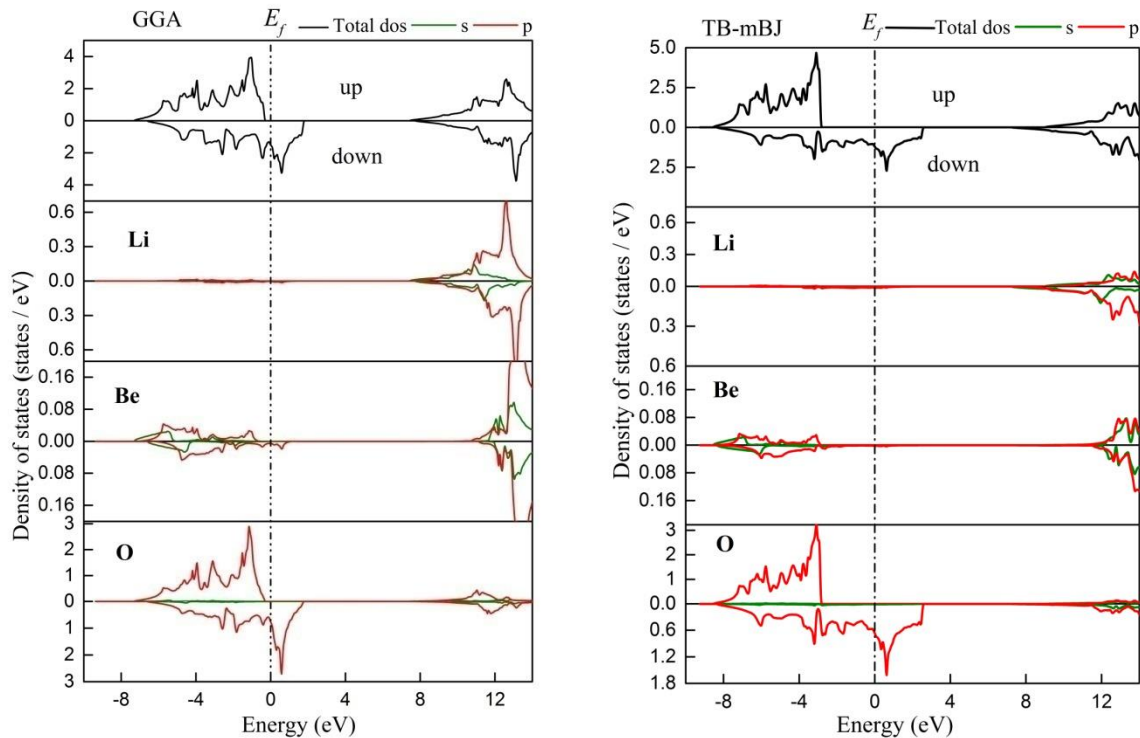

Figure III.9: Calculated DOS of LiBeO$_3$ compound in both spin-up and spin-down states by GGA and GGA+TB-mBJ approximations.
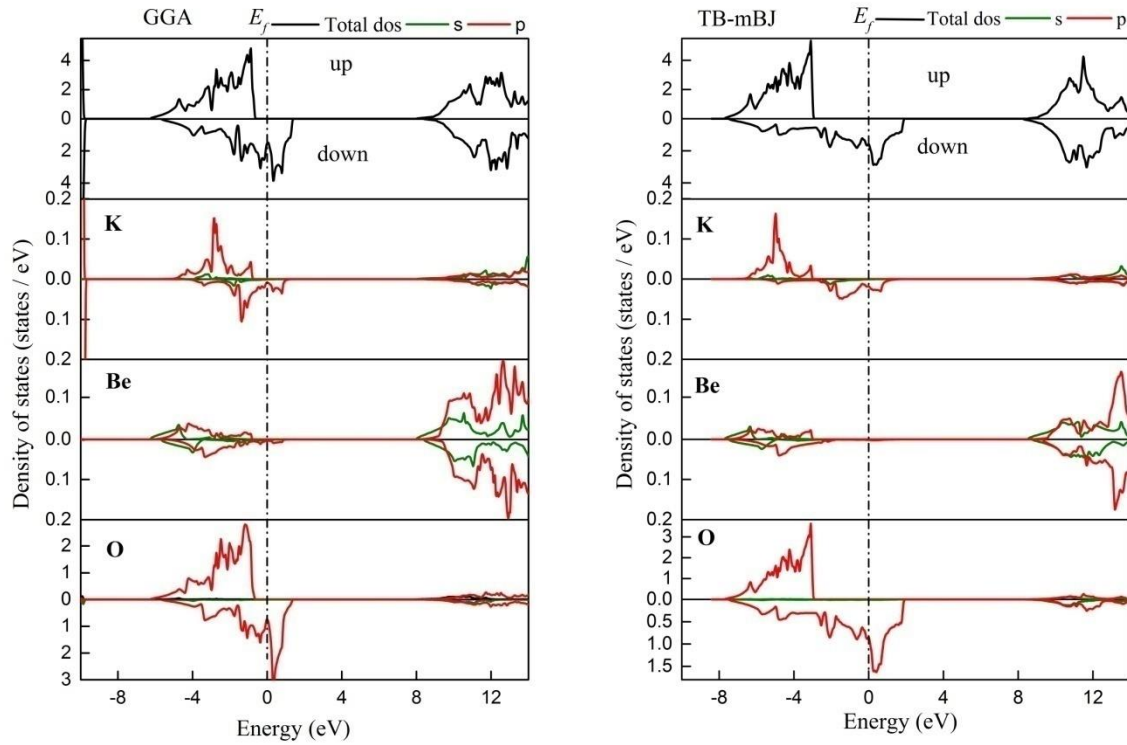
Fig III.10: Calculated DOS of KBeO$_3$ compound in both spin-up and spin-down states by GGA and GGA+TB-mBJ approximations.
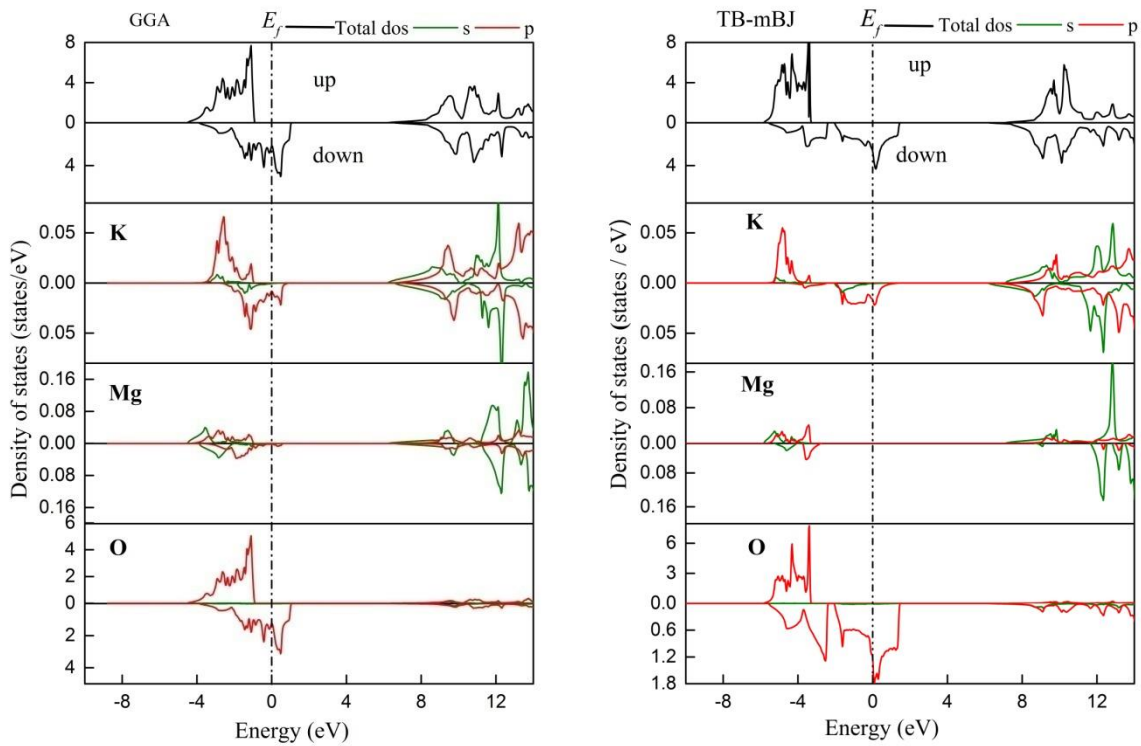

Figure III.11: Calculated DOS of KMgO$_3$ compound in both spin-up and spin-down states by GGA and GGA+TB-mBJ approximations.

III.2.4 Magnetic properties:

In order to describe the spin effect on our materials, we have computed the magnetic properties for our theoretical research.

The estimated local, interstitial and total magnetic moments for oxide perovskite compounds $LiBeO_3$, $KBeO_3$ and $KMgO_3$ by employing GGA and TB-mBJ approaches are gathered in **Table III.10**. It can be seen that the total magnetic moment for each studied compound has an integer value of 3μB per unit cell which fulfill the necessary condition of the half-metallic behavior for the three compounds in cubic phase.

From **Table III.10**, the main contribution, obtained by both GGA and TB-mBJ method, to the total magnetic moment comes from O atoms with the participation of the interstitial magnetic moment. The half-metallicity depend on the electronic and magnetic properties together.

Table III. 10: Calculated total, partial, and interstitial magnetic moments (in μB) in the unit cell for LiBeO3, KBeO3 and KMgO3. The values in parentheses are from [9-11].

LiBeO$_3$					
Method	M$_{tot}$	M$_{Li}$	M$_{Be}$	M$_O$	M$_{int}$
GGA	3.001 (3.000[9])	-0.006 (0.004 [9])	-0.01 (-0.010 [9])	0.768 (0.900 [9])	0.712 (0.314 [9])
TB-mBJ	3.000	-0.036	-0.035	0.936	0.264
KBeO$_3$					
Method	M$_{tot}$	M$_K$	M$_{Be}$	M$_O$	M$_{int}$
GGA	3.001 (3.000[9]) (3.000[10])	0.012 (0.0183[9]) (0.014[10])	-0.014 (-0.021[9]) (-0.019[10])	0.746 (0.919[9]) (0.933[10])	0.765 (0.258[9]) (0.207[10])
TB-mBJ	3.000 (2.999[10])	0.004 (-0.009[10])	-0.032 (-0.046[10])	0.898 (1.068 [10])	0.334 (-0.147[10])
KMgO$_3$					
Method	M$_{tot}$	M$_K$	M$_{Mg}$	M$_O$	M$_{int}$
GGA	3.000 (3.000[11])	0.001 (-0.019 [11])	-0.008 (-0.078 [11])	0.726 (1.040 [11])	0.830
TB-mBJ	3.000	0.002	-0.023	0.902	0.314

The origin of magnetic moment can be explained by the partially filled O-p orbitals: i.e. the element atom (Li, K) coming from the alkali metal group (I^A) loses one electron and the other atom (Be, Mg) coming from the alkaline earth metal group (II^A) two electrons to the oxygen atoms thereby forcing the oxygen atom to possess an oxidation state of −1 instead of −2. Therefore, the I^{A}II^{A}O3 valence electrons are distributed as follows: two electrons fill s-states of the O atoms and five electrons occupy their p orbitals, giving rise to one unpaired electron for each O atom, leading to a total magnetic moment of 3.0μB.
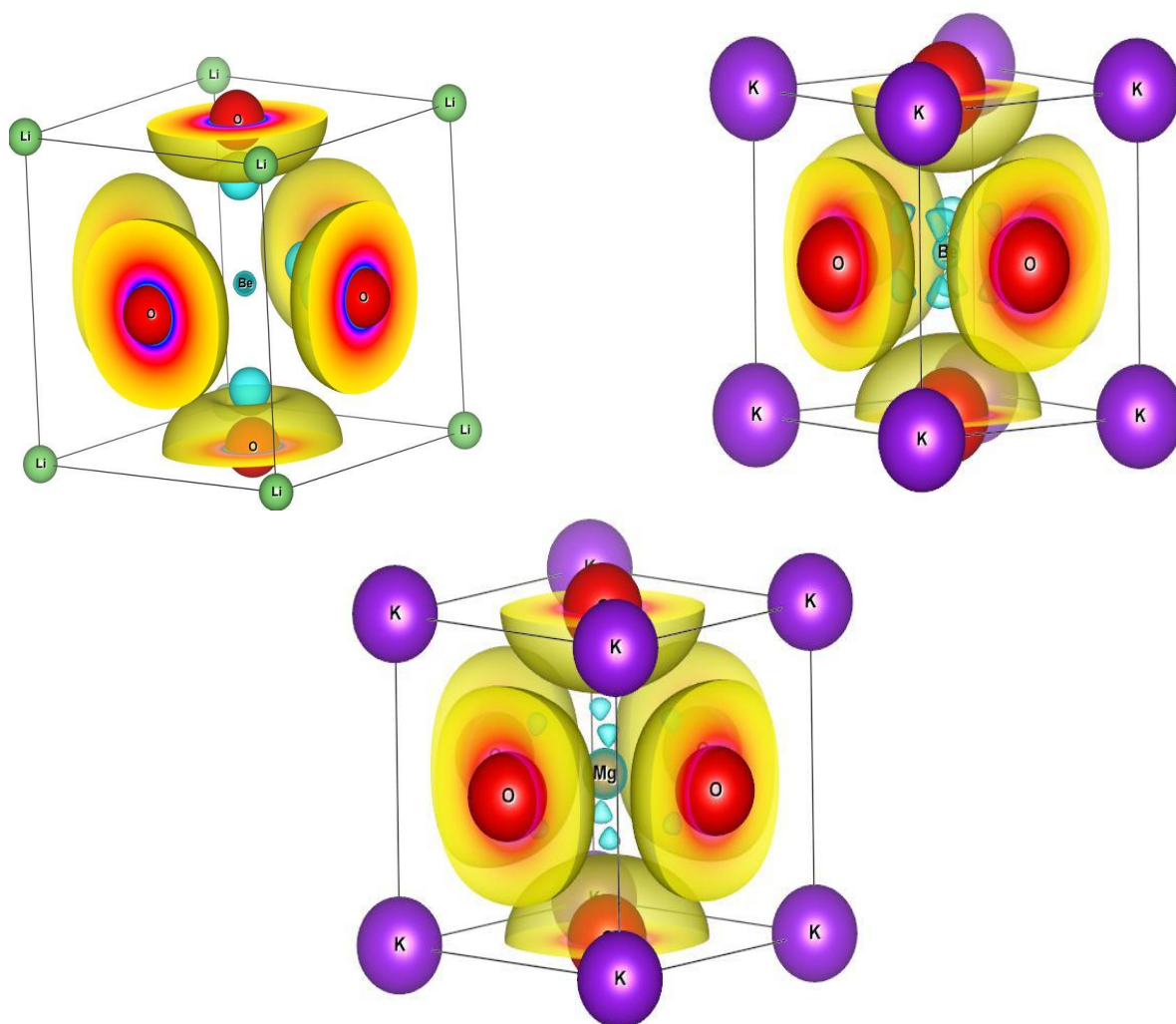

Figure III.12: Spin density of LiBeO$_3$,KBeO$_3$ and KMgO$_3$ (yellow and bleu isosurface colors correspond to positive and negative spin density, respectively).

To better highlight the origin of the magnetic moment of our considered compounds, we present in **Figure III.12** the spin density isosurfaces. It is clear from these figures that the spin magnetic moment for the three compounds are localized around O atoms which are shown to be ferromagnetically coupled, according to the yellow

isosurfaces with a positive spin density of $0.02/$ Å^3. In addition, a part of spin magnetic moment around Be and Mg atoms for LiBeO$_3$, KBeO$_3$ and KMgO$_3$, respectively, as shown by blue drop forms, indicates a small negative spin magnetic moment. On other hand, we can as well remark that there is almost no spin accumulated around Li, Be, K and Mg atom which means they have a negligible contribution to the total magnetic moment for each compound.

The Curie temperature (T_C), or Curie point, is the temperature above which ferromagnetic materials lose their permanent total magnetic moments. We have estimated the Curie temperature using the mean−field approximation (MFA) [25, 26]. In this method, T_C is expressed by:

$$T_C = \frac{2}{3xK_B} \Delta E \qquad\qquad\qquad (III.24)$$

Where x is the number of magnetic particles in supercell, K_B denotes the Boltzmann constant and ΔE is the total energy difference ΔE = E$_{AFM}$−E$_{FM}$ between the antiferromagnetic and ferromagnetic states. It is found to be 660.88K, 639K and 626K for LiBeO$_3$, KBeO$_3$ and KMgO$_3$, respectively

It's noticed that LiBeO$_3$ compound has a higher magnetic transition Temperature than KBeO$_3$ and KMgO$_3$ compounds, originated fundamentally from the robust exchange interaction O-O in our considered materials.

III.2.4. 1 Pressure effect on the half-metallic character:

The half-metallic behavior depends on the width and the existence of half-metallic band gap, which is defined as the smaller absolute energy difference: between VBM /CBM and Fermi level. By applying a pressure, the energy band gap decrease in the spin-up channel and the compound can loses its half-metallicity.

Figure III.13 presents the total, atomic, interstitial magnetic moments, VBM /CBM in the spin-up direction, and spin-polarization as a function of the pressure for LiBeO$_3$, KBeO$_3$ and KMgO$_3$. We can see that the total magnetic moment value keeps the integer value of 3µB for the three compounds in different range of pressure. LiBeO$_3$ loses its half metallicity once the pressure reached 24.7 GPa, whereas in KBeO3, this behavior remain up to 97 GPa where the total magnetic moment becomes 0 µB. KMgO$_3$ stay half-metallic up to116.2 GPa.
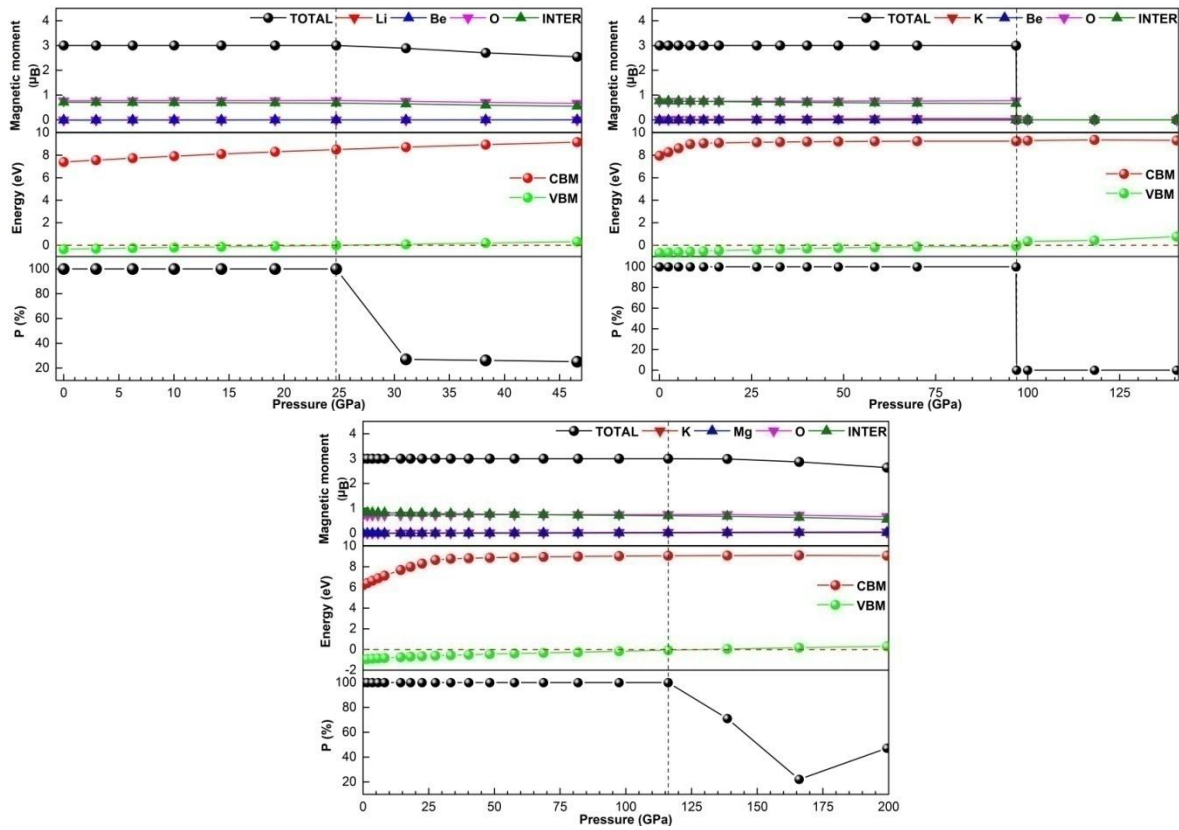
Figure III.13: Total and atomic magnetic moments, CBM and VBM in the spin-up channel, and spin-polarization as function of the pressure for $LiBeO_3$, $KBeO_3$ $KMgO_3$.

The spin polarization (P) at Fermi EF level is related to spin-polarized DOS by the expression:

$$P\left(E_f\right) = \frac{\rho\uparrow(E_f) - \rho\downarrow(E_f)}{\rho\uparrow(E_f) + \rho\downarrow(E_f)} \qquad \text{(III.25)}$$

Where $\rho\uparrow(E_F)$ and $\rho\downarrow(E_F)$ are the majority and minority state densities at Fermi level EF. As is clear from **Figure III.13**, the spin polarization at Fermi level is 100% up to the pressure of 24.7, 97 and 116.2 GPa for $LiBeO_3$, $KBeO_3$ and $KMgO_3$, respectively.

III.2.5 Thermodynamic properties:

In order to investigate the thermodynamic parameters, the quasi-harmonic Debye approximation has been applied which allows us to obtain all the thermodynamic quantities from the calculated (volume-energy) points, in which the unbalanced Gibbs function $G^*(V, P, T)$ is expressed as follows:[27]

$$G^*(V, P, T) = E(V) + PV + A_{Vib}[\theta(V), T] \qquad \text{(III.26)}$$

Where E(V) is the total energy of the unit cell. PV is the constant hydrostatic pressure condition and the A_{vib} is the vibrational Helmholtz free energy, expressed by:

$$A_{Vib}(\theta_D, T) = nk_BT \left\{ \frac{9\theta_D}{8T} + 3\ln\left[1 - e^{(-\frac{\theta_D}{T})}\right] - D(\frac{\theta_D}{T}) \right\} \qquad (III.27)$$

Where n is the number of atoms per formula unit and the Debye integral $D(\frac{\theta_D}{T})$, for anisotropic solid, is:

$$\theta_D = \hbar/k_B \left(6\pi^2 nV^{\frac{1}{2}}\right)^{\frac{1}{3}} f(\sigma) \left(\frac{B_S}{M}\right)^{1/2} \qquad (III.28)$$

Where, M is the molecular mass per unit cell. B_S is the adiabatic bulk modulus, which is approximately given by static compressibility:

$$B_S = B(V) = V\frac{\partial^2 E(V)}{\partial V^2} \qquad (III.29)$$

$f(\sigma)$ and B_S are mentioned in references [28], respectively. The non-equilibrium Gibbs function $G^*(V, P, T)$, as a function of (V, P, T) can be minimized with respect to volume V as:

$$\left[\frac{\delta^2 G^*(P,V)}{\delta V^2}\right]_{P,V} = 0 \qquad (III.30)$$

The isothermal bulk modulus B_T is given by [29]:

$$B_T(P, T) = V\left[\frac{\delta^2 G^*(P,V,T)}{\delta V^2}\right]_{P,T} \qquad (III.31)$$

The thermodynamic quantities such as heat capacity at a constant volume C_V and entropy S are calculated by the relation [27, 29]:

$$C_V = 3nk_B\left[4D\left(\frac{\theta_D}{T}\right) - \frac{3\theta_D/T}{e^{\frac{\theta_D}{T}} - 1}\right] \qquad (III.32)$$

$$S_{V=nk_B}\left[4D\left(\frac{\theta_D}{T}\right) - 3\ln(1 - e^{(-\frac{\theta_D}{T})})\right] \qquad (III.33)$$

The thermal properties are monitored in the temperature range between 0 and 1000 K, as well as the pressure effect is imposed in the range 0 to 30 GPa for $LiBeO_3$, 0 to 25GPa for $KBeO_3$ and 0 to 20 GPa for $KMgO_3$, where the pressure points are taken with a step of 5 GPa.

The relationship between the volume ratio V / V0 and the temperature at different pressures is clearly illustrated in **Figure III.1**, we observe that the volume ratio V/V_0

decreases linearly with an increasing temperature at a given pressure and decreases with an increasing pressure at a given temperature.
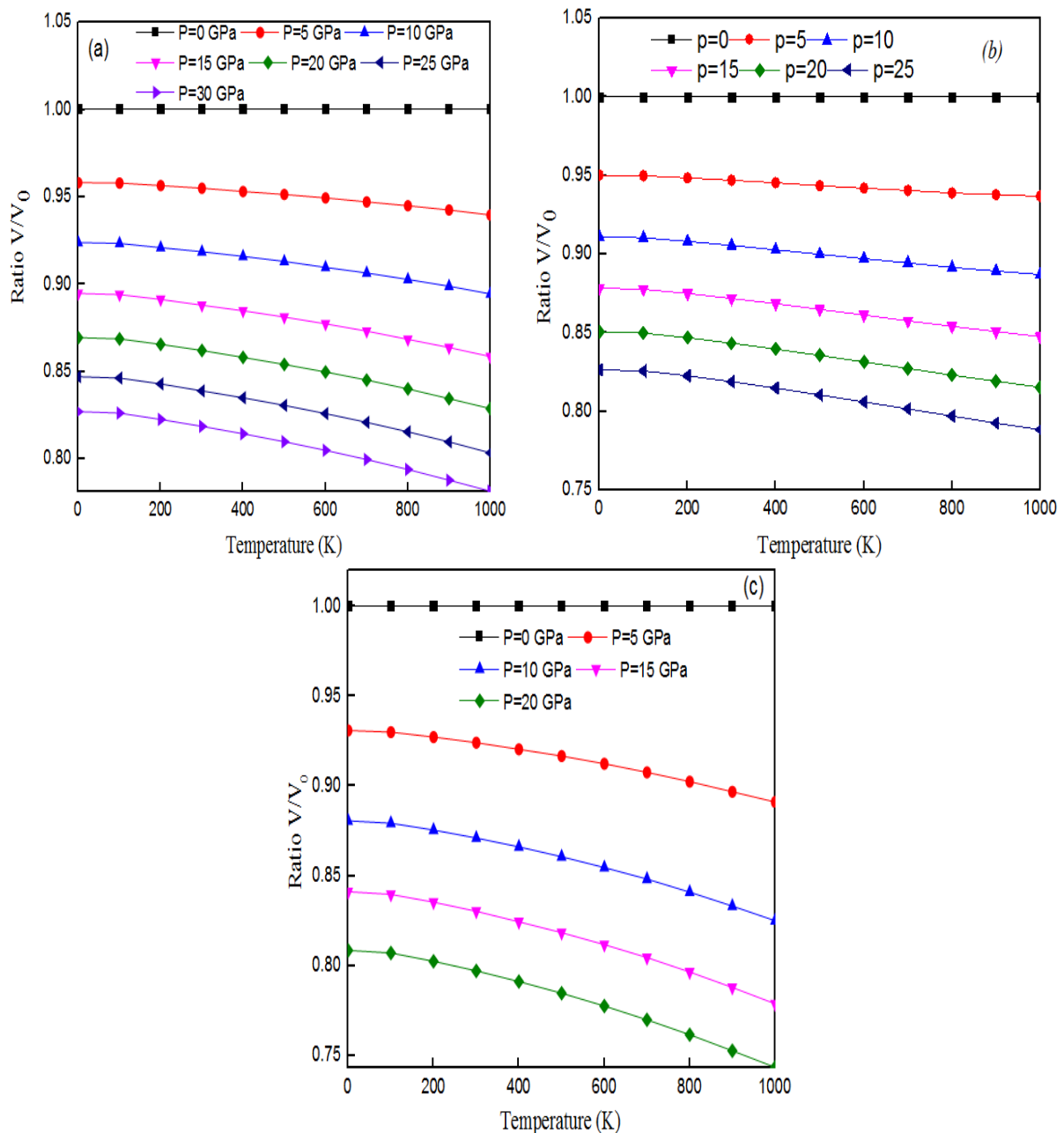

Figure III.14: Pressure and temperature dependence of the relative volume V/V_o: (a): LiBeO$_3$, (b): KBeO$_3$ and (c): KMgO$_3$.

The bulk modulus relates to the change in the volume of an object, when subjected to pressure changes, and is used to describe hardness. **Figure III.15** shows the evolution of the bulk modulii as a function of temperature in the range from 0 to 1000 K. We can see very clearly that they are almost constant in the range of 0 to 100 K, whereas from a temperature above 100 K they decrease with temperature for each

given pressure. These results mean that the increase in temperature within a material causes a reduction in its hardness (for the three compounds). The bulk modulus, at zero pressure and T=300K, is 98.46 GPa, 82.07GPa and 53.13GPa for LiBeO$_3$, KBeO$_3$ and KMgO$_3$, respectively.
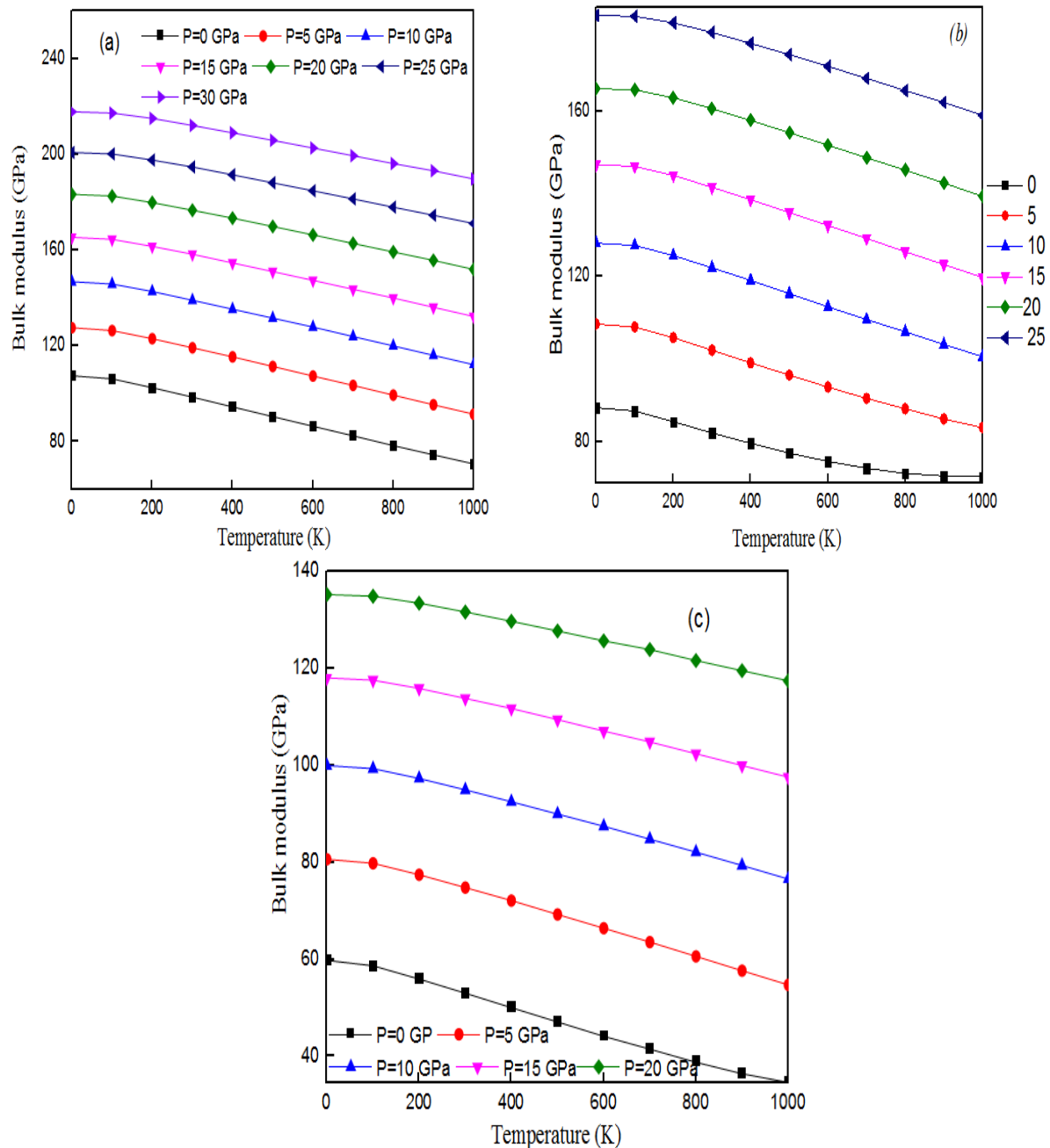

Figure III.15: Pressure and temperature dependence of the bulk modulus: (a): LiBeO$_3$, (b): KBeO$_3$ and (c): KMgO$_3$.

We present in **Figure III.16** the relation between the heat capacity at constant volume C$_V$ and the temperature for the three compounds. From this Figure, we notice that the specific heat (C$_V$) increases considerably with temperature in the

low temperature range (T<200) for KBeO$_3$ and KMgO$_3$ compound, and their variations are proportional to T^3 (Deby law), then the increase becomes slow in the high temperature range until it reaches the limit of Dulong and Petit (C$_V$ ~ 3R, where *R* is the universal gas constant).
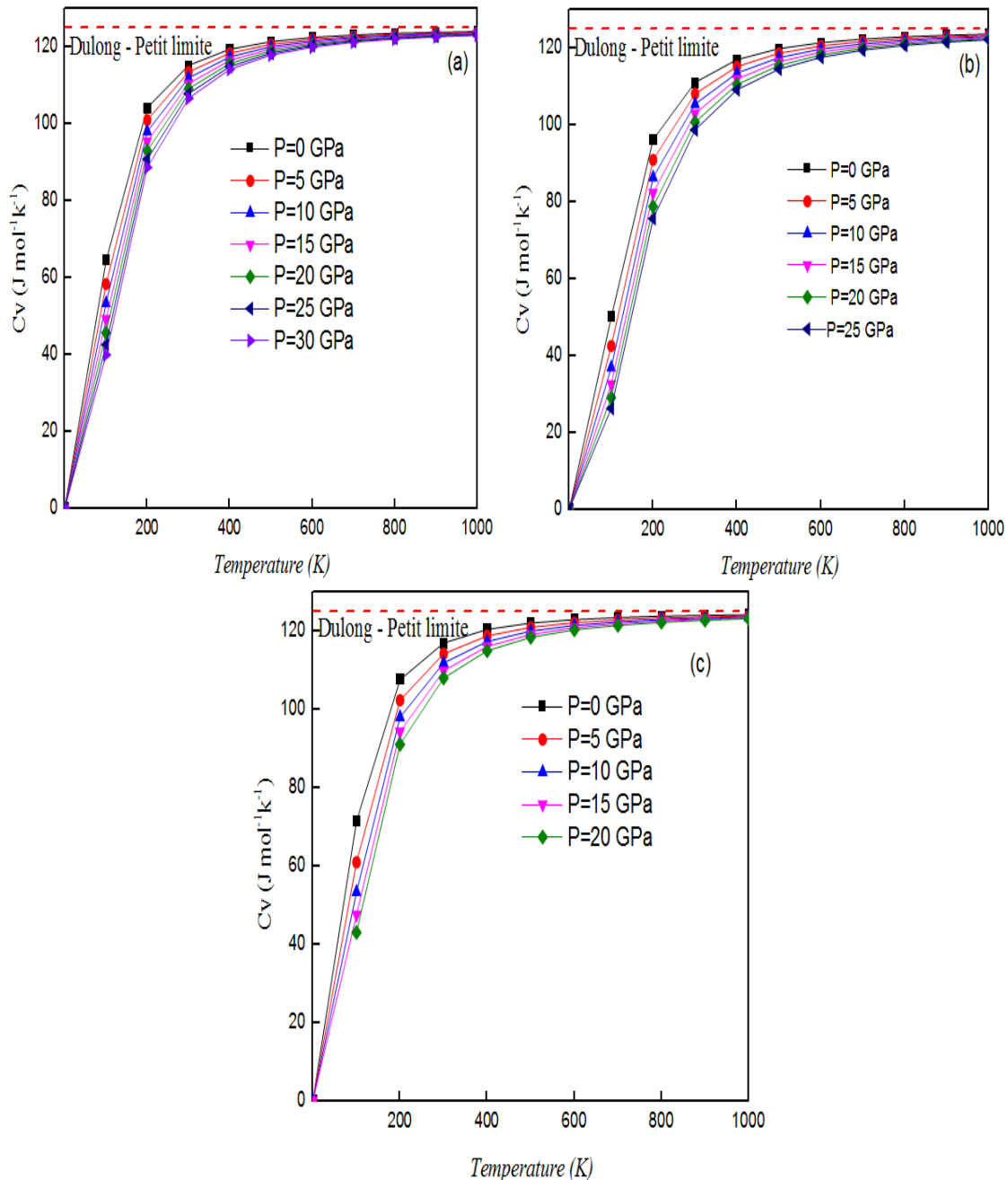

Figure III.16: Pressure and temperature dependence of the heat capacity C$_V$: (a): LiBeO$_3$, (b): KBeO$_3$ and (c): KMgO$_3$.

Another thermodynamic parameter, the thermal expansion (α), is illustrated in **Figure III.17**. From the three figures, it is clear that α rises rapidly from 0 K to 300 K, the increase in "α" is found to be quick under low temperatures values. Under

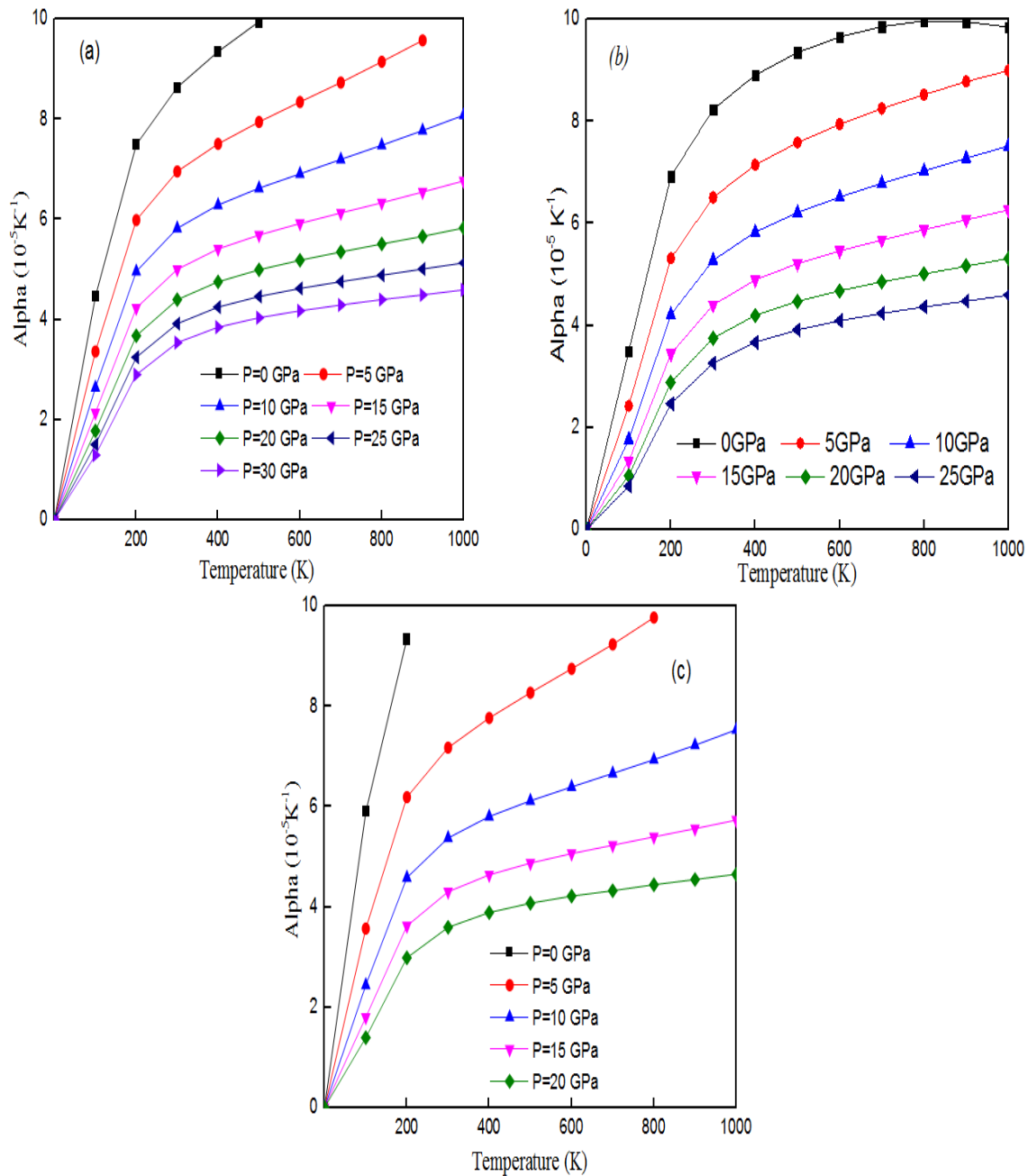higher temperatures value a weak increase in "α" is observed, exhibiting similar character as Cv.

Figure III.17: Pressure and temperature dependence of the thermal expansion (α): (a): LiBeO$_3$, (b): KBeO$_3$ and (c): KMgO$_3$.

Debye temperature θ_D is one of remarkable thermo-elastic parameters of solids. It is a good index of the stiffness of materials; materials with high θ_D exhibit high solidity and are somewhat hard than the materials with low θ_D.[30] In **Figure III.18**, the change in Debye temperature θ_D as a function of temperature and pressure is presented for the three compounds.

From the three figures, it can be seen that θ_D is nearly stable from 0 to 100 K and decreases with increasing the temperature. Moreover, it is evident that when the temperature is constant, the Debye temperature increases with the applied pressure. The calculated value of the Debye temperature of our compounds at 0 GPa and 300K temperature equals 380.05, 461.25K and 341.38K for $LiBeO_3$, $KBeO_3$ and $KMgO_3$, respectively.
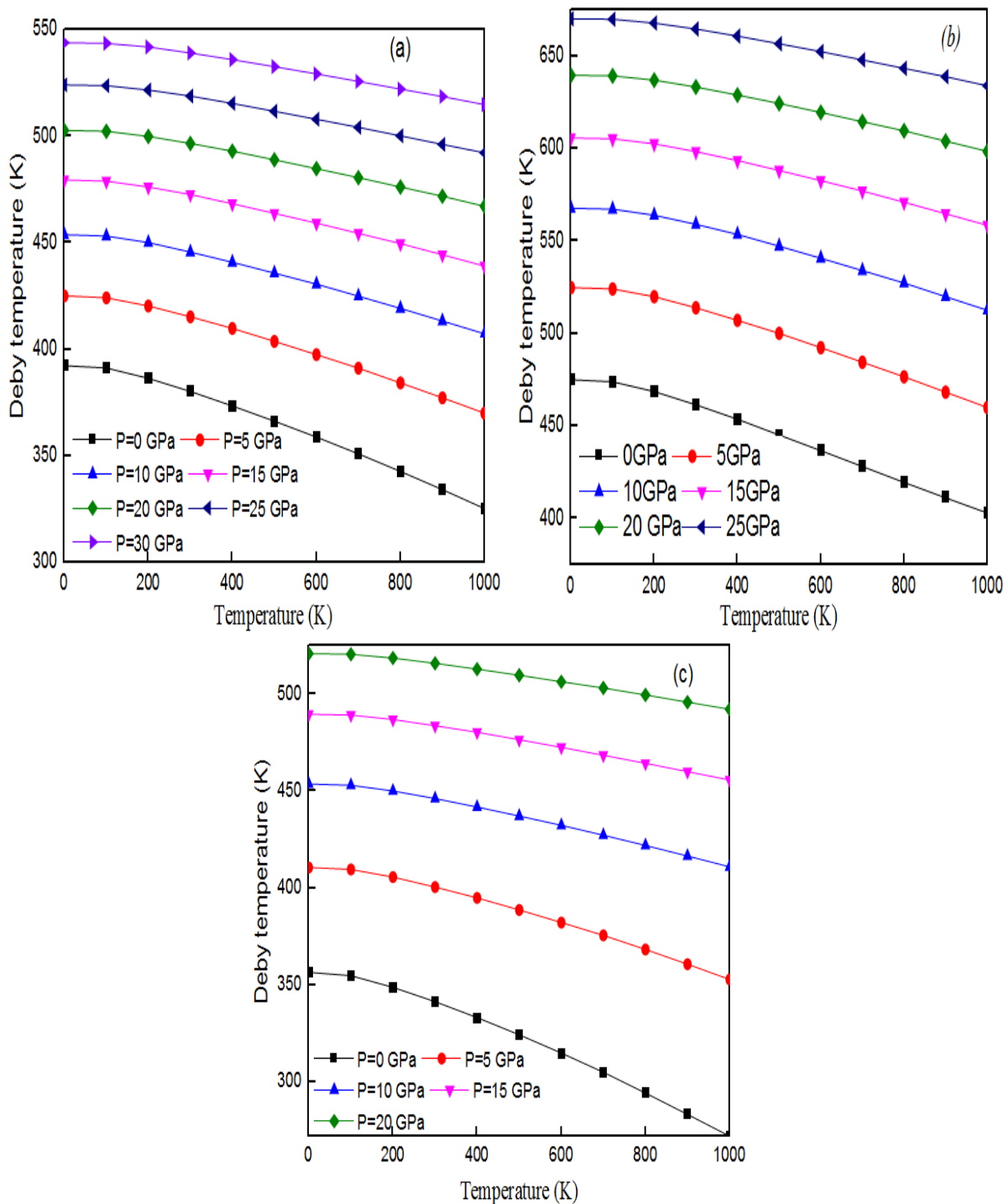

Figure III.18: Pressure and temperature dependence of the Debye temperature: (a): $LiBeO_3$, (b): $KBeO_3$ and (c): $KMgO_3$.

Bibliographical references:

[1] P. Hohenberg, W. Kohn, Inhomogeneous electron gas, Physical Review, 136 (1964) B864.

[2] W. Kohn, L.J. Sham, Self-consistent equations including exchange and correlation effects, Physical Review, 140 (1965) A1133.

[3] O.K. Andersen, Linear methods in band theory, Physical Review B, 12 (1975) 3060.

[4] P. Blaha, K. Schwarz, G.K. Madsen, D. Kvasnicka, J. Luitz, wien2k, An augmented plane wave+ local orbitals program for calculating crystal properties, 60 (2001).

[5] Z. Wu, R.E. Cohen, More accurate generalized gradient approximation for solids, Physical Review B, 73 (2006) 235116.

[6] D. Koller, F. Tran, P. Blaha, Improving the modified Becke-Johnson exchange potential, Physical Review B, 85 (2012) 155109.

[7] J. Camargo-Martinez, R. Baquero, The band gap problem: the accuracy of the Wien2k code confronted, arXiv preprint arXiv:1208.2057, (2012).

[8] F. Birch, The effect of pressure upon the elastic parameters of isotropic solids, according to Murnaghan's theory of finite strain, Journal of Applied Physics, 9 (1938) 279-288.

[9] Q. Mahmood, B.U. Haq, M. Yaseen, A. Shahid, A. Laref, Exploring the origin of p-type half-metallic ferromagnetism in beryllium doped alkali based perovskites, Solid state communications, 299 (2019) 113654.

[10] V. Ashwin, M.B. Ahamed, S.B. Elavarasi, Structural, electronic, magnetic and half-metallic properties of cubic perovskites NaBeO3 and KBeO3 using PBE-GGA and TB-mBJ approach: A DFT perspective, Applied Physics A, 126 (2020) 1-11.

[11] M. Babalola, B. Iyorzor, First-principles investigation of electronic, structural, magnetic and thermodynamic properties of $$\hbox {XMgO} _ {{3}} $$ XMgO 3 ($$\hbox {X}=\hbox {Na} $$ X= Na, K and Rb), Pramana, 96 (2022) 1-9.

[12] J.F. Nye, Physical properties of crystals: their representation by tensors and matrices, Oxford university press, 1985.

[13] R. Hill, The elastic behaviour of a crystalline aggregate, Proceedings of the Physical Society. Section A, 65 (1952) 349.

[14] B. Huang, Y.-H. Duan, W.-C. Hu, Y. Sun, S. Chen, Structural, anisotropic elastic and thermal properties of MB (M= Ti, Zr and Hf) monoborides, Ceramics International, 41 (2015) 6831-6843.

[15] Q. Wu, S. Li, Alloying element additions to Ni3Al: Site preferences and effects on elastic properties from first-principles calculations, Computational Materials Science, 53 (2012) 436-443.

[16] S. Pugh, XCII. Relations between the elastic moduli and the plastic properties of polycrystalline pure metals, The London, Edinburgh, and Dublin Philosophical Magazine and Journal of Science, 45 (1954) 823-843.

[17] D. Pettifor, Theoretical predictions of structure and related properties of intermetallics, Materials science and technology, 8 (1992) 345-349.

[18] G. Vaitheeswaran, V. Kanchana, R. Kumar, A. Cornelius, MF Nicol, A. Savane, A. Delin, B. Johansson, Phys. Rev, 75 (2007) 014107.

[19] H. Fu, D. Li, F. Peng, T. Gao, X. Cheng, Ab initio calculations of elastic constants and thermodynamic properties of NiAl under high pressures, Computational Materials Science, 44 (2008) 774-778.

[20] J. Haines, J. Leger, G. Bocquillon, Synthesis and design of superhard materials, Annual Review of Materials Research, 31 (2001) 1-23.

[21] V. Tvergaard, J.W. Hutchinson, Microcracking in ceramics induced by thermal expansion or elastic anisotropy, Journal of the American Ceramic Society, 71 (1988) 157-166.

[22] R.D. Shannon, Revised effective ionic radii and systematic studies of interatomic distances in halides and chalcogenides, Acta crystallographica section A: crystal physics, diffraction, theoretical and general crystallography, 32 (1976) 751-767.

[23] J. Philipp, P. Majewski, L. Alff, A. Erb, R. Gross, T. Graf, M. Brandt, J. Simon, T. Walther, W. Mader, Structural and doping effects in the half-metallic double perovskite A 2 CrWO 6 (A= Sr, Ba, and Ca), Physical Review B, 68 (2003) 144431.

[24] O. Volnianska, P. Boguslawski, Magnetism of solids resulting from spin polarization of p orbitals, Journal of Physics: Condensed Matter, 22 (2010) 073202.

[25] M. Shahjahan, M. Toyoda, T. Oguchi, Ferromagnetic Half Metallicity in Doped Chalcopyrite Semiconductors Cu (Al1– xAx) Se2 (A= 3 d Transition-Metal Atoms), Journal of the Physical Society of Japan, 83 (2014) 094702.

[26] L. Bergqvist, P.H. Dederichs, A theoretical study of half-metallic antiferromagnetic diluted magnetic semiconductors, Journal of Physics: Condensed Matter, 19 (2007) 216220.

[27] M. Blanco, E. Francisco, V. Luana, GIBBS: isothermal-isobaric thermodynamics of solids from energy curves using a quasi-harmonic Debye model, Computer Physics Communications, 158 (2004) 57-72.

[28] E. Francisco, J. Recio, M. Blanco, A.M. Pendás, A. Costales, Quantum-mechanical study of thermodynamic and bonding properties of MgF2, The Journal of Physical Chemistry A, 102 (1998) 1595-1601.

[29] F. Peng, H.-Z. Fu, X.-L. Cheng, First-principles calculations of thermodynamic properties of TiB2 at high pressure, Physica B: Condensed Matter, 400 (2007) 83-87.

[30] L. Ju, S.A. Dar, Probing the structural, electronic, mechanical strength and thermodynamic properties of tungsten-based oxide perovskites RbWO3 and CsWO3: first-principles investigation, Journal of Electronic Materials, 48 (2019) 4886-4894.

General conclusion

General Conclusion and perspectives:

The aim of this thesis was to present a theoretical study of the structural, elastic, magnetic, electronic and thermodynamic properties of some new perovskites type I^A-II^A-O_3 compounds based on the FP-LAPW method with the GGA and TB-mBJ approximations.

After extensive prospection, we turned our attention to three materials $LiBeO_3$, $KBeO_3$ and $KMgO_3$ which can be promising candidates for applications in spintronics technology. The principal conclusions through this study are highlighted below:

- The ferromagnetic phase (FM) is more stable than that of anti-ferromagnetic (AFM) and non-magnetic (NM) phases. Moreover, their stabilities are proven from negative formation energies.

- The necessary condition of half metallic behavior (net magnetic moment is integer) are fulfilled and its obtained value for each compound 3 μB. In these non-magnetic perovskites even without transition metals the Ferromagnetism was observed.

- The spin-down states display metallic behavior; whereas, spin-up states display insulating behavior (half-metallic character). Under GGA, $KBeO_3$ has an indirect band gap larger than $LiBeO_3$ and $KMgO_3$ in spin-up channel, while in TB-mBJ approach the band gap of $LiBeO_3$ becomes larger than $KBeO_3$ and $KMgO_3$.

- The half-metallicity of $LiBeO_3$, $KBeO_3$ and $KMgO_3$ is mainly resulted from the p-orbitals of oxygen.

- The mechanical profile suggests that $LiBeO_3$, $KBeO_3$ and $KMgO_3$ are ductile materials and show anisotropic nature.

- When compared, $KMgO_3$ has large HM gap than $LiBeO_3$ and $KBeO_3$ with same magnetic moment in both approaches.

- The half metallicity is maintained under the pressure up to 24.7, 97 and 116.2 GPa, for $LiBeO_3$, $KBeO_3$ and $KMgO_3$, respectively.

- From all these results, the reported perovskites might be valuable for future spintronic applications.

As perspectives, an interesting extension of this work would be to carry out a study of the dynamic and thermodynamic stability of perovskite oxides compounds of the I^A-II^A-O_3 type in order to better control the potentialities which can be offered by this family of materials.

Further research on bulk and surface half-metallicity of these and similar materials may shed more light on the physical mechanisms behind the half-metallic character.

Also, the investigation of this family in other phases is required.